2009

A self healing smart syntactic foam based grid stiffened sandwich structure

Manu Kuruvila John
Louisiana State University and Agricultural and Mechanical College, mjohn1@lsu.edu

A SELF HEALING SMART SYNTACTIC FOAM BASED GRID STIFFENED SANDWICH STRUCTURE

A Dissertation
Submitted to the Graduate Faculty of
Louisiana State University and
Agricultural and Mechanical College
in partial fulfillment of the
requirements for the degree of
Doctor of Philosophy
in
The Department of Mechanical Engineering

by

Manu Kuruvila John
B.Tech, Mahatma Gandhi University, India, 2001.
M.S., Tuskegee University, 2004.

December 2009

ACKNOWLEDGEMENTS

I would like to extend my heartfelt gratitude and thanks to Dr. Guoqiang Li, my major professor for his guidance and support provided during the course of this research work and the confidence he had in me. This work would not have been possible without his extensive help, valuable insight and time he invested in this research work. He has been my constant inspiration and mentor for both my course work and research work. I would also like to thank the support and guidance of my graduate committee, Dr. Dorel Moldovan, Dr. Su-Seng Pang, Dr. Muhammad Wahab, Dr. Steve Cai and Dr. Roberto Barbosa, who is acting as the Dean's representative. The help provided by Ms. Cindy Henk, Dr. Xiaogang Xie and Dr. Kun Lian in doing the TEM, SEM and DSC analysis is greatly appreciated. Also, the help from Dr. Phani Mylavarapu and my lab mates is greatly acknowledged.

I wish to extend a very special thanks to my wife, Chindu Rajan for the constant moral support and motivation she has provided throughout my life and work. She has been a constant source of inspiration and energy for me. I also would like to express my gratitude to my parents Mr. John Kuruvilla and Mrs. Susan John for their encouragement in pursuing my dreams and their help in getting a better education. Their sacrifices and prayers are really appreciated. The technical advice and expertise regarding the "polymerization" process, provided by my father Mr. John Kuruvilla, is highly appreciated at this point. I express my heartfelt gratitude to my younger brother, Dr. Jinu John and his wife Chinnu Simon for their love and moral support. I take this opportunity to thank my in-laws Mr. C.T. Rajan and Mrs. Gracy Rajan; sisters Anna Rajan and Sara Rajan.

Extreme gratitude goes to Mr. Abraham George and family, Hari and Archana; Arun, Reshmi and their lovely kid Aishwarya; Dr. Deepu, Ammu and their lovely kid Daya; Dr. Felix

and Suja; Fr. Boby Alex; Dr. Sundar, Mini and their handsome kid Vishnuh; Dr. Manoj and Sujitha; Gigi, Cherian, Prashanth, Jomish, Manjooran, Abhish and Ency, Ciby, Moncy, Reji, Surbhi, Aparna and Sitanshu.

I would like to acknowledge the Economic Development Assistantship (EDA) for providing funding for this study, Louisiana Transportation and Research Center (LTRC) and NASA-EPSCoR as well. Finally, no words can express my gratitude to the author and finisher of my life, Lord and Savior Jesus Christ, for His grace, wisdom and guidance.

TABLE OF CONTENTS

LIST OF TABLES

LIST OF FIGURES

ABSTRACT

Syntactic foams are composite materials synthesized by dispersing microballoons in a polymeric, ceramic or metallic matrix. In the past three decades, syntactic foams have gained immense importance as a lightweight and damage-tolerant material when used in foam-cored sandwich structures. Because of the structural-length scale damages by low velocity impact such as tool drops, runway debris etc., sandwich structures usually have a very low residual structural capacity. Unfortunately, macro-length scale damage, in particular internal damage such as impact damage, is very difficult to repair. Therefore, there is a genuine need to develop impact-tolerant and self-healing syntactic foams which can be used as a core in sandwich structures.

In this study, a new shape memory polymer (SMP) based syntactic foam was proposed, fabricated, characterized, and tested using DSC, TEM, SEM, and stress-controlled programming and free shape recovery by association with the foam cored sandwich. A micromechanics based model was employed to clearly visualize the microstructure and to quantify the geometrical and mechanical properties of the smart foam composite in the linear elastic region. An orthogrid stiffened SMP based syntactic foam cored sandwich was then fabricated, programmed, impacted, healed (sealed), and compression tested, for the purposes of sealing impact damage. Two impact energy levels (30J and 53J), two prestrain levels (3% and 20%), and two confinement conditions (2-D confined and 3-D confined) were used in the low velocity impact test, strain-controlled programming and constrained shape recovery, respectively. C-scan and visual observation were also conducted to visualize impact damage and evaluate the degree of sealing achieved.

It is found that the shape memory functionality of the SMP based syntactic foam can be utilized for the purpose of sealing impact damage with the developed programming and shape recovery. The developed foam and the hybrid sandwich structure are able to heal (or seal)

structural-length scale damage (here impact damage) repeatedly (up to 7 rounds of impact-healing cycles), efficiently (with a healing efficiency over 100%); and almost autonomously (the only human intervention is by heating). This study lays a solid foundation for the next generation of smart self-healing composite structures in engineering applications.

CHAPTER 1. INTRODUCTION

1.1 Syntactic Foams

Syntactic foams are light weight particulate composites that make use of hollow microspheres as reinforcement in a polymer resin matrix; see Figure. 1. Enormous work has been done in the field of syntactic foams since 1960s. The major work in this field started with a simple two-phase foam system with glass microballoons as reinforcement and a polymer system as the matrix. These systems were aimed at applications in the marine and submarine industry. Now this field has expanded to include polymer and metal hollow particles, rubber particles etc. to form three phase and four phase systems [1]. These multi-phased syntactic foams were aimed at applications that make use of the high specific strength properties, energy absorption characteristics, biocompatibility and flame retardant properties. Due to these innovations, syntactic foams have found applications in aerospace, automobile, transportations and biomedical fields.

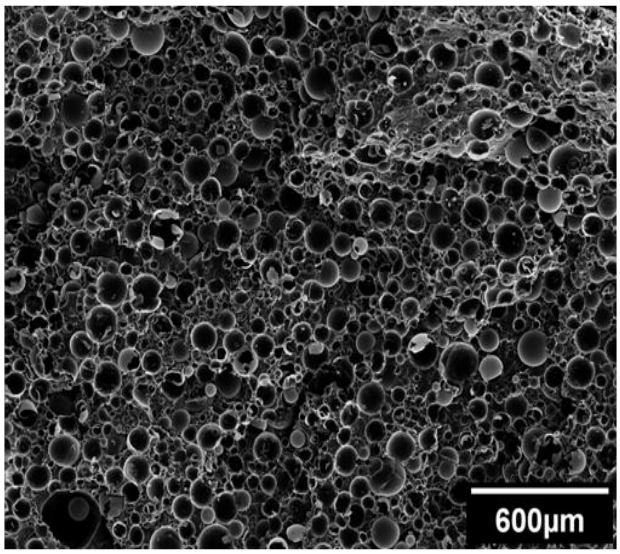

Figure 1. SEM image showing the microstructure of a syntactic foam

The physical and mechanical properties of these foams can be modified to suit the requirements of particular applications. These requirements in the material properties of the foams can be achieved by incorporating various reinforcing/filler materials. Varieties of foams have evolved through the incorporation of different filler materials like nanoparticles, short fibers, crumb rubbers, etc.

Thermosetting polymers as opposed to thermoplastic polymers are preferred matrix/binder materials due to their ease of manufacturing [2, 3] rather than specific material properties [4]. The mechanical properties of the resulting syntactic foams are related to the filler type and filler-matrix interaction. Normally spherical shaped fillers are preferred due to their good packing factor and hydrostatic compression strength [5]. The diameters of these particles range from 1-500μm with a wall thickness of 1-4 μm. Glass microspheres are usually preferred as filler materials due to their superior mechanical strength, smoothness and regularity of the surface, good wetting characteristics and low viscosity of the resulting foam, all combined with established production procedures and low cost. A comprehensive study on syntactic foams was reported by Shutov [6]. Concerning the mechanical behavior, syntactic foams display uniaxial compression strengths up to 100 MPa, hydrostatic compression strengths up to 150 MPa, uniaxial tension strengths up to 25~30 MPa and tensile Young's modulus up to 2500~3000 MPa. The behavior in compression is quite ductile, whereas tensile response is rather brittle [7].

The tensile modulus of syntactic foams containing low density microballoons can be increased with the decrease in microballoon volume fraction. An experimental investigation on the tensile strength and modulus of glass microballoon based syntactic foams were carried out by Gupta et.al [8]. From this study, they found that the tensile modulus of the foams with high density microballoons increased, but it was not related to the volume fraction. They concluded that the tensile strength enhancement was related to the matrix properties rather than the

microballoon characteristics. The modulus increased with microballoon density. A similar study was also conducted by Kishore et.al on the tensile strength and fractography of syntactic foams [9]. They concluded that the Young's modulus increased linearly from 2 to 2.47 GPa with the decrease in microballoon volume fraction. Fractographic studies revealed increased spacing between the microballoons and curvilinear deformation marks in the matrix with resin rich areas.

Addition of chopped fibers as reinforcements in syntactic foams helps in improving their flexural strength properties irrespective of the presence of voids. A study by Karthikeyan et.al on the flexural behavior of fiber reinforced syntactic foams validates this claim [10]. This emphasizes the importance of fibers as reinforcing materials in foams. Hence these foam materials with glass fibers can be used as a better core for sandwich structures in structural applications. Alonso et.al studied the mechanical performance of short fiber reinforced syntactic foams [11]. They used chopped glass and aramid fibers as the fiber reinforcements. Mechanical performance was measured using compression and shear tests. They concluded that the mechanical performance of the fiber reinforced foams was enhanced, and the aramid fiber performed better than the glass fibers. The compressive modulus of the fiber reinforced foams was also found to be higher than that of the fiber free syntactic foams. The compressive properties of chopped fiber reinforced syntactic foams were studied by Karthikeyan et.al [12]. The values increased with the content of fibers, thus emphasizing the influence of both densities and load bearing capacities of fibers on the compressive properties of these systems. Syntactic foams are therefore predicted to perform better with the incorporation of fibers without much of a change in the density for applications such as structural and sub-sea buoyancy aid materials.

The compressive strength and modulus of syntactic foams primarily depend on the relative strength of the microballoons and matrix resin. Also, in the case of foams with low strength microballoons incorporated, the mechanical properties show dependence on microballoon

properties. Gupta et.al [13] studied the compressive properties of syntactic foams having microballoons with four different wall thicknesses and five volume fractions. They found that the compressive modulus and strength varied linearly with the foam density, i.e., the compressive properties increased with microballoon wall thickness and decreased with microballoon volume fraction.

There are primarily two failure mechanisms that dominate in syntactic foams with varying densities. A study on the failure mechanisms of syntactic foams under compression were carried out by Kim et.al [14]. They concluded that longitudinal splitting occurred in the lower density foams and layered crushing occurred in the high density foams. The failure sequence associated with longitudinal splitting was (a) formation of multiple longitudinal cracks along the circumference of the compression specimen, (b) widening of longitudinal cracks and (c) failure at one end of the specimen resulting in further lateral expansion. The failure sequence associated with layered crushing was deduced from a model by which (a) the first failure initiation occurs at a weak microsphere, (b) failure of adjacent microspheres due to stress concentration resulting in propagation of microsphere failure laterally until it reaches the end of specimen wall, and (c) thickening of the crushed layer. Koopman et. al. investigated the micro-structural failure modes in three phase syntactic foams [15]. They conducted both compression and three-point bending tests on the syntactic foams. Microsphere strength had a strong effect on overall uniaxial compressive strength with interface strength playing a secondary, yet significant role. In three-point bending, the role of the interface was much more critical. SEM micrographs revealed primarily interface failure and were characterized as the presence of intact microspheres with clean surfaces, accompanied by corresponding areas of resin with concave spherical sections.

Enhancement of energy absorption by incorporation of rubber as filler and thereby improving the damage tolerance/resistance of syntactic foams has been widely studied in the past. Li and

Nji proposed and synthesized a rubberized syntactic foam to develop better impact properties in the conventional microballoon based syntactic foams [16]. The use of glass microballoons for fabricating syntactic foams is the most common due to their good chemical compatibility with polymers, lower cost, and higher strength. However, owing to the brittleness of the glass microballoons, the impact tolerance of syntactic foams made of glass microballoons is limited. Also there is a lack of mechanisms to contain or arrest the microscopic damage from propagating into macroscopic damage. Together with the brittleness, current syntactic foams cannot absorb sufficient amount of impact energy without significantly compromising structural strength. To take care of this, they proposed rubber coated microballoons dispersed in a nanoparticle and microfiber reinforced polymer resin. They found out that this unique microstructure provided a number of mechanisms for absorbing impact energy in micro-length scale and prevented the micro-scale damage from propagating into macro-length scale damage. A similar study by Nji and Li [17] showed that the incorporation of CaO improved the mechanical properties of the rubberized syntactic foam. CaO helped in removing the water contained in rubber latex by generating an exothermic reaction within the rubber latex/microballoon mixture and eventually reacting with water to form calcium hydroxide. Also the heat generated due to the exothermic reaction helped in evaporating the water, resulting in microballoons coated with calcium hydroxide reinforced rubber layer.

A study on crumb rubber based syntactic foams was conducted by Li and John [18]. The foam had a hybrid microstructure bridging over several length scales. In this study they showed that the presence of crumb rubber helped in reducing the stress concentration centers, thereby improving the impact tolerance and also flexural strength. The initiation energy increased and propagation energy decreased when a portion of the microballoons were replaced with crumb rubber particles. It was found that the rubberized syntactic foam possessed a higher capacity to

dissipate impact energy and to retain bending strength. There was a positive composite action between the hollow glass bead particles and crumb rubber particles by means of stress field interaction and reduction in stress concentration. Azimi et al. [19] investigated the fatigue crack propagation and fracture toughness of a modified syntactic foam containing both glass microballoons and reactive liquid rubber. They contributed the enhanced crack propagation resistance and fracture toughness to a synergistic action between the microballoon and the rubber modified epoxy matrix.

The elastic properties of syntactic foams have been predicted using suitable models as well in the past. Song et.al performed dynamic modeling of the constitutive behavior of syntactic foams [20] using damage mechanics. The effective elastic properties of these syntactic foams were also modeled by different researchers. Bardella et.al [21] studied the elastic behavior of foams based on a micromechanics point of view. Using a concentric spherical model, Marur et.al estimated the effective elastic constants [22] and compared the results with theoretical and experimental values. It was found that the model had good agreement with the experimental results.

Compression studies on syntactic foams with lateral confinement results in high stress levels in the specimen due to densification of the foam. This was studied by Subhash et.al [23], by conducting edgewise quasi-static compression tests and dynamic tests with and without rigid steel confinement. They concluded that when deformed uniaxially without confinement, the foams reach a maximum stress and then exhibit a softening response that eventually results in the fracture of the specimen on random planes. On the other hand, compression tests with the confinement resulted in densification of the foams and thereby resulting in high stress levels being generated in the specimen.

The addition of glass microballoons results in an increase in the glass transition temperature (T_g) of the thermoset resin. A Dynamic Mechanical Analysis (DMA) of syntactic foams was

conducted by Sankaran et.al [24]. From their studies they concluded that the T_g values of the syntactic foams were higher than that of the neat resin. The maximum use temperature could be interpreted based on the T_g values and could be used as a design input. The storage modulus values decreased with increasing temperature, but the reduction was less than the reduction of neat resins. A thermal stability analysis was performed by doing Thermo Gravimetric Analysis (TGA) on syntactic foam samples by Alonso et.al [11]. They concluded that the thermal stability of the fiber reinforced foams was enhanced, and the aramid fiber performed better than the glass fibers.

From the previous work on syntactic foams in the past few years, it is very clear that the damage induced in the foam when subjected to tension, compression or impact is on a macroscopic length scale or in other words results in a brittle failure. Even though several methods to improve the impact tolerance have been devised, such as adding rubber particles to contain this type of damage, there is no effective solution to recover the strength of the foam lost due to low velocity impact events. In other words there are no self healing properties inherent in the syntactic foam to heal a damage caused due to different types of failure. So there is an urgent need to develop self healing smart foams that can sense the damage and actuate the healing process in conventional syntactic foams and at the same time are impact tolerant materials. In another word, there is a strong need to repair internal damage autonomously, repeatedly, efficiently, and at molecular-length scale.

1.2 Syntactic Foam Cored Sandwiches

A sandwich is a special class of structure that is fabricated by attaching thin but stiff skins to a light weight but thick core. Woven glass fabric infused with a polymer is generally used as the skin. Currently, various core materials are available to dissipate impact energy, including foam

core. Among them, syntactic foam – a light weight and closed cell material with polymeric, ceramic, or metallic microballoons dispersed in a polymer matrix, is becoming more and more accepted in impact tolerant sandwich structures. A schematic of a typical sandwich structure showing the skin and core is depicted in Figure 2. Fiber reinforced polymer composite sandwich structures have been used in almost all man-made engineering structures such as space shuttle, aircraft, ship, auto, pressure vessel, piping, bridge, building, platform, etc., primarily due to their high specific strength and stiffness, tailor-ability, corrosion resistance, and functionally graded construction.

Figure 2. Schematic of a Sandwich structure

Impact has been a critical problem for engineering structures. Failure of engineering structures due to impact has been well documented [25-34]. Therefore, sandwich structures must be designed to have a certain impact tolerance or impact resistance. The top and bottom skins of the sandwich structure serve the function of carrying the bending loads and thereby protecting the syntactic foam core from catastrophic failure. One of the main functions of the core is to absorb impact energy during low velocity and high velocity impact events. It also serves as a means of shielding radiation and insulating heat transfer. More or less the core plays an important and vital role as part of the sandwich structure.

Composite sandwich panels can absorb more energy than laminates and at the same time undergo less deflection to absorb the same maximum energy as the laminates. A comparative study on the impact resistance of composite laminates and sandwich panels was conducted by

Ferri et.al. [35]. They showed that the overall response of the sandwich panel depends on the properties of the face sheets (skins) and the foam core. Also, they found that impact energies above a statically determined threshold level resulted in extensive foam core damage. Transverse load induced impact damage has been a critical problem for composite sandwich structures. This type of impact events can result in reduction of the residual strength of the sandwich panel. An enormous amount of work has been done towards this direction to improve the residual load bearing capacity of sandwich structures subjected to low velocity impact events.

Sandwich structures have been widely used in load bearing structures due to their high specific stiffness and high specific strength. Some sandwich structures, such as those used in high speed transportation applications, are required to have high impact energy absorption characteristics. Vaidya et.al studied the impact damage of partially foam filled co-injected honeycomb core sandwich composites [36]. They performed both low velocity and high velocity impact studies on two different foam filled sandwich structures. They concluded that the foam filling not only provided support to the cells, they also helped in improving the impact tolerance. Another noticeable fact was that the resistance to penetration, energy absorption and damage modes were a function of core stiffness, extent of filling the foam and number of face sheet plies. Low velocity impact tests were conducted on syntactic foam cored sandwich structures by Hazizan et.al [37]. They concluded that the dynamic response of the sandwich structures mainly depends on the elastic properties of the foam material. Three prominent modes of failure were detected. Shear cracking in the brittle core, fiber buckling close to the point of impact and finally delamination of the skin resulting in complete failure of the sandwich. The static and impact failure modes of foam cored sandwich beams were investigated by Lim et.al [38]. The impact energy absorption was related to the failure mode strongly and also they suggested that for enhancement of the impact properties, the failure should occur at the face.

Failure in syntactic foam cored sandwich structures under bending loads is governed by the tensile properties of the core and not on the radius ratio of the microballoons [39]. This study concluded that the core shear stress and skin bending stress decreases with decrease in radius ratio. Radius ratio is defined as the ratio of the inner radius to the outer radius of the glass microballoons. A mechanical and numerical characterization of a syntactic foam/glass fiber composite sandwich intended for naval applications was conducted by Corigliano et.al [40]. They concluded that the sandwich core helped in improving the stiffness and strength quite remarkably. Also a weakness at the skin/core interface could result in delamination of the skin materials. Rocca et.al conducted static and dynamic fatigue tests on a sandwich structure comprised of glass fiber reinforced polymer skins and a fiber reinforced foam core [41]. They noticed no considerable change in the residual compressive strength and failure modes.

Various types of core materials have been used in fabricating sandwich panels. Among them the foam core which can be sub-divided into syntactic foam, polymeric foam, metallic foam, ceramic foam, balsa wood etc. has enjoyed enormous attention in the past few decades [42-44]. Web cores like truss and honey comb [45-48] have also gained much attention as core materials in sandwich structures due to their superior mechanical properties. Hybrid foam cores are another category of core materials that can be used in structural applications. These hybrid foam cores include 3-D integrated core [49,50], foam filled web core [21,36,51], laminated composite reinforced foam core [52,53], grid stiffened syntactic foam core [54,55], etc. Among the different core materials available, the hybrid foam cores predominate. Some of the drawbacks of the other core materials are as follows. For example, the foam cores are brittle which results in macro-length scale damage, sacrificing the residual strength; the web cores on the other hand, possess lack of proper bonding with the skin and also consist of impact windows; and 3-D

integrated core results in pile buckling. This leaves the grid stiffened syntactic foam as the ideal candidate for energy absorption and hence resulting in good impact tolerance.

1.3 Grid Stiffened Syntactic Foam Cored Sandwiches

Some of the limitations of the present foam cores such as brittle behavior, macroscopic length scale damages etc. were listed in the previous section. Li and Muthyala [54] and Li and Chakka [55] conducted manufacturing, testing, and modeling of a new composite sandwich structure with a hybrid grid stiffened core. The hybrid core consists of a continuous fiber reinforced polymer orthogrid skeleton [54] or isogrid skeleton [55] that is filled with light weight syntactic foam in the bays or cells. Low velocity impact tests and compression after impact (CAI) tests were conducted to evaluate the impact response and residual strength of the sandwich structure. C-scan and SEM observation were implemented to investigate the impact damage. A finite element analysis using ANSYS was conducted to validate the compression test results. It is found that these integrated cores enhance impact energy transfer, energy absorption, and positive composite action, ensure quasi-static response to impact, and have higher CAI strength. They concluded that implementing the use of a grid stiffened core in the sandwich structure helped in containing the damage within one cell or several neighboring cells due to the boundary controlled impact response. On the other hand one of the major limitations of these sandwich structures, similar to other sandwich structures, is that the core is brittle and also due to the generation of micro/macro cracks and the lack of self-healing mechanisms, the post impact residual load bearing capacity is still low [54,55].

1.4 Limitations of Syntactic Foams and Foam Cored Sandwiches

While syntactic foam and foam cored sandwich have been widely studied and used in practice, they have certain limitations. Due to the brittle nature of the thermoset polymer matrix

used for fabricating the foam material, the energy absorption during an impact event is at macro-length scale. In other words, energy absorption is facilitated by macro-length scale damages. These type of macro-length scale damages will lead to a very low residual structural capacity in the impact damaged sandwich structures. This calls for immediate maintenance or repair of the structure. Unfortunately it is extremely difficult to repair this type of damage induced in the sandwich structure due to impact. Because of the difficulty in repairing internal damage, it usually leads to the replacement or rebuilding of the entire structure. Therefore there is a genuine need to develop impact tolerant and self-healing syntactic foams that will actuate a healing process when triggered by an internal stimulus.

1.5 Self Healing Methods in Thermoset Polymer Systems

The current way of repairing impact damage is through external structural repair such as welding or patching [56]. They are costly, time consuming, and require reliable detection techniques and a skilled work force. They are mainly applicable to the repair of external and accessible damages instead of internal and invisible microcracks. Thus, there is a strong need to repair internal damage autonomously, repeatedly, efficiently, and at molecular-length scale.

Self healing process is very evident in thermoplastics. They can achieve molecular level healing by just heating the thermoplastic above its melting temperature and allowing them to flow into the damaged region. Upon cooling, they become rigid and thus heal the damage. But due to their low stiffness and thermal instability they are not widely used in structural applications. So this research work is primarily focused on thermoset resin systems. Chemical crosslinks provide appropriate anchorage which in turn results in the superior strength, stiffness and thermal stability for the thermoset polymer systems. The fracture of one polymer chain results in the transfer of the damage force to the adjacent chains through the crosslinks and

eventually results in crazing, cracking and ultimate fracture at a small strain. Thus it is very clear that the fracture in thermoset polymer systems is brittle in nature. So, developing thermoset self healing polymer systems are very challenging as opposed to their thermoplastic counterpart.

Enormous interest has been generated in the recent years in the area of self-healing internal damage in thermoset polymer and its composites [57]. In an effort to develop a self sustained repair procedure for a sandwich structure that has lost its structural capacity due to damage, several self healing schemes have been devised. Scientists and researchers started thinking of implementing self healing schemes similar to the biological systems in humans as well. The ability to heal wounds is one of the truly remarkable properties of biological systems. A big challenge facing the materials science community is to design 'smart' synthetic systems that can mimic this behavior by not only 'sensing' the presence of a 'wound' or defect, but also actively re-establishing the continuity and integrity of the damaged area. Such 'self-healing' materials would significantly extend the lifetime and utility of a vast array of manufactured structures. Researchers have worked on the feasibility of adding hollow fibers having healing agents, microencapsulated spheres, thermoplastic additives etc. to help in the process of self healing.

1.5.1 Hollow Fiber Approach

The pioneering research of using hollow fibers to hold healing agents to be released for damage repair was done by Dry and Sottos [58-60]. This concept was initially developed in the field of cementitious materials to alter the cement matrix permeability, prevent corrosion, repair cracks etc. This was further extended to polymeric materials. In this approach, healing was achieved when a propagating crack encounters one of the dispersed hollow glass fiber, the fiber bursts/fractures and the encased fluid flows into the cracked region and cure *in-situ*. In the initial studies on hollow glass fibers with healing agents, the researchers had problems of void formation in the entire system. A major reason for this behavior was attributed to the larger size

of the fibers holding the healing agent when compared with the reinforcing fibers. This might have resulted in stress concentration centers which in turn resulted in failure within the composite structure [61]. Bleay et.al [62] used smaller glass fibers to hold the healing agents to account for the problems faced by the previous researchers. But the filling and release of the healing chemicals proved to be more problematic. Pang et.al [63] continued the work on synthesis of self healing composites based on hollow fiber concept. The idea was to tailor the self healing systems according to the specific application by varying the healing chemicals.

Some of the drawbacks of the hollow fiber approach were the difficulty in filling the hollow fibers, the proper release of the healing agents at the right time and also the inability of the system for repeated healing. Even though some work has been done to address this issue [64, 65], these systems still possess drawbacks like excess discharge of healing agent from the micro-hollow fibers. Another important issue was the sealing effectiveness after damage. There is also a need to develop rehealing systems which provide high strength and reactivity only when required.

1.5.2 Microencapsulation Approach

Microencapsulation is the most studied self-healing concept in recent years. This particular approach involves incorporation of a microencapsulated healing agent and a catalyst within a polymer matrix [66-68]. When a crack is induced in a polymer system, the microcapsules are damaged by the propagating crack and release the healing agent into the cracks by capillary action. Further, the healing agent and catalyst react to heal the crack and prevent subsequent crack propagation. This approach alleviates the manufacturing problems caused by using the hollow fiber approach. Another variation of this approach was coined by Skipor et.al [69]. In this approach, they proposed attaching catalyst molecules to the exterior of microcapsules filled with the healing agent. They claimed to have improved the healing efficiency.

But this method also possesses similar limitations to the hollow fiber approach. Some of the limitations include limited availability of the healing agent at the damaged site, limited environmental stability of healing agents, immobility of healing agents at low temperatures, shelf life of the healing agents, and inability to heal damage more than once.

1.5.3 Thermoplastic Additives

The inclusion of thermoplastic additives as healing agents in a thermoset resin system was first reported by Zako and Takano [70] in 1999. Upon heating, the particles melted, flowed into internal cracks or flaws and healed them when cooled down. The feasibility of this system was studied by many researchers and the different factors affecting the healing efficiency can be listed as follows:

(a) Compatibility of the two polymers, the thermoplastic polymer should be miscible with the thermoset polymer system and at the same time should not react with it at ambient temperature.

(b) The T_g of both the thermoplastic and the thermoset should be close so that the thermoplastic melts above ambient temperature and at the same time not so high to cause thermal degradation of the thermoset.

(c) Low molecular weight polymer diffuses faster resulting in quicker healing, while high molecular weight polymer possess better mechanical properties. A balance should be attained between these two essential characteristics.

(d) Healing process is diffusion in nature. So the healing temperature is expected to affect the healing rate and efficiency.

This self healing scheme possesses the advantages of autonomous and repeatable healing. The feasibility of this system depends highly on the four factors mentioned above. The mechanism behind this method is based on the melting of the thermoplastic particles and their eventual flow

into the cracks through diffusion when heating; the molten thermoplastics bond the two sides of the cracks and establish continuity at molecular level when cooled below T_g. In another word, the thermoplastic serves as an adhesive at micro-length scale. While this method can heal damage autonomously, repeatedly, and at molecular level, there are two limitations: (1) its healing efficiency is still low. This is because the thermoplastic within the crack behaves like the bulk due to the relatively wide opening of the crack. Multiple impact-healing cycles were used to test composites containing 7–10% polybisphenol-A-co-epichlorohydrin in an epoxy matrix. These samples were assessed visually, and only 30–50% healing efficiency was reported [71]; (2) the amount of thermoplastic additive is high (typically over 10%), again due to the relatively wide opening of the crack, which may adversely affect the stiffness and thermal stability of the thermoset matrix.

1.5.4 Thermally Reversible Cross-linked Polymers

This class of polymers makes use of the thermo-reversible covalent bonds to self-heal internal cracks in the polymer system. The mechanical properties of these systems are comparable to the conventional systems used in fiber reinforced composites. Thus they can be used as the matrix materials for structural applications as well. A thermally reversible cycle such as Diels-Alder (DA) reaction for self healing applications was pioneered by Chen et.al [72]. They described a remendable system which could heal cracks multiple times. This system had advantages over the popular microencapsulation technique because it eliminates the need for catalysts, healing agents etc.

The first generation of a highly cross-linked and transparent polymer was synthesized via the DA cycloaddition of furan and maleimide moieties, and the thermal reversibility of the chemical bonds is accomplished via the retro-DA reaction [73]. Solid state reversibility of the cross-linking structure via DA and retro-DA reactions was tested and confirmed by subjecting the

polymerized films to different heating and quenching cycles, and analyzing the corresponding chemical structure by solid state 13C NMR.

Liu et al [74,75] further investigated the applicability of self-healing polymers using DA reactions in advanced composite production. They employed epoxy precursors to prepare multifunctional furan and maleimide monomers. These monomers possess the desirable characteristics of the traditional epoxy resins such as solvent and chemical resistance, low melting point, and solubility in a number of organic solvents. These characteristics enable them to be processed in a similar fashion to the epoxy resins.

The use of thermally reversible covalent bonds to heal the cracks eliminates the need to incorporate self healing agents, catalysts etc in the polymer system. Another important advantage is the repeatability of the healing process. Depending on the extent of the damage area which in turn is related to the fracture of specific covalent bonds, this healing process can be repeated multiple times. Thus these types of polymer systems with thermally reversible covalent bonds are autonomous as well as capable of healing cracks multiple times. However, this scheme is a very lengthy process. First decoupling of the covalent bond is required so that the component can flow into the damaged space; after that, the system is cooled down to re-develop the covalent bond so that the material can be healed. The re-establishment of covalent bond at room temperature usually takes several days. A more time-efficient healing scheme is thus needed.

A concluding remark on self healing mechanisms in thermoset resin systems can be made as follows. Most of the preliminary work done in the field of self healing resin systems has tried to mimic the biological method of healing in human beings. In humans, healing is based on the development of new cells/tissue after initially forming patch surfaces to protect the damaged tissue lying beneath. Natural healing is also a lengthy process depending on the extent of the wound. Replication of the simplest biological self healing system in polymer systems, and

thereby making the thermoset polymer based syntactic foam sandwich structures behave in a smart way to damage is a long route towards realization. Therefore, there is an urgent need to develop such polymer systems that can self heal on demand and also be compatible with most of the additives to make them more functionally useful or active.

1.6 Shape Memory Polymers (SMP)

Chang and Read revolutionized the field of active materials research by the discovery of shape memory effect in 1932 [76]. Shape memory effect is the ability of a material to fix a temporary shape in response to an elastic deformation and recover the original shape after application of external stimuli like temperature, light, magnetic field etc. This property is not an inherent material property, but it is a result of material structure and specific functionalization techniques. Shape Memory Alloys (SMAs) have received considerable attention as stimuli responsive materials due to their small size and high strength. On the other hand, they possess obvious disadvantages like high manufacturing costs, limited recoverable deformation and appreciable toxicity. However, in the past decade, Shape Memory Polymers (SMPs) have gained more importance over SMAs due to their superior properties like high recoverable strains of up to 300% when compared with only 5-14% of recoverable strains in SMAs, low density, low cost etc. Also, SMPs can be tailored according to a specific application by changing the recovery temperature with changes in chemical formulations. The activation temperature can be changed by changing the co-polymer composition or degree of cross-linking. These properties have helped SMPs in becoming functionally attractive in many fields these days and are mode widely used when compared with the SMAs for structural, aerospace and defense applications.

Shape memory polymers were first introduced by Nippon Zeon Co. in Japan. The first SMP was polynorborene based having a T_g range of 35^0C to 40^0C [77]. SMPs are a class of polymers

that can undergo deformation at high temperatures, retain the deformed shape when cooled and return to its original shape upon heating above the T_g. Shape memory polymers possess two phases, which are clearly separated by the glass transition temperature. Above the glass transition temperature they are soft and rubbery, thus making it easily deformable. While below the glass transition temperature they are rigid and cannot be easily deformed [78]. SMPs are regular polymer resin systems that exhibit shape memory effect (SME). The consequences caused by an intended or accidental damage can be ironed by heating the SMP above a defined transition temperature. This is mainly possible due to the flexibility of the polymeric chains in the structure. Shape memory property is not related to a specific property of a single polymer; but it is a combination of polymer structure and morphology together with applied processing and programming technologies. The potential applications of these SMPs range from consumer goods to medical supplies. Shape memory polymers find applications in biodegradable sutures, repairable automobile skins, satellites and other space vehicles as well. Although some SMPs have applications in the engineering industry, they are far from technological potential of the SMP. This is mainly due to the weakness in mechanical strength and stiffness when compared to metals and ceramics [79-81]. Fiber reinforcements could improve the strength and modulus while retaining considerable large recoverability properties. Discontinuous fiber reinforcements showed strain recoverability in all directions, while continuous fiber reinforcements showed recoverability only in the transverse direction [82].With the use of the proper reinforcement these SMPs could be used as an active structural material for vibration and acoustic control, damage control and shape control capabilities.

The shape memory effect of the thermoset polymers can be explained based on two perspectives: the first one would be from a thermodynamic point of view and the second one from a molecular perspective. Polymers can be classified broadly into crystalline and amorphous

polymers. This study deals with amorphous polymer systems. Amorphous polymers are those polymers in which the polymer chains are not in an orderly fashion. In other words, they take a completely random distribution in space. If W expresses the probability of a conformation, a strongly coiled conformation (state of maximum entropy) represents the most probable state for an amorphous linear polymer chain according to the Boltzmann equation [83]:

$$S = k \log W \quad (1)$$

Here, S is the entropy of the system and k is the Boltzmann's constant. The driving force for shape recovery is the conformational entropy of the molecular segments in terms of micro-Brownian thermal motion. Thermodynamically, the molecular segments experience a change from a temporary and ordered configuration to its random and coiled configuration during the shape recovery process. Since this process is accompanied by an increase in entropy, it is an autonomous process. It is the recovery in strain and in stress that makes SMP a viable choice as sensors and actuators. In order to make the polymer smart, it is usually subjected to a typical three-step thermomechanical cycle called programming; see Figure 3 for a 1-D tensile stress (σ), tensile strain (ε), and temperature (T) relationship during the programming cycle. The programming starts at a temperature above the glass transition temperature (T_g) of the SMP. It involves a high-strain deformation in the rubbery state, which is called ''pre-deformation'' or ''pre-strain". Step 2 is a ''strain storage'' process by maintaining the pre-strain constant while cooling down to below T_g. Because of the thermal contraction of the SMP during cooling, the tensile stress needed to maintain the pre-deformed shape increases as the temperature drops. The third step is a ''low temperature unloading'' process, which is defined as the removal of the stress in the glassy state. The low temperature unloading process may be accompanied by ''spring back", i.e., some pre-strain may be rebounded. This completes the three-step programming.

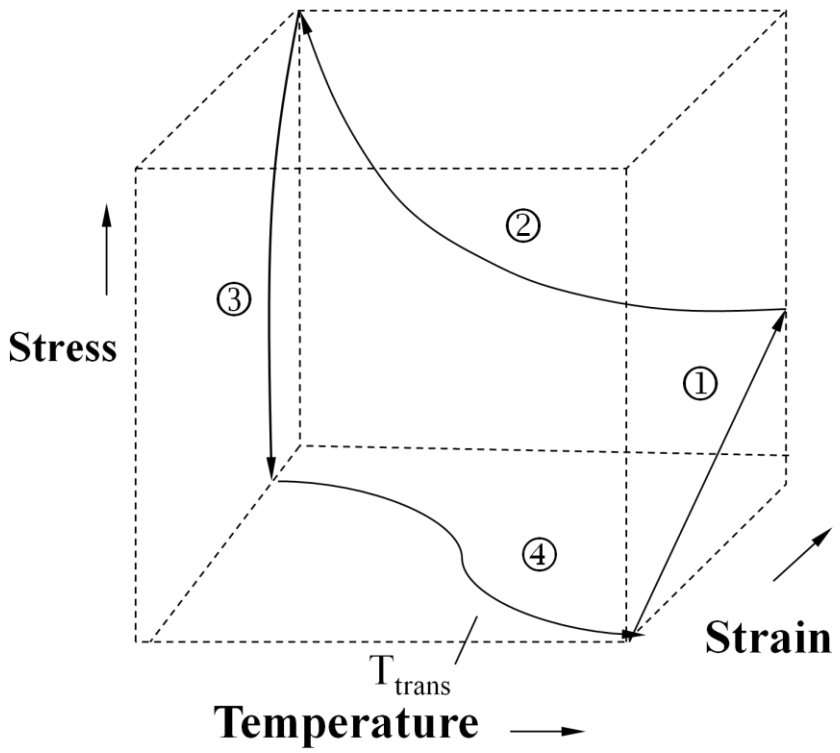

Figure 3. Schematic of four-step strain controlled programming

In step 4, which involves reheating to its starting temperature (above T_g) without applying any constraint, sometimes called ‘‘free strain recovery’’ or ‘‘unconstrained recovery’’, brings the pre-strain back to zero (if the recovery rate is 100%). This completes the typical four-step thermomechanical cycle.

This strain-controlled programming and free-shape recovery are schematically shown in Figure 4 for a polymer with glass transition temperature (T_g) as its transition temperature (T_{trans}) and the molecular mechanisms involved are schematically shown in Figure 5.

The efficiency of a shape-memory polymer is empirically controlled by its composition, as defined by the polymer’s chemical structure, molecular weight, degree of cross-linking, and fraction of amorphous and crystalline domains [76,83]. The energy that is restored with shape recovery is a growing function of the energy supplied during the deformation at a high

temperature [84,85]. A critical science and technological implication of SMP is that one can utilize its shape memory functionality for self-sealing purposes.

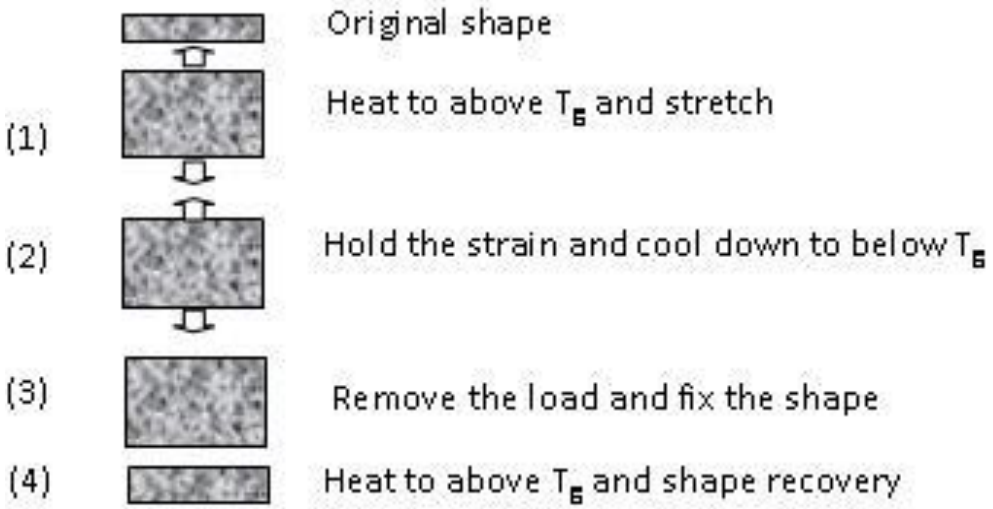

Figure 4. Experimental Procedure of Programming

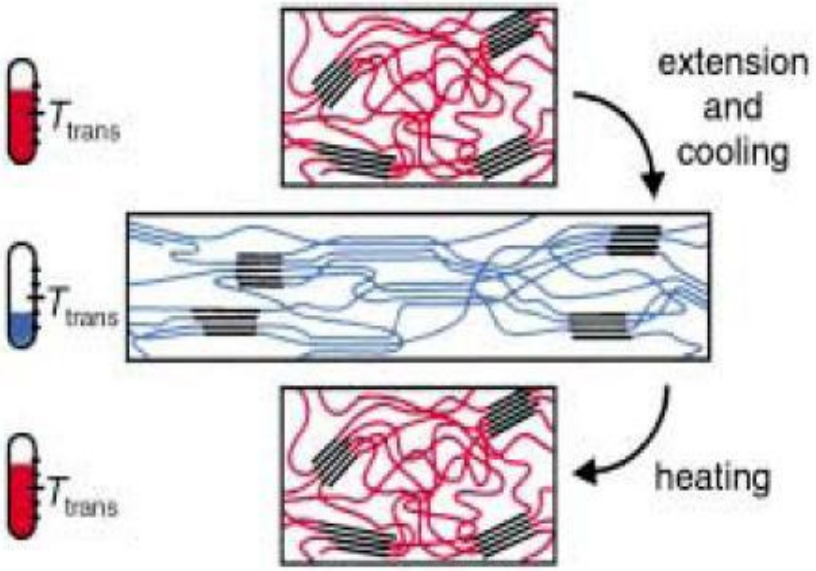

Figure 5. Molecular mechanism of the thermally induced shape-memory effect for a multiblock copolymer [83]

SMPs can be perceived as possessing two phases: (1) a frozen (hard segment) phase and (2) a reversible switching (soft segment) phase. The hard segment is responsible for the permanent/original shape of the SMP by providing permanent cross-links and the soft segment is responsible for the shape recovery or in other words strain recovery. The soft segments deform upon application of a prestrain above a transition temperature, either the glass transition temperature (T_g) or the melting temperature (T_m) [86]. A high value of the ratio of elastic modulus is essential to fix the deformed shape easily and recover the original shape rapidly. The modulus is dependent on the hard segment content and this in turn is related to the extent of crosslinks. If the hard segment content is below a critical value (30%-60%) it will not show proper shape recovery characteristics. On the other hand, if it is above the critical value then it can result in brittle behavior of the system.

As mentioned earlier in section 1.5, the current self-healing schemes have their own limitations in achieving self-healing. One major aspect is the inability to heal the damage multiple times. Another important drawback is that these systems are not autonomous. So there exists an urgent need to develop a self-healing scheme that is autonomous and at the same time can heal damages multiple times. The use of SMPs will help in nullifying the drawbacks in the present self-healing schemes. The only human intervention for these SMP systems is to provide the required external stimuli to achieve shape recovery. Since the shape recovery mechanism depends on the conformational entropy restoration, the system can be considered to be autonomous. The ability to heal damages multiple times depends on the amount of energy supplied during the initial impact or deformation event. In other words, depending on the amount of energy stored in the system due to the deformation (shape fixity), the extent of shape recovery of the material can be achieved. The energy supplied during the shape fixing process can be used to recover the damage fully. Another possibility is that the amount of energy supplied during the

fixity process be utilized for healing multiple damages, i.e., one shape fixity process correspond to several shape recoveries. Research in this direction is very scarce and is still evolving. Some studies have dealt with SMP based foams and studied the thermomechanical behavior of these foams. But they were open cell foams which lack the required strength and stiffness as compared to the closed cell syntactic foams. Details of these foams are discussed in the next section.

1.7 Shape Memory Polymer Based Foams

In order to identify the most appropriate SMP candidate to be used as a thermoset polymer matrix in a syntactic foam based sandwich structure, it should essentially meet the following self healing criteria. (1) healing of damaged region in an almost autonomous fashion, with almost no human intervention, (2) capability to heal the damage multiple times or in other words repeatability of healing is quite essential, (3) the chemical crosslinks/ covalent bonds provide the necessary strength and stiffness for these polymer systems and they break as a result of damage. The restoration of these bonds at a molecular level is also a very desirable criterion in order to restore the strength in the sandwich structures and (4) high healing efficiency of the structure is an aftermath of re-establishment of chemical bonds. The ideal and smart foam should satisfy these four criteria simultaneously.

Shape Memory Polymer (SMP) based foams were developed by many researchers in an effort to make the foam core smart. Tobushi et.al studied the influence of shape holding conditions on the shape recovery of polyurethane based shape memory polymer foams [87]. Thermomechanical analysis of these foams suggested that if it was compressed above its glass transition temperature (T_g) and then cooled below its T_g, then it will maintain the deformed shape. If the deformed SMP foam is held above its T_g, secondary shape forming occurs, or in other words it returns to its original shape. In a similar study by the same author [88], they

concluded that the deformation resistance of the SMP foam is large at low temperatures and high strain rates. At temperatures above the T_g, the strain is recovered by unloading.

Huang et.al conducted compression, free recovery, constrained cooling and gripping tests on SMP foams [89]. In contrast to the work by Tobushi et.al, they found that the compressive force did not diminish upon cooling to room temperature. The effect of long term storage on the properties of compressed elastic memory polyurethane foam was investigated by Tey et.al [90]. The SMP foams were pre-strained at temperatures above the T_g, and then cooled back to room temperature for hibernation. But in a span of two days they returned to their original shape. This was due to the fact that the T_g of the shape memory polymer was very close to the room temperature. They concluded that the foam retained its shape memory properties even after storing it in a compacted state for a long period.

These foams are not syntactic foams. In other words, they are open cell foams. Open cell foams are manufactured by using foaming agents or blowing agents in the foaming process. Air bubbles are trapped during this process and they are considered as a different phase in the system. Syntactic foams are manufactured by incorporating glass microspheres which gives it a closed cell structure. These syntactic foams are closed cell foams which possess some distinct advantages over open cell foams. The specific compressive strength of these closed cell syntactic foams is much higher than its open cell counterpart. They also absorb less moisture than the open cell structured foams. So there is an urgent need to design, fabricate and characterize closed cell syntactic foams based on shape memory polymers and use them in sandwich structures for structural applications. The use of an SMP as the matrix material for the foam core and in turn use the core in a sandwich will help in self-healing the sandwich multiple times due to the driving force by conformational entropy.

In this study, the shape recovery functionality of the SMP was used for the purpose of self-healing damages. Shape memory polymer based syntactic foams were fabricated and characterized, and their structural applications were evaluated. In an effort to make these sandwich structures smart, an SMP based syntactic foam was used as the core material in a sandwich structure. Low velocity impact properties and residual compressive strength of the smart sandwich structure was evaluated. The shape memory functionality was utilized for self healing of the damage due to multiple impacts at the same location. Another set of similar tests were also conducted on a grid stiffened sandwich structure with the smart foam filled within the bay areas of the grid structure. As discussed in section 1.1, the hybrid foam core proved to outperform all other types of foam cores. More specifically the grid stiffened hybrid core is preferred, due to the positive composite action between the ribs and the foam core. This grid stiffened structure is envisaged to contain the impact damage within the boundary or in other words, it results in a quasi-static behavior within the bay area and also heals the damage multiple times. The foam in the bay area is confined from the sides by the glass fiber ribs (2-D) and from the top and bottom by the glass fabric sheet resulting in a 3-D confinement. Thus during the recovery process (by heating above the T_g of the SMP), the foam will try to regain its original shape or in other words there will be an increment in the volume. But since the entire bay is constrained in all directions it will be forced to fill the microcrack generated due to impact, leading to self-sealing. Further, if the recovery stress is high enough, the cracked surfaces may be pushed so close that some physical entanglement of the broken polymer chains or Van De Waals force may be possible, leading to healing at molecular level. The only human intervention during shape recovery process is to provide external stimuli such as heat, light, magnetic field, etc. [91-99]. Out of the different external stimuli, light and magnetism are non-contact types and require no human intervention for activation. Since self healing is driven by conformational entropy, it is

autonomous. Also, the rate of recovery can be fully controlled by the programming used and the constraint applied. Therefore, this is an almost autonomous and controlled self-healing process. Unlike the currently available self-healing schemes, which are based on *in-situ* polymerization and need new and fresh supply of monomer and catalyst for self-healing new damage, SMP can repeat its shape recovery or self-healing process many times.

CHAPTER 2. SHAPE MEMORY POLYMER BASED SMART SYNTACTIC FOAM*

As discussed in Chapter 1, the current self healing schemes employed to make thermoset polymer systems smart (sensing the damage and actuating a healing process) faces considerable challenges which are still not resolved completely. Some of the conventional healing systems lack repeatability of healing and also in turn have lower healing efficiency. Even though some of them like the thermo-reversible covalent bond polymer systems take care of the multiple healing issues and molecular level healing, they turn out to be deficient when it comes to the time involved in achieving the required healing efficiency. So there is an urgent need to design polymer systems that meets the four criteria of healing, (1) autonomously, (2) repeatedly, (3) efficiently and (4) at molecular length-scale. In this chapter, an SMP based syntactic foam with carbon nanotubes was fabricated and characterized. A syntactic foam without carbon nanotube incorporation was also prepared.

This chapter mainly deals with the fabrication and characterization of the smart foam (SMP based syntactic foam) and is subdivided into the following sections: (1) SMP formulation, which gives the technical details involved in formulating the particular SMP used in this study. This section also details the curing cycle that could be used to formulate the SMP and also the polymerization process involved which results in the final shape memory polymer system. (2) Materials and fabrication section which gives details about the raw materials used in fabricating the SMP based smart syntactic foam and also the fabrication route adopted to cure the smart foam. (3) Smart foam characterization section which involves transmission electron microscopy studies to check if the dispersion of carbon nanotubes in the SMP was uniform, differential

scanning calorimetry to determine the T_g of the smart foam, thermal conductivity studies to see if the addition of nanotubes improved the heat conduction and uniaxial compression tests to determine the compressive behavior of the smart foam.

2.1 SMP Formulation

The shape memory polymer used in this study can be formulated by following a particular chemical reaction process. Depending on the manufacturing conditions and amount of each constituent, the T_g can be varied significantly. The shape memory polymer formulation is based on a reaction product of (a) styrene, (b) a vinyl compound other than styrene, (c) a cross-linking agent and (d) an initiator. Sometimes a fifth component called a modifying polymer may also be added to improve the toughness of the final SMP. By varying the composition of each component, the T_g of the SMP can be tailored to the required application. The cross-linking agent should be having a polymerizable functionality of at least 2, meaning it should help in the cross-linking process of both the 1^{st} monomer and 2^{nd} monomer. This system with 2 different monomers is called a copolymer.

2.1.1 Suggested Components and Curing Cycle

The components listed below are mixed in the following order (a-d) and then refrigerated before use [100].

(a) Styrene – 90% (1^{st} monomer, styrene)

(b) Vinyl neodecanoate - 7% (2^{nd} monomer, vinyl compound)

(c) Divinyl benzene -1% (Cross-linking agent)

(d) Benzoyl peroxide – 2% (Initiator)

The mixture is polymerized preferably at a temperature range between 65^oC-75^oC and a pressure of 14.7 psi for a duration in the range of 4 hours to 1.25 days. Then the solution is

injected into a mold for curing at 75°C for 24 hours. After curing, the SMP sheet sample is demolded. A clear sheet of the SMP is thus obtained [100].

2.1.2 Polymerization Process

Part A of the Veriflex (CRG Industries, Ohio) shape memory polymer system consists of three monomers namely styrene, vinyl neodecanoate and Divinyl benzene (cross-linking agent). Divinyl benzene helps in the cross-linking process of the other two monomers as shown in Figure 6.

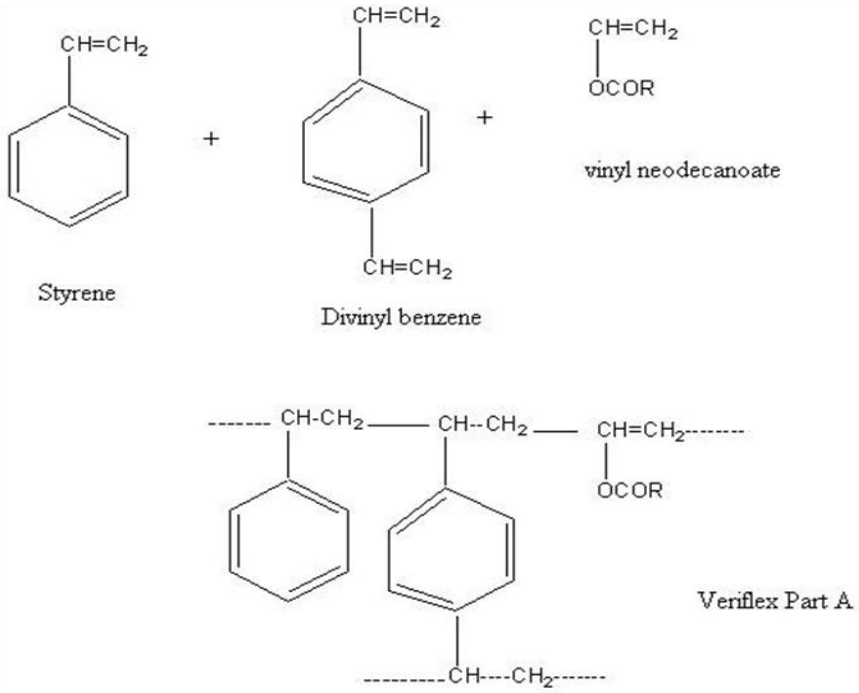

where R= C_9H_{19}

Figure 6. Cross-linking process during the polymerization of the polystyrene SMP

When the initiator, Benzoyl peroxide (Part B of Veriflex) is added to Part A, a free radical initiation process starts which is shown in Figure 7. Because the polymerization process is proprietary, it is assumed that the process consists of three steps, (1) the first step involves free radical generation from Benzoyl peroxide. (2) The free radical thus formed attacks one of the

monomers in Part A which is called chain initiation process (step 2). This secondary radical further attacks either of the remaining two polymers to form the final shape memory polymer. The process is called chain propagation (step 3).

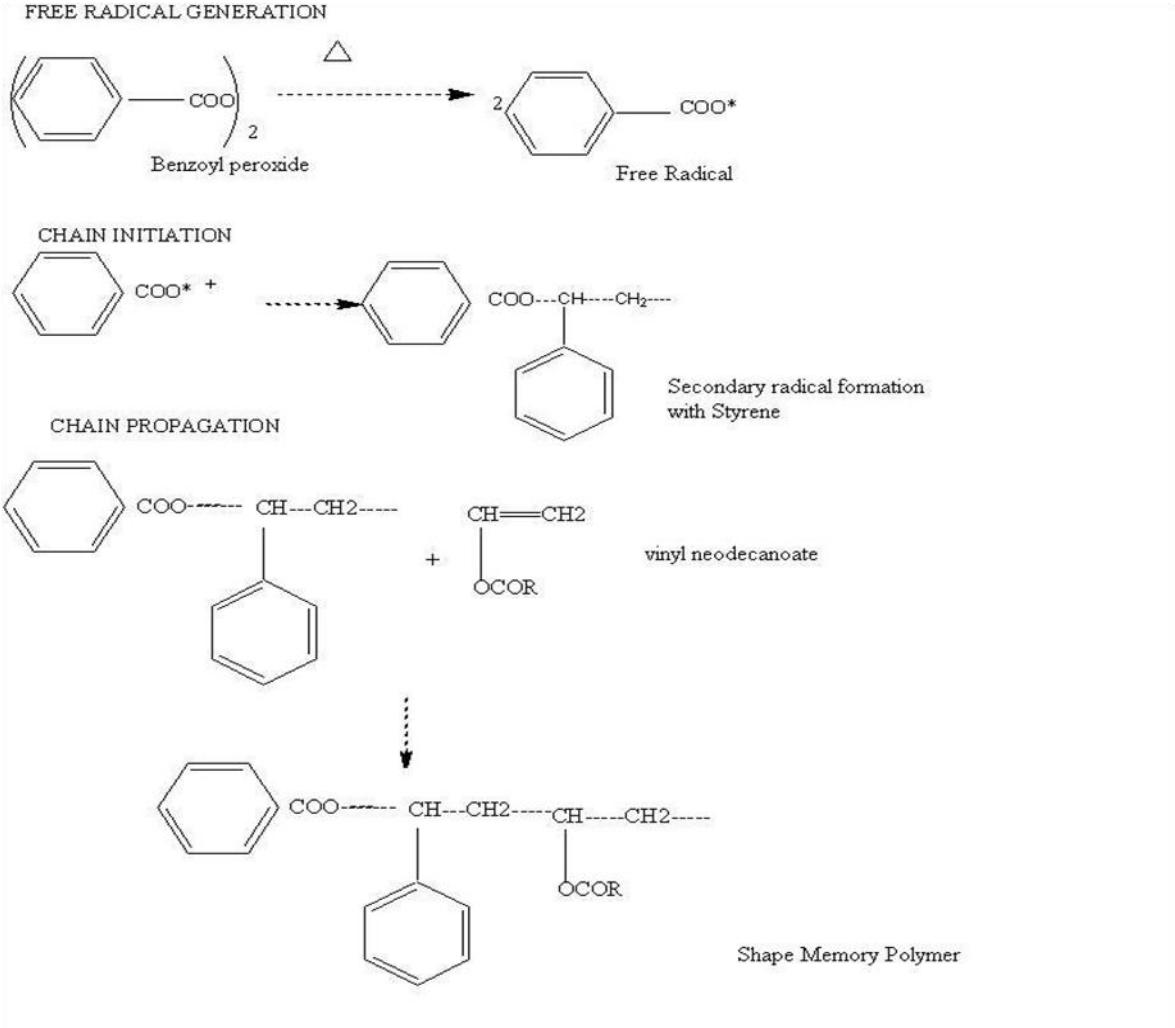

Figure 7. Free Radical Initiation and Polymerization Process

2.2 Materials

The syntactic foam was fabricated by dispersing glass microballoons and multi-walled carbon nanotubes into the shape memory polymer matrix. The shape memory polymer (Veriflex, CRG industries) has a T_g of 62 ^oC (143^oF), tensile strength of 23MPa and modulus of elasticity of 1.24

GPa at room temperature. The foam was fabricated by dispersing 40% by volume of glass microballoons (Potters Industries Q-cel 6014: bulk density of 0.08g/cm^3, effective density of 0.14g/cm^3, particle diameter range of 5 - 200μm, average diameter of 85μm, and crushing strength of 1.72MPa), and 0.15% by volume of multi-walled carbon nanotubes (Cheap Tubes Inc.: density of 2.1g/cm^3, diameter of 20-30nm, and length of 10-20μm) into the polymer matrix. Carbon nanotubes were used for a couple of reasons. The addition of carbon nanotubes can result in enhancement of the strength, stiffness and recovery rate of the SMP after damage is induced in the SMP. This is very critical when the working temperature is above the glass transition temperature. Another reason for using nanotubes is that they have a potential to serve as a medium for heating and triggering phase change if its content is higher than the percolation threshold, such as by electricity. Percolation threshold can be defined as that volume fraction of carbon nanotubes in the polymer system at which the conductivity of the carbon nanotube composite shoots up drastically.

2.3 Smart Syntactic Foam Fabrication

The primary task in the fabrication of shape memory nano-foams is the dispersion of the Multi-Walled Carbon Nanotubes (MWCNT) in the SMP matrix. Poor dispersion will result in agglomerates thereby leading to poor interfacial shear strength due to inefficient load transfer from the matrix to the MWCNT. Also normal mixing methods like mechanical mixing can lead to large agglomerates. These agglomerates can act as voids leading to an earlier failure of the specimen. Proper dispersion is also required for obtaining improved thermal and electrical conductivity. It has been found from previous work by many researchers that the addition of MWCNT to polymers helps in enhancing their mechanical properties and at the same time making the pristine insulating polymer matrix a conducting medium.

The smart foam fabrication process involved primarily two steps. The first step involved dispersion of carbon nanotubes in the SMP matrix. In the second step, the glass microballoons were added to the SMP-nanotube mixture along with the hardener and were eventually poured into a steel mold, covered from all sides and transferred into an industrial oven for final curing. A review paper by Coleman et.al. indicates Young's modulus enhancement in different polymer systems due to reinforcement with carbon nanotubes [101]. That work showed that an incorporation of very low volume fractions of nanotubes can result in mechanical and thermal property improvements. So in this study low volume fractions of carbon nanotubes (0.5%, 1% and 2% by volume) were dispersed in the SMP foam and kept for curing. But due to the very sensitive nature of the SMP, the polymer did not cure at these loading rates of the nanotubes. Eventually, a volume fraction of 0.15% of nanotubes turned out to be the best composition that resulted in complete curing of the foam slab. Dispersion of nanoparticles in a polymer matrix is a very crucial factor affecting the overall strength and stiffness of the particulate composite. Many techniques for the dispersion of nanoparticles like manual mixing, high temperature mixing, ultrasonic mixing and three-roll mill mixing have been adopted in the past. A recent study by Ji and Li [102] shows that a combination of ultrasonic and three-roll mill mixing helps in achieving the optimum dispersion of nanoparticles within the matrix. Therefore, a similar approach was adopted in this study.

The nanotube-polymer mixture was mixed with the assistance of an ultrasound mixer for 30 minutes at a frequency of 20kHz (Sonics Vibracell VC 750W) and a three-roll mill for one pass (NETZSCH type 50). When using the three-roll mill, care was taken to set the gap between each roller not too close to result in the breaking of carbon nanotubes. Breakage of nanotubes will lead to lower aspect ratio and in turn lower mechanical and thermal properties. Second, glass microballoons (40% by volume) and the hardener (Veriflex Part B) were added to the carbon

nanotube-polymer mixture and mixed with a spatula for 15 minutes to make sure that a uniform, homogeneous mixture was obtained. The ultrasonic mixer and the three-roll mill are depicted in Figure 8.

Figure 8. Ultrasonic mixer and three-roll mill

The whole mixture was then poured into a steel mold and sealed on the top with a steel plate for curing. The surface of the top and bottom steel plates used to seal the mold were covered with teflon sheets to facilitate easy removal of the foam after curing. The sides were also protected with a double sided taci tape to prevent the foam from leaking through the sides. Curing in a closed mold was recommended by the manufacturer due to the volatile nature of the polymer system used as the matrix. The curing process started at 75°C for 24 hours, 90°C for 3 hours and then 100°C for 3 hours in an industrial oven. This curing cycle was chosen by a *trial and error* process because the curing cycle for the pure polymer recommended by the manufacturer could not cure the foam. After curing, the smart foam was demolded and cut according to the specifications for TEM, DSC, thermal conductivity and uniaxial compression tests. The cured smart syntactic foam is depicted in Figure 9. The striations that can be seen on

the surface are due to the teflon sheet that was spread on the mold to facilitate easy demolding of the foam after completion of the curing cycle.

Figure 9. Cured Smart Syntactic Foam

2.4 Transmission Electron Microscopy (TEM)

Approximately 70 nm thick sections were cut with a Rondikn diamond knife on a DuPont MT 5000 Sorvall Ultramicrotome. Sections were collected on collodion-coated copper grids and imaged with a JEOL 100CX TEM. TEM images of the pure SMP and the ones with MWCNTs are depicted in Figure 10. It was found that the combination of the ultrasonic mixer and the three-roll mixer was adequate to uniformly disperse the carbon nanotubes in the polymer matrix as validated by the TEM image in Figure 10 (b). Thus the dispersion of carbon nanotubes in the thermosetting SMP matrix was found to be effective by using a combination of the ultrasonic mixer and the three roll mill in accordance with the study conducted by Ji and Li [102]. The gap between each roller of the three roll mill was selected such that damage of the carbon nanotubes will not occur during the shear mixing process.

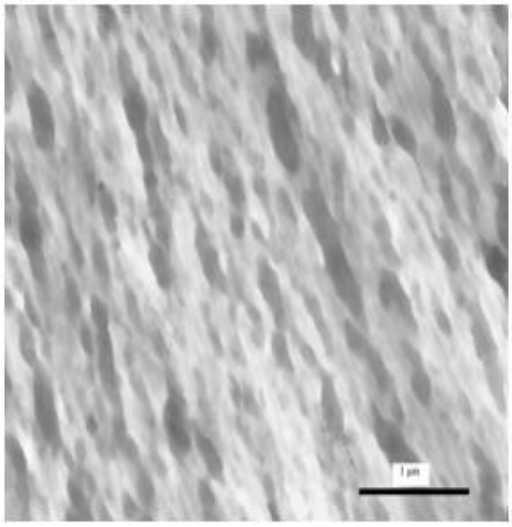

(a) Shape Memory Polymer

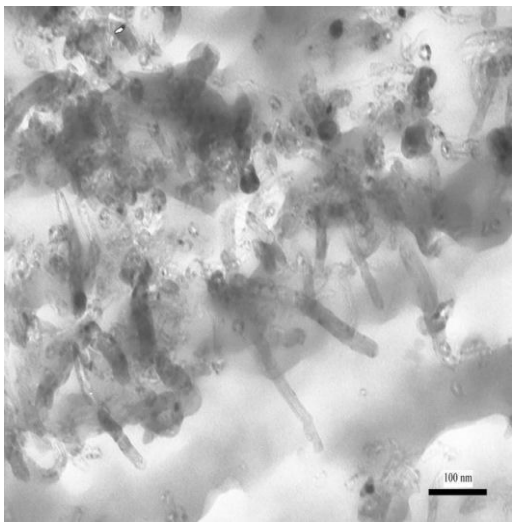

(b) Smart Foam

Figure 10. TEM image of Shape Memory Polymer and Smart Foam

2.5 Differential Scanning Calorimetry (DSC)

Glass transition temperature (T_g) is an important parameter in the programming of the SMP. As discussed previously, the programming must start at a temperature higher than T_g. Also, in applications that can experience temperature extremes, it is important to know what the potential exposure temperatures are and how they will affect the mechanical behavior of the material. The DSC is primarily used to measure the glass transition temperature (T_g), below which the material/polymer is rigid and brittle, and above which they are elastic and ductile. Knowledge of T_g helps in devising a systematic testing procedure for the characterization of the shape memory polymer. In addition, it also helps in predicting when material recovery will occur upon heating. Shape memory effects are more pronounced in the vicinity of T_g , because this temperature corresponds to the relaxation of the polymeric chains.

Differential Scanning Calorimetry is a technique used to study the thermal transitions occurring in a polymer when it is heated. The operation of a Differential Scanning Calorimeter is

based on measurement of the thermal response of an unknown specimen as compared with a standard when the two are heated uniformly at a constant rate. The DSC has several useful capabilities, primarily the ability to measure glass transition temperature.

A schematic representation of the DSC is given in Figure 11. From the figure it can be seen that the DSC has 2 pans, the reference pan and the sample pan. The shape memory polymer is placed in the sample pan and the reference pan is empty. Both the pans are heated at the same rate by cylindrical furnaces. Due to the presence of the polymer in the sample pan, it will take more heat to keep the temperature of the sample pan increasing at the same rate as the reference pan. This additional heat absorbed is measured by the DSC.

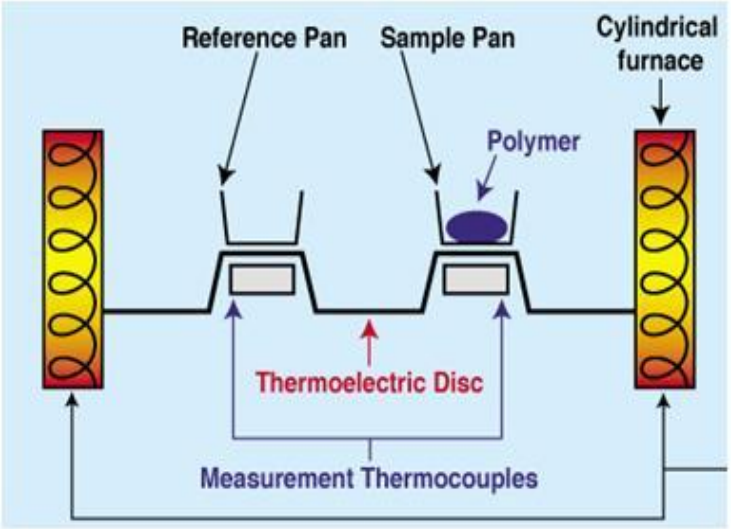

Figure 11. Schematic of the Working of DSC

A typical DSC curve obtained from experiments conducted on the carbon nanotube reinforced SMP foam is shown in Figure 12. The DSC test was conducted from 35^{o}C to 90^{o}C at a ramp rate of 5^{o}C/min. As the temperature increases, the internal energy of the material changes with an inflection point at the glass transition temperature. Three effective specimens were tested to obtain an average of the glass transition temperature. In Figure 12 we can see a change in slope corresponding to the inflection point around 62^{o}C, suggesting the T_g value.

From Figure. 12, it is noted that the peak has been significantly flattened due to the presence of the elastic components (glass microballoons and nanotubes). Relaxation of the shape memory polymer chains occur in the vicinity of the glass transition temperature and this in turn corresponds to the shape recovery process of the SMP. Previous studies have showed that large variations of T_g can occur at the interface between nanoparticles and the polymer matrix [103]. In this case, the polymer surrounding the carbon nanotubes can overlap and percolate resulting in different polymer-to nanotube distances that ranges from molecular contact to several nanometers. Due to this wide range of confinement, the widening of the relaxation time domain occurs which in turn results in a broadened glass transition region as seen in Figure 12.

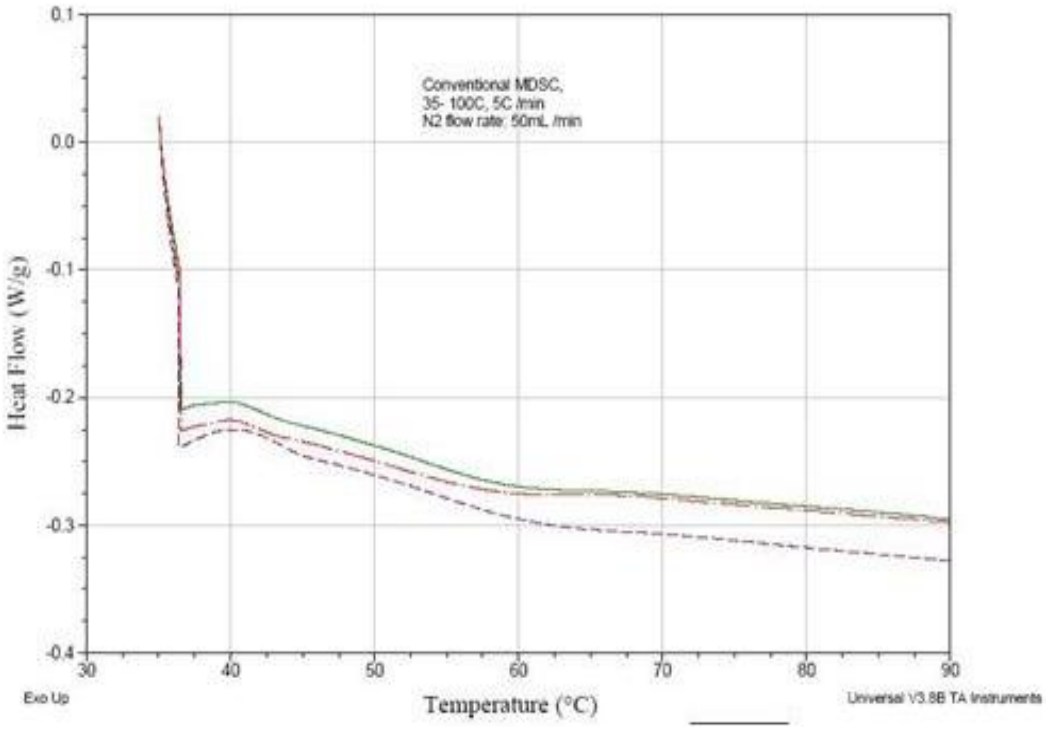

Figure 12. Typical DSC curve for the smart syntactic foam

2.6 Thermal Conductivity Measurements

In order to measure thermal property enhancements due to the addition of nanotubes in the shape memory polymer, thermal conductivity and specific heat of the foam were analyzed. This

was done with the help of a Flash line 5000 series thermal analyzer. Figure 13 depicts the flash line 5000 series thermal conductivity measurement device and the inset is a more clear view of the specimen holder. The method involves uniform irradiation of a small, disc-shaped sample over its front face with a very short pulse of energy. The time-temperature history of the rear face is recorded through high-speed data acquisition from a solid-state optical sensor with very fast thermal response. Cylindrical specimen with a diameter of 12.5mm and thickness of 3mm were used for taking the thermal conductivity measurements. An average of 3 specimens was taken to obtain the effective thermal conductivity of the smart foam.

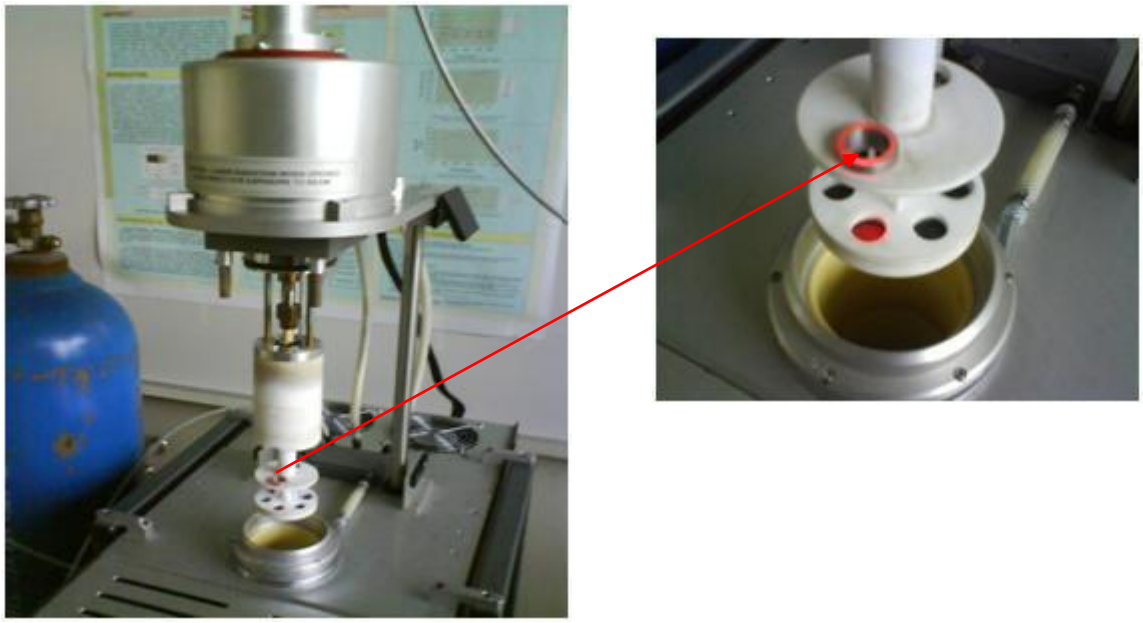

Figure 13. Flash Line 5000 Thermal Analyzer

The thermal conductivity and specific heat of the neat SMP and the smart foam is summarized in Table 1. It can be seen that the thermal conductivity of the foam specimen remained the same when compared with the neat SMP (0.14 W/m·K). There was no increase in the conductivity of the foam specimen mainly due to the lower volume fraction of nanotubes used for the fabrication process. On the other hand, the specific heat of the smart foam (1364.5 J/kg·K) was reduced by

about 2.2%, when compared with the neat SMP (1395.6 J/kg·K). This clearly shows that the amount of heat energy required to increase the heat of a unit quantity of the foam is less when compared with the neat SMP. The reduction in specific heat is probably due to the voids in the hollow glass microballoons.

Table 1. Thermal Conductivity and Specific Heat Capacity Measurements

Specimen	Thermal Conductivity (W/m.K)	Specific Heat Capacity (J/kg.K)
Neat SMP	0.14	1395.6
Smart Foam	0.14	1364.5

2.7 Uniaxial Flat-wise Compression Tests of Smart Foam

In order to evaluate the mechanical properties of the prepared foam, uniaxial compression test was conducted. The foam specimens were 25.0mm long, 25.0mm wide, and 12.5mm thick blocks, which were tested flat-wise per ASTM C 365 using an MTS 810 machine. The test was strain controlled and the loading rate was 1.3mm/min. The test was conducted at room temperature. Three effective specimens were tested. The compression test setup is shown in Figure 14. The stress-strain curve was obtained and the yield strength, ultimate strength, and modulus of elasticity were determined. Yield strength suggests the end of elastic region and start of elastic-plastic region. The ultimate strength suggests the maximum load carrying capacity of the specimen. Typical compressive stress-strain plots of three smart foam specimens are shown in Figure 15. It is clear that the stress-strain curve can be characterized by 3 distinct regions. The initial region (region 1) is a linear elastic region. In this region the foam undergoes elastic deformation which is recoverable at room temperature. This is followed by a plateau region

(region 2) which corresponds to the densification of the foam material; and the last region (region 3) corresponds to the compaction and consolidation of the foam material, which may include the crushing and further densification of the microballoons.

Figure 14. Uniaxial compression of smart foam

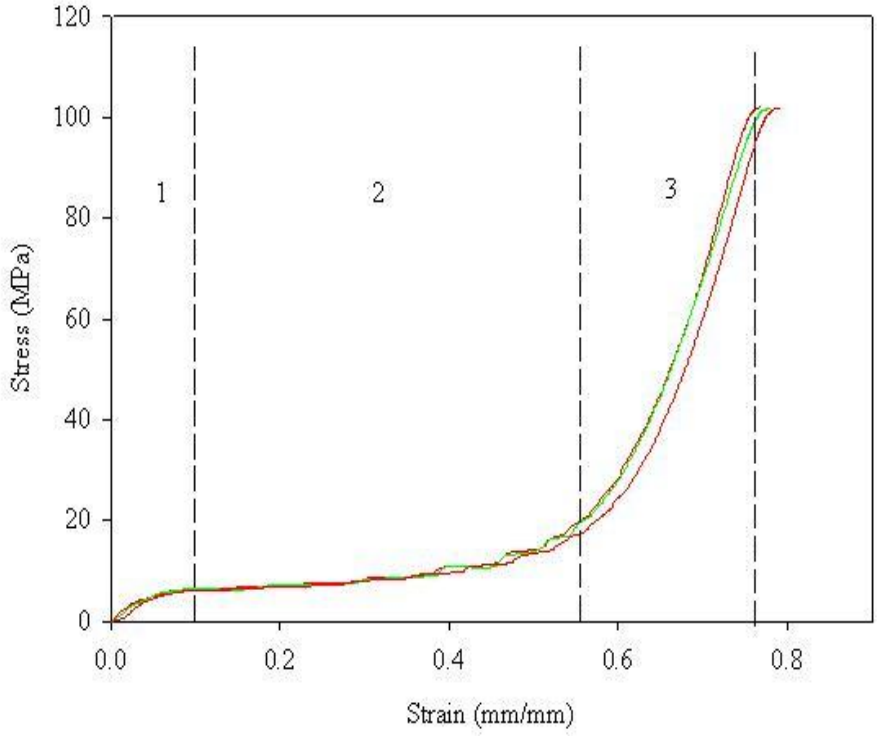

Figure 15. Typical compressive stress – strain behavior for the foam material

Compared with regular syntactic foam, it is obvious that the deformation in the plateau region is much higher**.** This suggests that the smart foam would be able to absorb more impact energy without disintegration.

Another batch of syntactic foam was also fabricated without carbon nanotubes. The purpose is to evaluate the effect of carbon nanotubes on the mechanical properties and self-healing efficiency. The foam was cured at 79.4^{o}C for 24 hours, followed by a cycle at 107.2^{o}C for 3 hours and finally at 121.1^{o}C for 6 hours. Uniaxial compression tests were conducted on 5 effective specimens using the same Q-TEST150 test machine setup as described previously. Typical stress-strain plots are depicted in Figure 16. Compared to Figure 15, it is seen that the tendency of these two types of foams are similar. However, the one without carbon nanotubes has a considerably higher yield strength and modulus of elasticity (the slope in region 1). Therefore, it seems that the foam without carbon tubes is more suitable for carrying load. Of course, better mechanical properties are just one side of the equation, self-healing efficiency is another one. Therefore, in the following, both foams will be utilized in fabricating sandwich structures to evaluate their impact response and self-healing efficiencies.

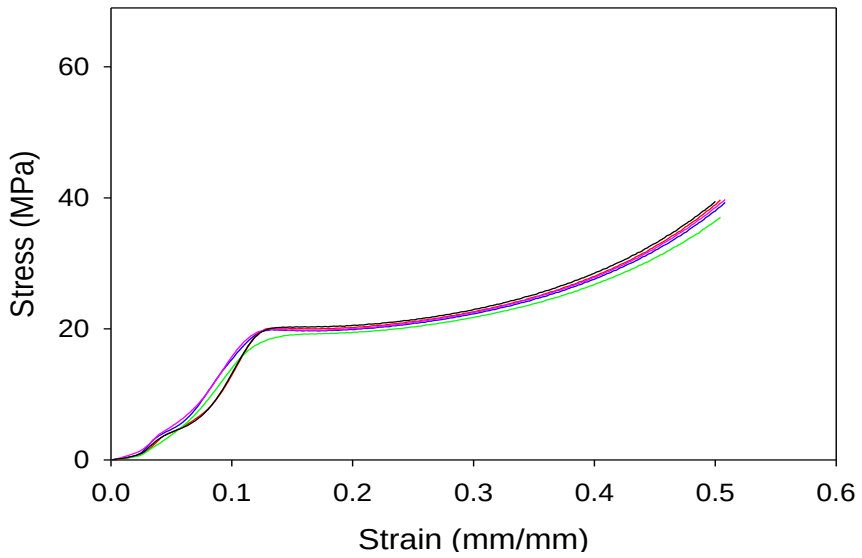

Figure 16. Typical compressive stress – strain behavior for the syntactic foam with no nanotubes

CHAPTER 3. MICROMECHANICS MODELING OF MICROSTRUCTURE OF THE SMART FOAM

From chapters 1 and 2, it can be concluded that the smart foam possesses a multiphase microstructure. The unit cell of the smart syntactic foam essentially consists of at least three phases. One is the solid shell of the hollow glass microballoon, the second is the void within the glass shell, and the third is a layer of SMP coated on the outer shell of the glass microballoon. However, due to the interaction between the microballoon and the SMP, there may be an interfacial transition zone (ITZ) or interphase in between the glass microballoon and the SMP. Hence, the basic building block of the foam may essentially consist of four phases. From inside to outside, they may be void, solid glass shell, ITZ, and pure SMP. The assumption of a four-phase microstructure was further validated by the studies of Xu and Li [104] and Li and Nettles [105] by conducting Fourier Transform Infrared (FTIR) spectroscopy and Dynamic Mechanical Analysis (DMA) of the pure SMP and the smart syntactic foam, respectively. Based on the study conducted by Xu and Li [104], by comparing the FTIR peaks of the pure SMP and the smart foam, it was evident that there exist weak hydrogen bonds at the interface of the glass microballoon and the SMP, possibly due to some chemical reactions between them. The DMA tests conducted by Li and Nettles [105] characterized the glass transition temperature (T_g) of the pure SMP and the smart foam. An increase in the T_g of the smart foam by about 2.8^{o}C was observed when compared with the pure SMP. This increase in the T_g can be attributed to the layer of SMP that could be adsorbed around the vicinity of the glass microballoon, possibly through the weak hydrogen bond as evidenced by the FTIR test. This is also in accordance with the studies conducted by Berriot et.al. [103] in which they claimed that the T_g can be shifted up by more than 100°C when the polymer is confined at 1 nm from the interface and by a few

degrees Celsius at 10 nm. The effect becomes negligible at greater distances. Berriot et.al. [106] and Kaufman et.al. [107] studied carbon black interactions with rubber by conducting Nuclear Magnetic Resonance (NMR) tests. They concluded that there exist two different micro domains of the immobilized and mobilized layers and were able to determine the thickness of the immobilized layer. Thus it is clear that there is an ITZ layer in the building block and the smart foam consists of essentially four phases. It is noted that it is very difficult to obtain the detailed physical and mechanical properties of the ITZ layer. Therefore, in this study, we treat the ITZ layer and the pure SMP layer to be an equivalent SMP layer. In such a way, the foam becomes an equivalent three phases: void, solid glass shell, and equivalent SMP. The purpose of this study is to obtain the size and elastic properties of the equivalent SMP layer so that the basic building block of the foam can be better understood.

3.1 Micromechanics Modeling

Given the visco-elastic and visco-plastic nature of the SMP foam, along with damage such as microballoon crushing, it is a challenging task to model the properties of the smart foam in the three regions of the compressive stress versus strain plots. This section will primarily quantify the elastic properties of the smart foam in the linear-elastic region (region 1) of the stress-strain plots. A more detailed study on the constitutive behavior of the SMP based smart syntactic foam can be found in the studies by Xu and Li [104].

A micromechanics based modeling of the smart foam was conducted by following the four phase sphere modeling of concrete by Li. et.al. [108]. In that study, the effective bulk modulus of concrete was evaluated based on the four phase sphere model. The model was solved by embedding a three-phase unit cell (aggregate, ITZ, and cement paste) into an infinite equivalent concrete medium. Because the ITZ and the pure SMP layer has been treated as an equivalent

SMP layer for the foam, as shown in Fig. 17, the model developed by Li et al. [108] can be directly utilized. In Figure 17 (a) the microballoon possesses an inner radius denoted by “a” and an outer radius denoted by “b”. This is followed by the ITZ layer with a radius of “e”. Then a layer of the SMP with a radius of “f” can be found. This is converted into an equivalent three-phase system in Figure 17 (b) with “a” and “b” the same and “c” denoting the radius of the equivalent SMP layer around the glass microballoon.

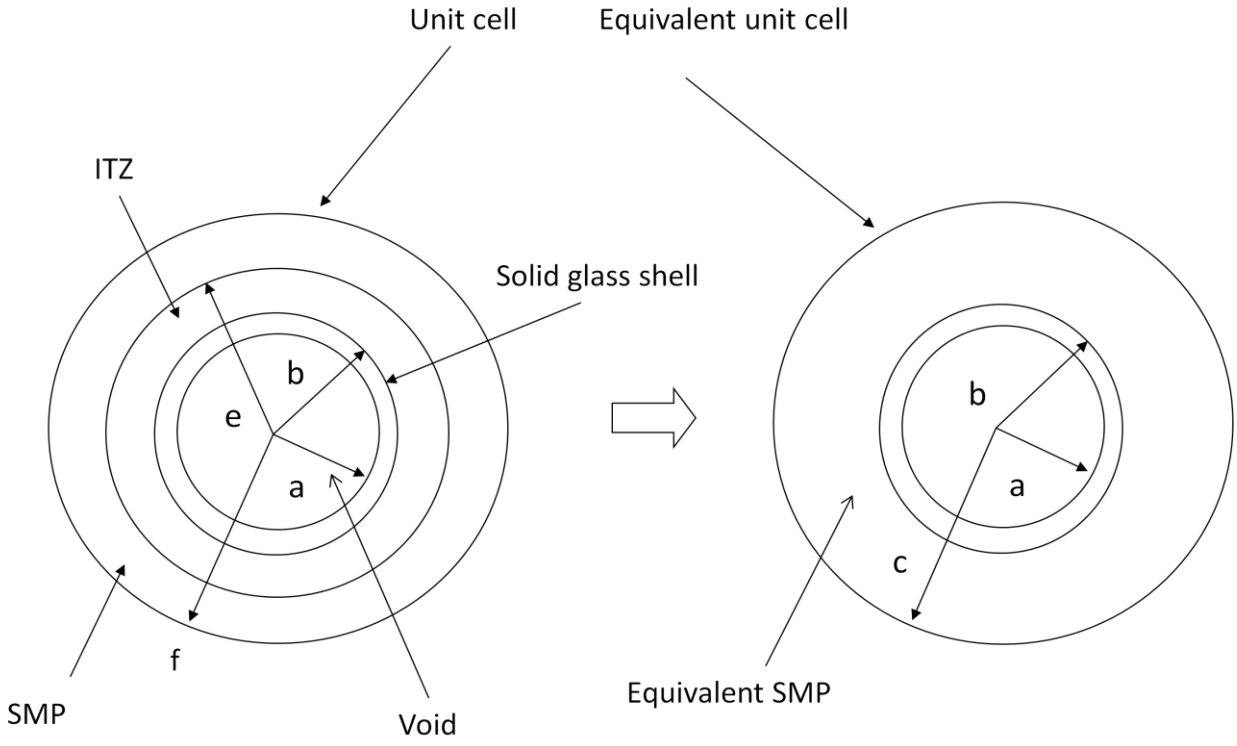

Figure 17.Four-phase foam been transformed into an equivalent three-phase foam

3.2 Model Formulation

The glass microballoon is hollow with an inner radius of 41.69µm (a) and outer radius of 42.5 µm (b). The outer radius was obtained from the manufacturer data sheet (Q:cel 6014, Potters Beads Inc.). The inner radius was calculated using equations for radius ratio (η), which is defined as the ratio of the inner radius (a) to the outer radius (b) of the hollow glass microballoon. The

radius ratio can also be expressed in terms of the densities of the glass microballoon (ρ_{mb}) and bulk glass (ρ_g). The calculations leading to the estimation of the inner radius (a) of the glass microballoon is given below.

$$\eta = \frac{a}{b} = \sqrt[3]{\left(1 - \frac{\rho_{mb}}{\rho_g}\right)} \quad \ldots\ldots\ldots\

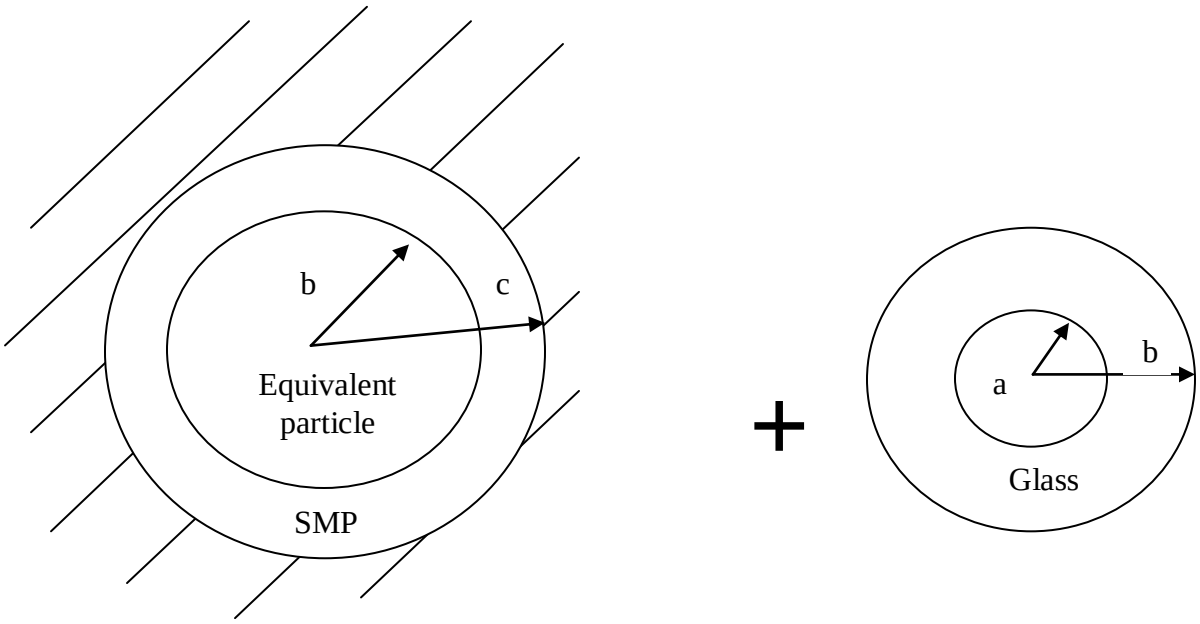

(a) (b)

Figure 18. Scheme to solve the modulus of the foam

Using theory of elasticity [109] and Eshelby's equivalent medium theory [110], Christensen [111] proved that the effective bulk modulus in Figure 18 (a) can be predicted by Equation (4):

$$K_0 = K_1 + \frac{(K_e - K_1)(b^3/c^3)}{1 + [(1 - b^3/c^3)(K_e - K_1)/(K_1 + \frac{4}{3}G_1)]} \quad \ldots\ldots\ldots\ldots\ldots\ldots\ldots\ldots\ldots\ldots\ldots\ldots\ldots\ldots (4)$$

where K_0 is the bulk modulus of the model described by Figure 18 (a) and in this case is the modulus of the equivalent smart syntactic foam obtained from uniaxial compression tests performed on the smart foam in section 2.7. K_e is the equivalent effective bulk modulus of the equivalent particle in Figure 18 (a), which can be solved by Equation (5) in terms of Figure 18 (b):

$$K_e = K_2 + \frac{(K_3 - K_2)(a^3/b^3)}{1 + [(1 - a^3/b^3)(K_3 - K_2)/(K_2 + \frac{4}{3}G_2)]} \quad \ldots\ldots\ldots\ldots\ldots\ldots\ldots\ldots\ldots\ldots\ldots\ldots\ldots\ldots (5)$$

The terms a, b and c were described in the earlier paragraph. E_i, K_i, G_i and ν_i (i=1, 2, 3) are the Young's modulus, bulk modulus, shear modulus and Poisson's ratio of the equivalent SMP system (i=1), solid glass microballoon shell (i=2) and the void of the glass microballoon (i=3) respectively. K_3 is taken to be zero in these equations because the modulus of the void is zero. Thus the only unknown is K_1, which is the effective bulk modulus of the equivalent SMP layer around the glass microballoon. Once K_1 is determined by solving Equations (4) and (5), and using Equation (6), we can find E_1.

$$\left.\begin{aligned} E &= 3K\,(1-2\nu) \\ E &= 2G(1+\nu) \end{aligned}\right\} \quad \ldots\ldots\ldots\

Table 2. Elastic Constants and Poisson's ratio of different phases in the smart foam

Layer	**Young's Modulus E, (GPa)**	**Bulk Modulus K, (GPa)**	**Poisson's Ratio, ν**
Equivalent Solid Glass Microballoon	1.94	1.29	0.25
Equivalent SMP layer	0.15	0.25	0.35
Equivalent SMP Foam	0.27	0.22	0.30

Based on Table 2, the equivalent smart foam is well quantified. Of course, if the ITZ layer can be further defined and the parameters such as thickness of the ITZ layer are obtained, a clearer picture of the foam can be given and the unit cell of the smart foam can be better understood.

CHAPTER 4. SMART FOAM CORED SANDWICH*

The core plays a vital role in any sandwich construction. The core is responsible for separating and fixing the skins, resisting transverse shear, carrying in-plane loads etc. The core is also a good insulator of heat and shields electromagnetic radiation. It also helps in absorbing impact energy, both low velocity and high velocity impact. But the core as a single entity is brittle under impact loads due to the macro length scale damages induced in them. So a sandwich construction with the core sandwiched between two polymer infused glass fabric skins will be the most ideal configuration to protect the core from catastrophic failure (glass fabric skins helps in containing the bending loads in the system). The glass fabric skins are also responsible for eroding and breaking the projectile, thereby protecting the core lying beneath. The shape memory polymer based syntactic foam can be used as a core material in composite sandwich structural applications and thus the sandwich panel can actuate a healing process when triggered by an external stimulus like heat. Therefore, the work in this chapter is primarily focused on the fabrication methodology, impact, structural, morphological and visual characterization of a sandwich structure incorporating the smart foam as the core.

This chapter can be sub-divided into the following sections. (1) the raw materials and fabrication methodology utilized in manufacturing the smart foam cored sandwich structure, (2) thermomechanical programming of the smart sandwich coupled with post curing of the skin infused with the SMP, (3) low velocity impact studies to determine the impact tolerance and energy absorbing characteristics, (4) compression after impact studies on the impacted and healed specimen to determine the residual strength and hence the healing efficiency, (5) non-

destructive ultrasonic C-scan evaluation of the impacted and healed specimen and (6) morphological and visual inspection of impacted and healed specimen.

4.1 Materials

The smart foam with carbon nanotube incorporation described in Chapter 2 was used as the core for the sandwich construction. A woven roving fabric 7725 (Fiber Glast) was used as the top and bottom skin or face sheet. The warp and fill yarns run at 0 and 90 degrees respectively. Thus these woven glass fabrics are strong in both directions. These woven glass fabrics have high tensile strength, dimensional stability, high heat resistance, chemical resistance, fire resistance and durability when compared with other fabrics.

4.2 Smart Foam Cored Sandwich Fabrication

The sandwich panels were fabricated using Vacuum Assisted Resin Infusion Molding (VARIM) system (Airtech). The whole setup is depicted in Figure 19 (a) and the resin infusion process is shown in Figure 19 (b) and (c). VARIM process involves the utilization of a distribution mesh to uniformly distribute the SMP through the glass fabric skins. However, at the same time the distribution mesh should not stick to the glass face sheet after curing. Hence a porous teflon sheet was used in between the face sheet and the distribution mesh. This helped the resin flow through the panel and at the same time go through the pores in the porous teflon and wet the glass fabric sheet uniformly. On top of the sandwich panel the mesh was bonded to a spiral wrap tube which in turn was connected to a tube for polymer infusion. A similar arrangement of the teflon sheet and distribution mesh was also adopted at the bottom face sheet. Meanwhile, the bottom tube from the mesh was connected to an excess resin collecting container which in turn was connected to a vacuum pump. The whole system was put under vacuum using

a vacuum bagging sheet. The vacuum pump pulls the resin through the skin and once the SMP passed through the entire skin, the system was closed using valves at both ends.

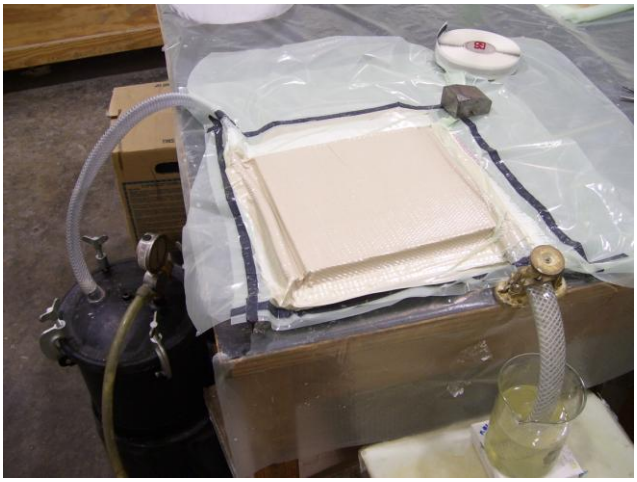

(a) System set-up

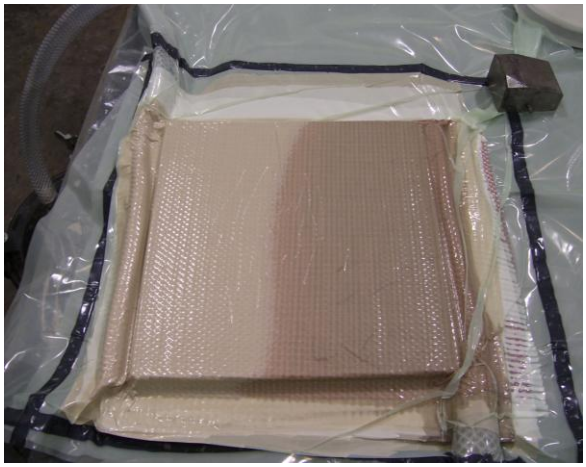

(b) Infusion in progress

(c) Infusion completed

Figure 19. VARIM system for SMP infusion

After leaving the system under vacuum at room temperature for about 15 minutes, the setup was transferred into the oven for curing the skins. In order to maintain chemical compatibility, the polymer used in the skin was the same shape memory polymer as the foam core. The cured thickness of the skin was 0.736mm. The glass fabric sheet skins infused with the SMP was cured

following a similar curing cycle as that of the SMP based syntactic foam core. A unique feature of this manufacturing process is that the curing of the sandwich face sheet was coupled with programming of the SMP foam core (shape fixity). Shape fixity and recovery will be discussed in section 4.3. The foam cored sandwich panels with a dimension of 152.4mm × 101.6mm × 12.7mm were prepared for impact and self-healing tests. This particular dimension was selected in order to conduct compression after impact test per the anti-buckling test fixture.

4.3 Thermomechanical Programming

The shape fixity or programming of the smart foam core was coupled with the curing of the sandwich panels. Shape fixity can be defined as the level of deformation that may be fixed upon cooling of the deformed material to room temperature. In this study, stress-controlled programming with a constant compressive stress of 0.05MPa was used, instead of the regular strain controlled programming. The programming process started by heating the sandwich panel to 75^{o}C. After that, the pressure of 0.05MPa was applied by the vacuum system. This temperature and pressure was maintained for 24 hours. Then the temperature was raised to 90^{o}C and maintained for 3 hours. The sandwich was then heated up to 100^{o}C and the temperature was maintained for another 3 hours (Step 1). After that the sandwich panel was cooled down to room temperature in about 6 hours while maintaining the stress level (Step 2). After 0.5 hour at room temperature, the pressure was removed (Step 3). This completed the three-step shape fixity process and the sandwich panels were ready for impact testing.

In order to examine the shape recovery capacity, the fourth step was also conducted on a control sandwich panel. Shape recovery can be defined as the level of deformation that can be regained upon heating above the T_g of the material. The sandwich panel was heated up again to 100^{o}C to determine the shape recovery without applying any stress (free or unconstrained shape

recovery). In order to quantitatively obtain the four-step thermal-mechanical cycle, strain gages were installed along the edges of the control sandwich panel in the thickness direction. This helped in determining the strain in the thickness direction.

A Yokogawa DC100 device was used to monitor the changes of strain with time and temperature. A DAQ 32 plus software in conjunction with the data acquisition system was used to record the strain and temperature data. The temperature was monitored with the help of thermocouples connected to the same device. The Yokogawa DC 100 strain and temperature measurement setup along with the strain gage attached sandwich specimen is depicted in Figure 20 (a). Figure 20 (b) gives a clearer picture of the strain gage attached to the smart foam cored sandwich structure in the thickness direction. The strain gages (Vishay Micromeasurements Inc.) were rated at a resistance of 350Ω±0.3% and a gage factor of about 2.105±0.5%. The permissible strain limits on this gage was about 3-5% of strain.

(a) Yokogawa DC 100 Data Acquisition

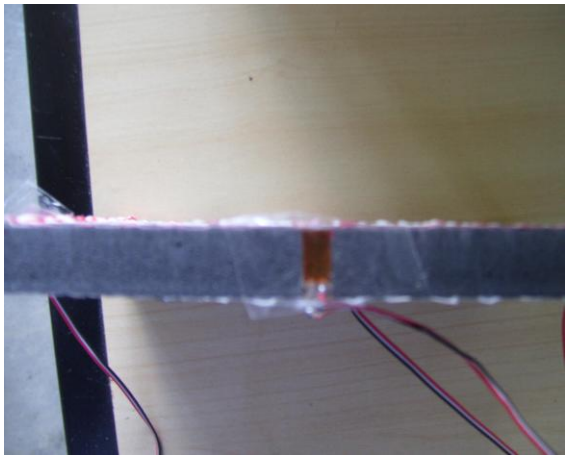

(b) Strain gage attached to the sandwich specimen in loading/thickness direction

Figure 20. Yokogawa DC 100 data acquisition system and strain gage

In the literature, the shape fixity and recovery rates are determined in terms of strain during the thermomechanical cycle by Equation (8) [83]:

$$R_f(N) = \frac{\varepsilon_u\,(N)}{\varepsilon_m} \text{ and } R_r(N) = \frac{\varepsilon_m - \varepsilon_p\,(N)}{\varepsilon_m - \varepsilon_p\,(N-1)} \quad \ldots\ldots\ldots\

From Figure 21, it is found that the shape fixity rate R_f = (529 × 10^{-5} mm/mm) / (534 × 10^{-5} mm/mm) = 99%. The shape recovery rate R_r = (534 × 10^{-5} mm/mm – 13× 10^{-5} mm/mm) / (534 × 10^{-5} mm/mm - 0× 10^{-5} mm/mm) = 97.6%. From the above calculation, it is clear that the shape fixity rate is close to 100% and the shape recovery rate is very high, suggesting good shape memory functionality of the smart foam. Also, an inflection point is found in the shape recovery step (step 4) around the glass transition temperature of the SMP (62^{o}C).

The shape fixity results indicate that the smart sandwich structure was able to store a majority of the strain introduced into the system during the high temperature deformation process. A value of shape fixity close to 100% is also an indication of minimal spring-back of the specimen during the low temperature unloading process. This is very important because it maintains the shape stability of the specimen. Shape recovery values were also close to 100%, indicating good shape memory behavior of the smart foam cored sandwich. This result suggests that the shape memory functionality of the smart foam has a great potential to seal internal damage upon heating.

4.4 Low Velocity Impact (LVI) Tests

Low velocity impact has been a critical problem in composite structures. Tool drops, runway debris, etc are examples of low velocity impact incidents. The finished structures made up of these composite materials could be subjected to low velocity impact events at the time of transportation or in service. For instance the foam materials / sandwich structures may be used as a layer beneath a bumper layer to absorb energy and protect the more important and vital part beneath. During a high velocity impact event like a bullet shot, the bumper layer gets shattered and the broken pieces will hit the underlying sandwich foam. This simulates a low velocity impact event in the sandwich. But these types of damages could be invisible and they cause a

reduction in the residual strength of the sandwich. So it is essential to conduct LVI tests on these sandwich structures and also do compression tests after impact to evaluate their residual strength.

All the low velocity impact tests were performed with the help of an Instron Dynatup 8250 HV drop weight impact machine. The Dynatup machine shown in Figure 22 is also equipped with an impulse data acquisition system. The fixture on which the sample was mounted is housed within an environmental chamber at the bottom of the drop tower which can be heated or cooled according to the requirements. The impact energy and velocity can be varied by changing the mass and the height of the drop weight. The impactor is hemispherical in shape with an instrumented tup of capacity 15.56kN and a diameter of 12.5mm. Transient response of the specimen includes the velocity, deflection, load and energy as a function of time. The machine also possesses a velocity detector that measures the velocity of the tup before it strikes the specimen. Pneumatic brakes are also provided which prevent multiple impacts on the specimen.

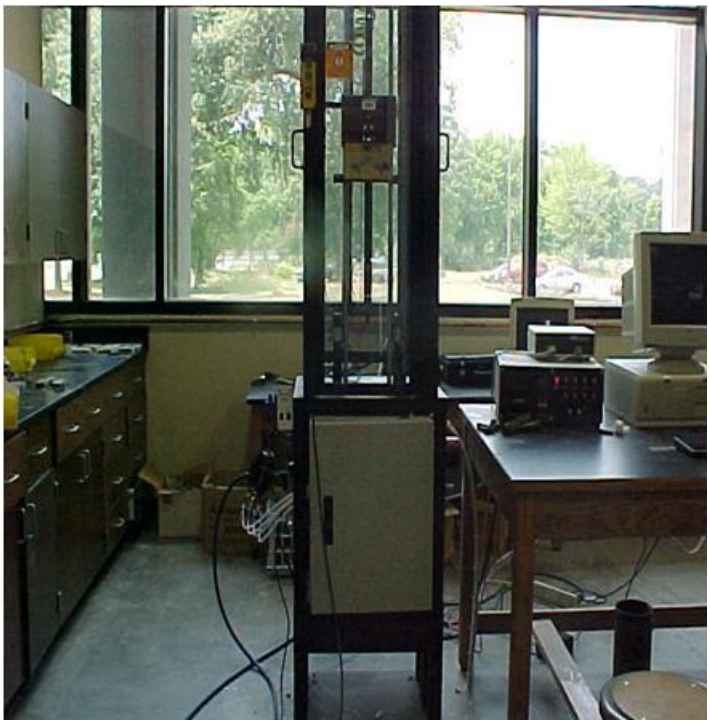

Figure 22. Low velocity impact machine

The maximum impact force, maximum deflection, and impact duration were directly obtained from the load and energy traces. The initiation energy and propagation energy were calculated based on these traces. Impact energy corresponding to the maximum impact force is defined as initiation energy. Propagation energy is defined as the difference between the maximum impact energy and the initiation energy. These definitions have been used previously [16-18, 54]. It has been suggested that the initiation energy is basically a measurement of the capacity for the target to transfer energy elastically and higher initiation energy usually means a higher load carrying capacity; on the other hand, the propagation energy represents the energy absorbed by the target for creating and propagating gross damage.

Low velocity impact tests were performed on each sandwich panel at the same impact location (center of the panel) repeatedly using drop tower impact machine at a velocity of 3 m/s and a hammer weight of 6.64 kg per ASTM D 2444. This is equivalent to about 30 Joules of energy. After each impact cycle, the sandwich specimens were taken into an industrial oven for performing the recovery/healing process. No external confinement was provided when the impact damaged sandwich was recovered by heating the sandwich specimen to 100^{o}C for 3 hours. However, it is noted that recovery was not free for the foam core. The reason is that the damaged form core was partially confined by the skin and by the surrounding undamaged foam. Therefore, this was a partially confined recovery test.

Typical load and energy traces are shown in Figure 23. The maximum impact force, maximum deflection, impact duration, initiation energy, and propagation energy after each impact are summarized in Figure 24. From Figure 24, the impact response is statistically the same for each round of impact. This suggests that the damage induced by each impact has been effectively healed by the shape recovery process. The impact tolerance has been effectively recovered by self-healing. Actually, it seems that the impact tolerance after the 7^{th} round of

impact is slightly better than that after the 1st round of impact, as indicated by slightly higher initiation energy and slightly lower propagation energy. This 'abnormal' behavior suggests that repeated impact and healing cycles may have adjusted the microstructure of the foam, making it more beneficial for impact tolerance. This fact is also reflected in the C-scan images as will be described in section 4.6. Another possible reason is the post-curing effect caused by the healing process, which was conducted for 3 hours at 100°C for each healing cycle. This will be discussed further in section 4.5.

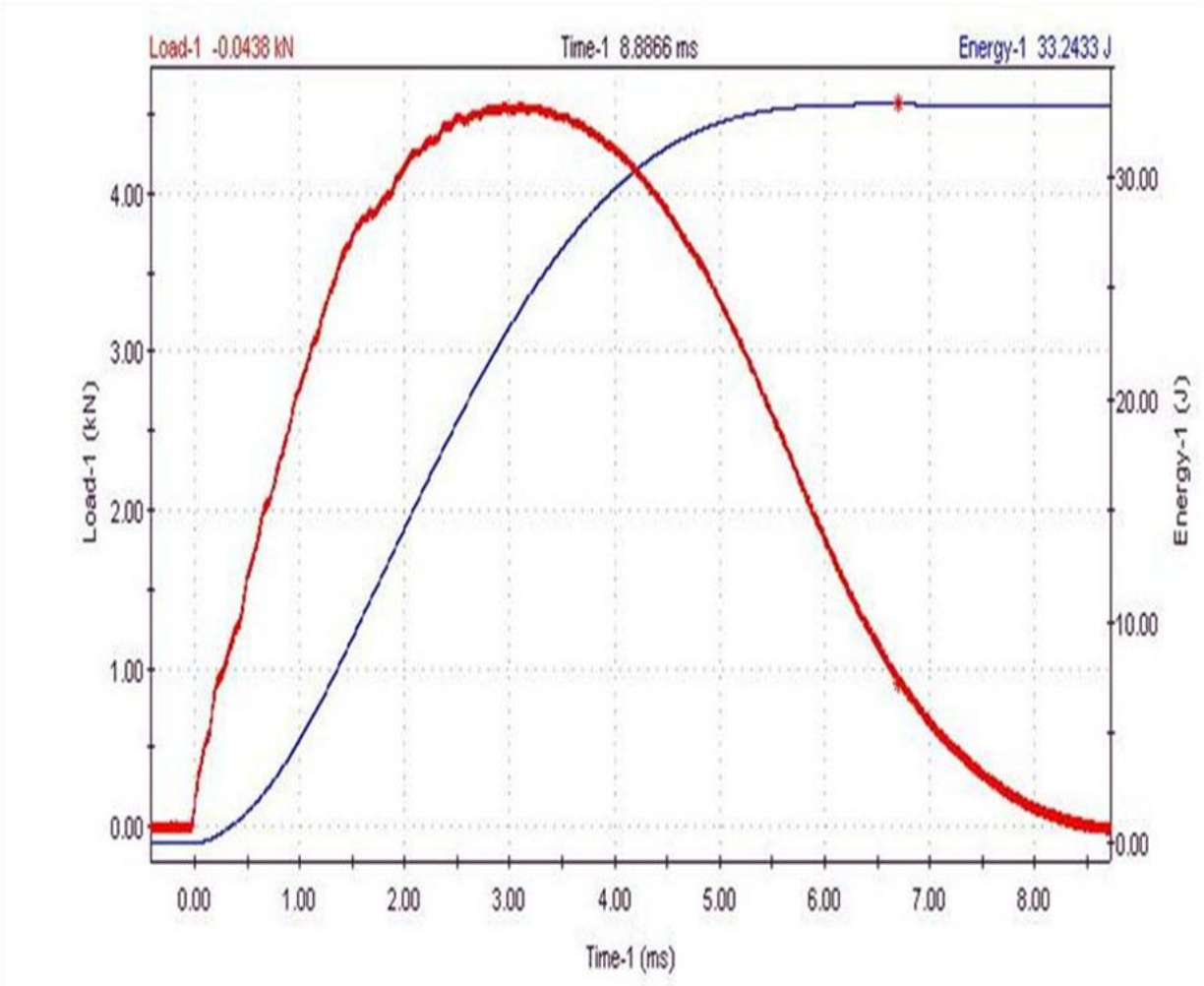

Figure 23. Typical Load-Energy versus time plots

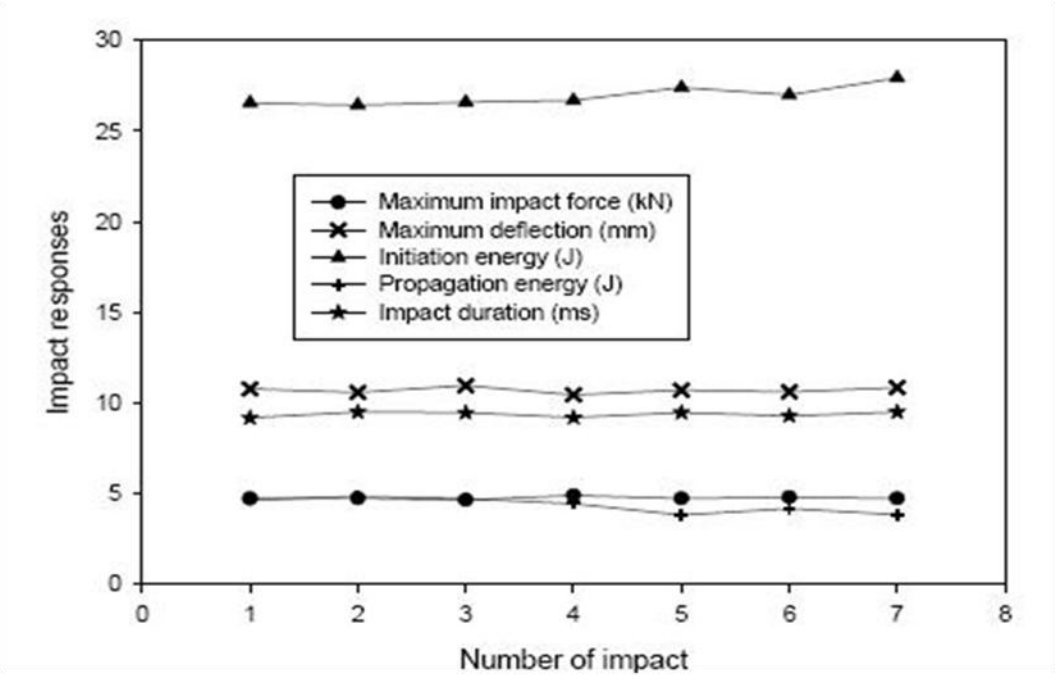

Figure 24. Impact response of the smart foam cored sandwich panels under multiple impacts

4.5 Compression After Impact (CAI)

Low velocity impacts might not create any damages visible to the naked eyes on the sandwich structure. In practice, however, this type of damage can adversely affect the strength of the sandwich and hence result in low residual load carrying capacity. To have a better understanding of the residual strength in the sandwich structure, generally compression after impact or bending after impact tests are performed on the impacted sandwich specimen. This will help in determining the residual compressive strength or bending strength in the specimen and hence in determining their permissible stress levels.

The testing was conducted using an MTS QTEST 150 machine and the fixture used was a "Boeing Compression after Impact Compression Test Fixture" per BSS7260 standard. A strain controlled testing mode experiment was conducted at room temperature and the loading rate was 1.3 mm/min. Each test was conducted on 5 effective specimens. For comparison purposes, 5

effective specimens without impact were also tested using the same anti-buckling fixture as controls. Figure 25 depicts the compression after impact test setup for the smart foam cored sandwich.

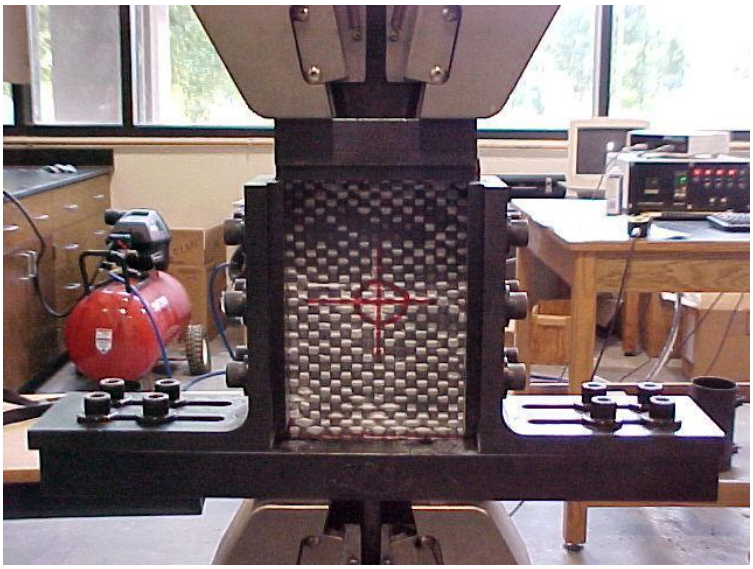

Figure 25. Compression after impact test setup

The typical CAI stress versus strain curves for CAI tests conducted on the control (without impact), after 1st impact and 1st healing, and after 7th impact and 7th healing of the smart sandwich specimens are shown in Figure 26. From Figure 26, the compressive modulus, yield strength and ductility (strain corresponding to the maximum stress) values are obtained. It is found that the modulus for the 1st impacted, 1st healed and 7th impacted specimen reduced to 85.04% (556 MPa), 94.04% (614 MPa) and 95.4% (623 MPa) of the original unimpacted control specimen (653 MPa), respectively. On the other hand the modulus for the 7th healed specimen increased to 110.9% (725 MPa) of the control specimen.

Figure 27 shows the variation of the residual yield strength with up to 7 consecutive impact-healing cycles. Two observations can be made: (1) each impact considerably decreases the CAI strength as compared to the control specimens.

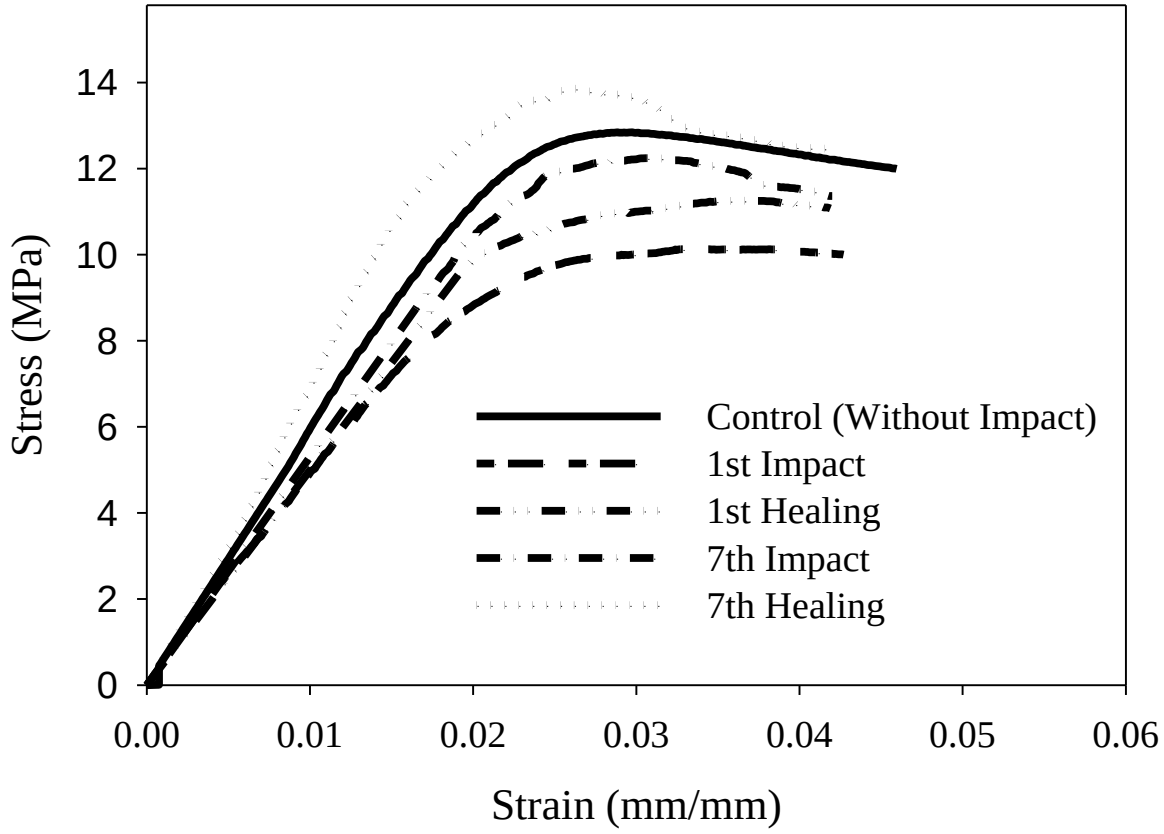

Figure 26. Typical CAI stress versus strain plots for various impact and healing cycles

Also, the CAI strength gradually decreases as the impact cycle increases until the 6th impact cycle. For the 7th impact cycle, a significant rebound in CAI strength is observed; (2) each healing cycle recovers a considerable portion of the compressive strength lost due to impact. However, the healed specimens still have a slightly lower strength than the control specimen. This tendency holds true until the 6th healing cycle. For the 7th healing cycle, its strength after healing is higher than the control specimens. These qualitative observations can also be detailed by quantitative analysis. The following quantitative estimation can be concluded from Figure 27. For instance, the CAI yield strength after the 1st impact is about 83.9% of the original yield strength without impact (control specimens, 12.23MPa); after 1st healing, the yield strength is about 93.8% of the original strength. This

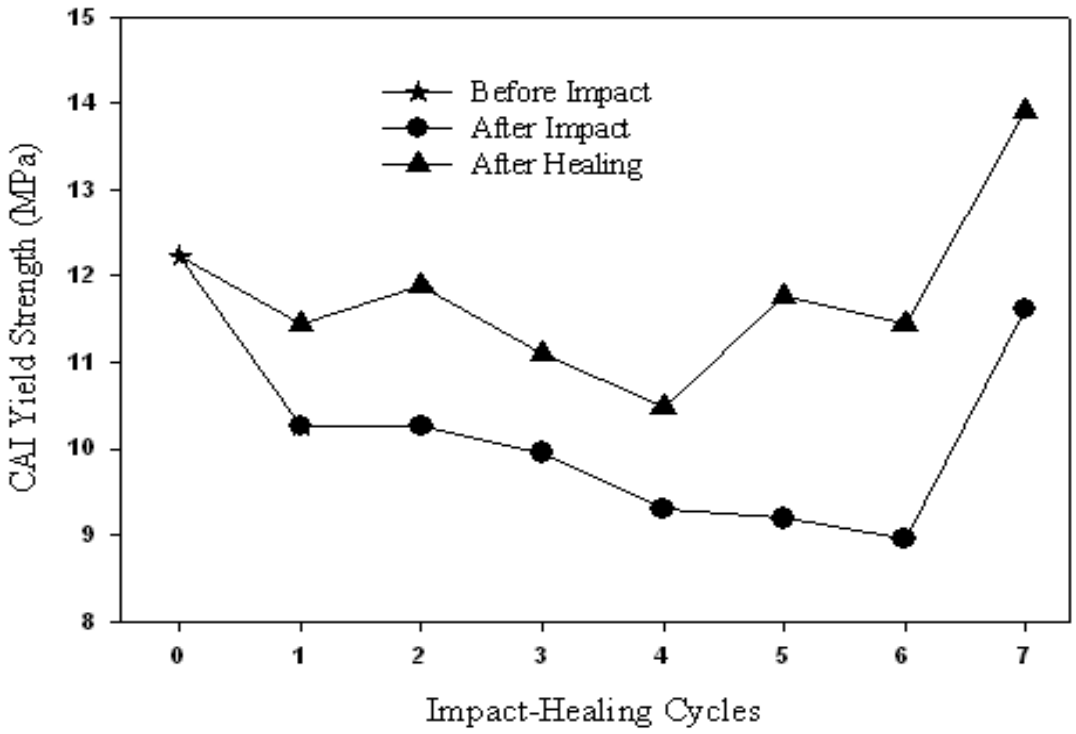

Figure 27. Variation of CAI yield strength with impact-healing cycles

suggests that the self-healing has recovered a major portion of the lost strength. After the 7th impact, the CAI yield strength is about 94.9% of the original yield strength; after the 7th healing, the residual strength is about 113.6% of the original yield strength. This suggests that after 7 rounds of impact-healing cycles, the sandwich specimens are actually gaining some strength. This result echoes the impact test results, i.e., at the 7th impact-healing cycle, the sandwich panels are becoming better in resisting impact damage. It is believed that the healing process may have coupled with the post-curing of the foam.

As mentioned previously, the curing time for all the specimens at 100^{o}C was 3 hours. Because each specimen was reheated to 100^{o}C for three additional hours during each healing cycle, the specimens subjected to different impact-healing cycles experienced different exposure time at the curing temperature of 100^{o}C. This is called as post-curing in this study. For example, for the specimens subjected to the first impact-healing cycle, the post-curing time is 3 hours; for

specimens subjected to 7th round of impact-healing cycles, the post-curing time is 21 hours. In order to understand the post-curing effect, uniaxial compression test was conducted on a group of block foam specimens which experienced various additional post-curing time periods simulating the actual high temperature healing. The temperature was fixed at 100°C and the period of post-curing was equal to the time period of healing. One group of 5 specimens was post-cured for 3 additional hours to simulate the 1st healing cycle; another group of 5 specimens was post-cured for 21 additional hours to simulate the total healing hours up to the 7th healing. The specimen size was the same as the flat-wise specimens and the test was conducted per ASTM C365. The test results show that after the 3 additional hours of post-curing, the average yield strength of the foam is 5.10MPa, which is about 0.81MPa lower than the regularly cured specimens (5.91MPa). This reduction may explain why the CAI strength of the sandwich specimens after 1st healing is only about 93.8% of the original strength. If the reduced strength of 0.81MPa were added to the yield strength of the sandwich specimens after 1st healing (0.81MPa + 11.44MPa = 12.25MPa), it is clear that the 1st healing would fully recover the original strength (12.23MPa). After 21 hours of additional post-curing, the yield strength of the foam becomes 7.60MPa, which is about 7.60MPa – 5.91MPa = 1.69MPa higher than the regularly cured foam without additional post-curing. This additional gain in strength is obviously due to the post-curing effect. If this additionally gained strength is removed from the sandwich panel after 7th healing (13.90MPa – 1.69MPa = 12.21MPa), it is clear that this corrected yield strength is close to the original strength (12.23MPa) (control sandwich panels). From the C-scan images, it is clear that both impact and healing change the microstructure of the foam. The reduction in the yield strength of the foam after 3 additional hours of post-curing may be due to the changed microstructure which is unfavorable for the strength development. Of course, further study is needed to fully understand the mechanism.

4.6 Ultrasonic and SEM Inspection

Ultrasonic inspection was performed on all specimens both after impact and after healing for each impact-healing cycle using a 1MHz transducer for the foam cored sandwich. An UltraPac inspection machine from Physical Acoustics Laboratory was used in conjunction with UltraWin software to acquire the C-scan images and identify damages. Scanning electron microscope (SEM) observation of micro-length scale damage was conducted using a JEOL JSM-840A scanning electron microscope. The Ultrapac inspection machine is shown in Figure 28.

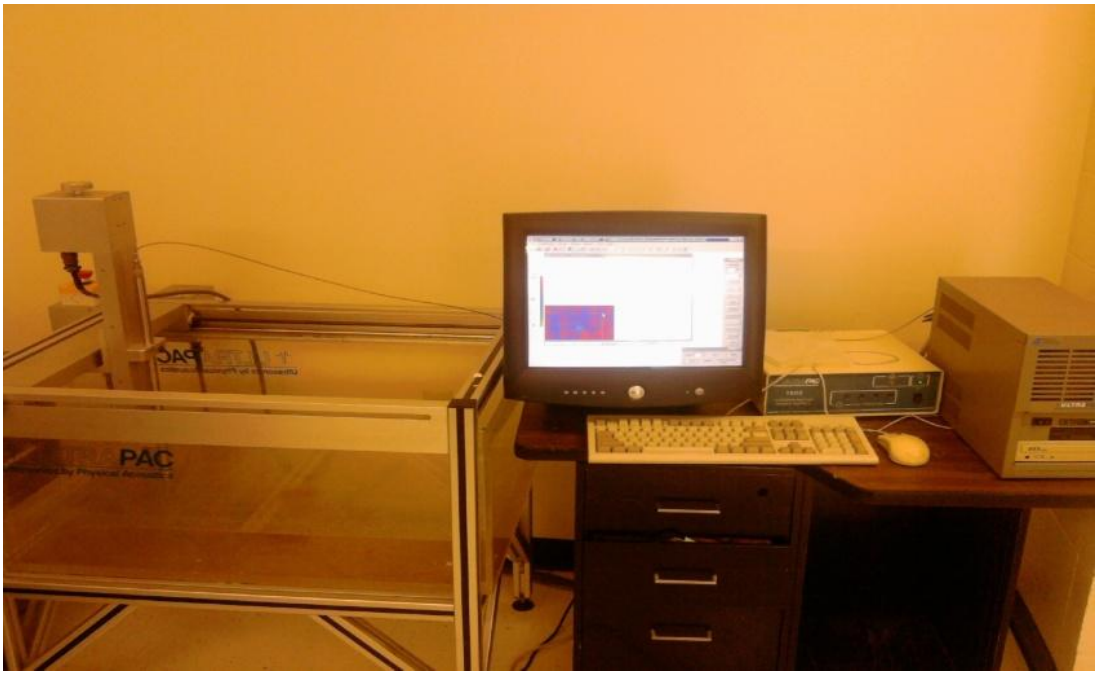

Figure 28. Ultrapac ultrasonic C-scan equipment and a typical C-scan Image

The impact damage can be visualized by C-scan and the damage at micro-length scale can be observed by SEM. Figure 29 shows the C-scan results of one sandwich panel before impact, after 1st impact, after 1st healing, until after 7th impact and 7th healing. In these pulse-echo C-scan images, red color represents an excess of 80% of the signal returning to the receiver, whereas blue color indicates that 50-80% of the signal is being received. White color represents a

complete attenuation of the ultrasound signal or 0% of signal received. Therefore, the white spot at the center of the specimen indicates a certain type of damage.

Two observations can be made: (1) the damage after each impact has been effectively healed, as evidenced by the removal of the white spot; (2) the microstructure has been changed after each impact-healing cycle as indicated by the change of the color distribution. These observations are supported by the impact responses, which show that the healing has helped the sandwich panel not only recover, but also slightly enhance its impact tolerance.

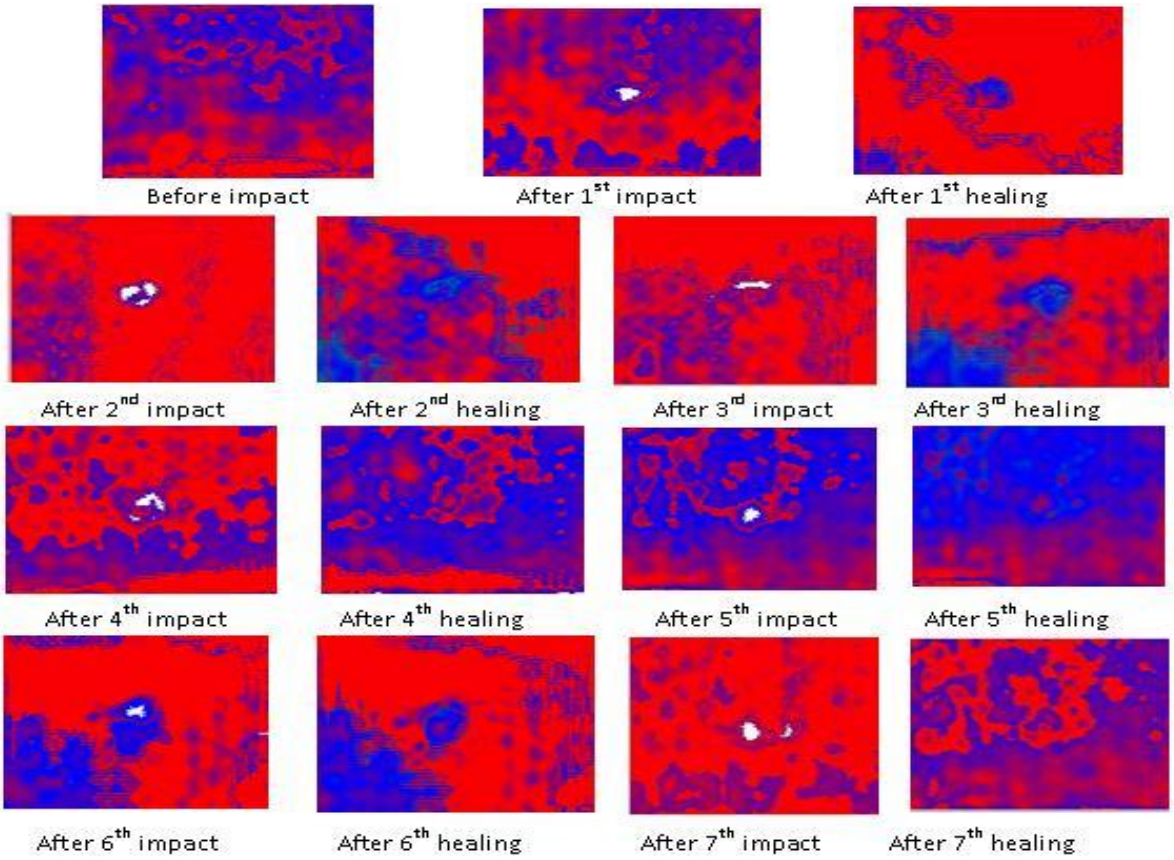

Figure 29. C-scan images of the sandwich panels after each impact and healing

Figure 30 shows a comparison of a microcrack in the foam core immediately after impact and immediately after healing. It is clear that the microcrack length has been reduced and the microcrack opening has been narrowed after healing. It is noted that during healing the sample, the shape recovery is stress-free, i.e., unconfined free shape recovery. In the sandwich panel, the

foam core directly under impact is partially confined by the skin and by the surrounding materials. Therefore, the confinement may produce a certain stress which may help in pushing the microcrack from two sides and thus may help close the crack. In another word, the microcrack in actual sandwich panels may have a better healing effect than that seen in Figure 30.

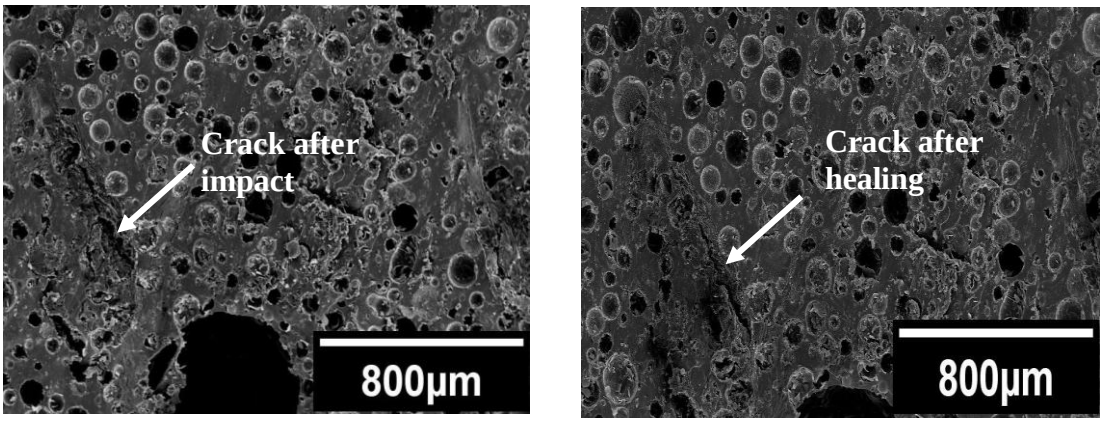

Figure 30. SEM pictures showing the effect of healing on the microcrack

A visual inspection of the impacted sandwich specimen was also conducted after each impact-healing cycle. The visual photographs corresponding to the unimpacted, 1st and 2nd impact-healing cycles are shown in Figure 31. specimen. It is also seen that the damage has been effectively repaired or healed by each healing cycle. These visual inspection pictures echoes the C-scan and SEM observation and suggests a high efficiency of healing by shape memory functionality.

Before impact

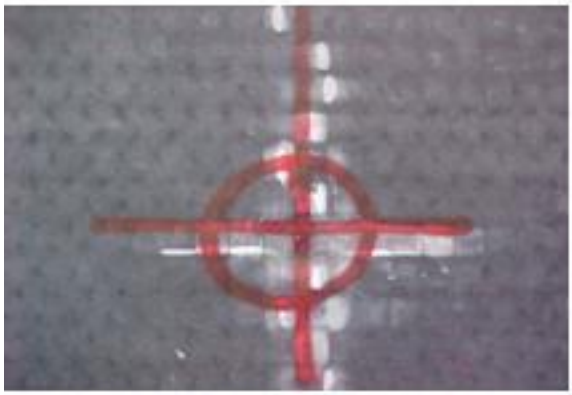

After first impact

After first healing

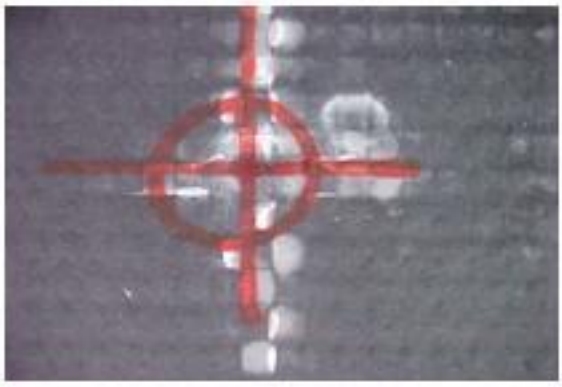

After second impact

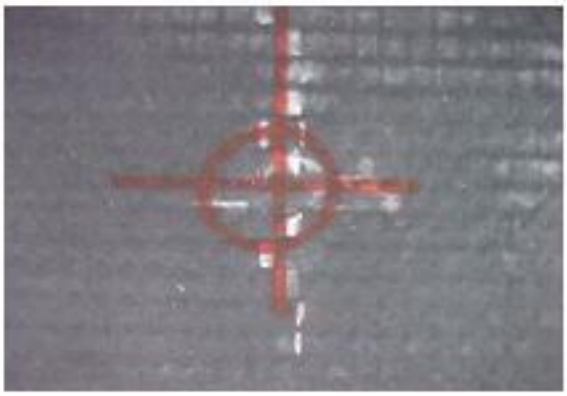

After second healing

Figure 31. Visual Inspection of healing efficiency

CHAPTER 5. GRID STIFFENED SMART SYNTACTIC FOAM CORED SANDWICH

As discussed in the introduction chapter, most of the conventional cores used in sandwich constructions (foam core, web core, 3-D core etc.) suffer from some limitations one way or another. The brittle nature of the foam core due to macro length scale damages, improper bonding of the skin to the core in web cores and pile buckling in 3-D cores are some of the disadvantages of the existing cores. This makes the hybrid core a suitable candidate for manufacturing sandwich structures. As a result special emphasis is given to grid stiffened structures in this study. The previous works by Li and Muthyala [54], and Li and Chakka [55] have shown that grid stiffened structures can perform in a better way by containing the impact damage in a quasi-static manner. So, the primary objective of this chapter is to fabricate, test and evaluate the healing efficiency of a grid stiffened sandwich structure with an SMP based syntactic foam filled within the bay areas of the grid. This makes the grid structure respond to damages in a smart way. The quasi-static behavior of the sandwich under impact is also validated in this study.

This chapter mainly discusses the fabrication of grid stiffened sandwich structures and the characterization procedures employed. Also, it is further sub-divided into the following sections. (1) materials used and the fabrication methodology employed for manufacturing the grid structures, (2) 3- step thermomechanical programming to two different pre-strain levels (3% and 20%), (3) low velocity impact tests (two different energy levels, 30 J and 53 J) at the same location (center of the bay) until 7 rounds of impact and healing, (4) two different routes of healing (in-plane 2-D confinement by the grid skeleton and 3-D confinement by the grid skeleton and the external transverse confinement) to compare the healing efficiency achieved, (5) wave

propagation within the bay area of the sandwich with the help of strain gages attached to the specimen to validate the claim of a quasi-static response in the grid stiffened sandwich, (6) compression after impact tests on the impacted and healed specimen and (7) ultrasonic C-scan imaging and visual observations of the healing efficiency achieved by the two routes of healing employed.

5.1 Materials

Glass fiber rovings (Saint Gobain) were used for dry weaving the ribs of the grid skeleton. The fiber rovings have a modulus of elasticity of about 70GPa and tensile strength of 1700MPa. They possess very low thermal conductivity and possess high corrosion resistance. A woven roving fabric 7725 (Fiber Glast) was used as the top and bottom skin or face sheet. The shape memory polymer with glass microballoons (smart foam) was filled in the bay area of the grid stiffened sandwich structure.

5.2 Grid Stiffened Smart Syntactic Foam Sandwich Fabrication

The grid skeleton was made by a dry weaving process similar to that in [54]. Initially pins were nailed down on a sheetrock board such that the space between the nails was 254.0 mm which corresponds to the length and width of the bay area. After nailing down the pins, a layer of teflon was put on the board and then the 7725 glass fabric was laid on top of it. Then the fiber roving was dry wound around the pins in an orthogonal fashion. In other words, no resin was used along with the fiber for the weaving process. The fiber weaving pattern and the finished grid stiffened sandwich structure can be seen in Figure 32. The smart syntactic foam was then prepared and poured into the bay area. The smart foam consisted only of the glass microballoons and the SMP. The MWCNTs were not included because the foam with nanotubes and glass microballoons did not perform better than the foam with the glass microballoons only. Hence the

time involved in fabrication of the smart foam was reduced considerably as well. The next step involved placing the top skin (7725 glass fabric) and closing the whole system with a vacuum bag (Airtech). After running the vacuum for about 15minutes the system was transferred into an industrial oven for curing at 79.4^{o}C for 24 hours, followed by a cycle at 107.2^{o}C for 3 hours and 121.1^{o}C for 6 hours to complete the total curing procedure. This modified curing cycle was used to avoid excessive heating of the specimen in the oven at the higher temperature and thereby resulting in loss of the foam due to its highly volatile nature.

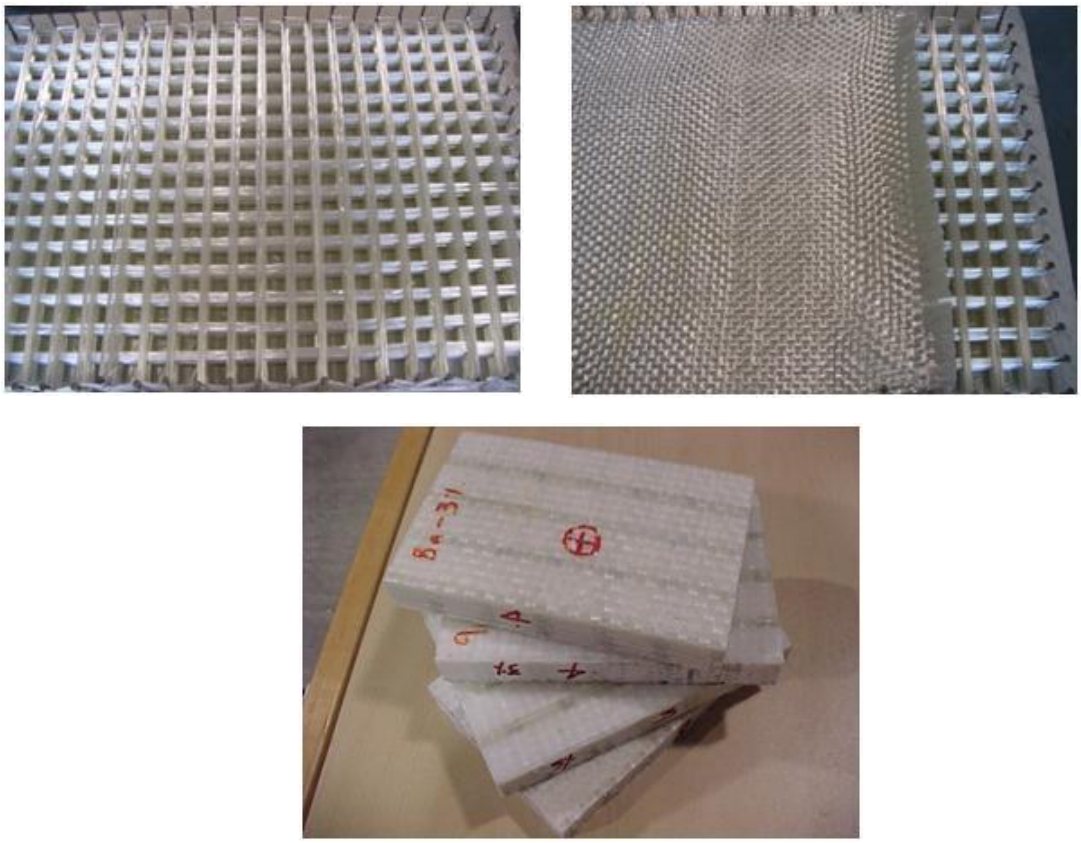

Figure 32. Grid weaving, fabrication and finished grid stiffened sandwich structure

A total of 17 different groups of specimens depending on the 2 prestrain levels of programming, 2 types of confined recovery, 2 impact energy levels, and 7 rounds of impact/healing cycles were fabricated, tested and analyzed. Each group contained at least 5 effective specimens. The total number of effective specimens was 105. The nomenclature used

for each group of specimens is as follows: NP means control specimens without programming; P means control specimens after programming; C1 means compression after first round impact; C1FR1 means compression after first round impact and first round 2-D confined recovery (or 'free recovery (FR)' without external confinement); C1CR1 means compression after first round impact and first round 3-D confined recovery (or 'confined recovery (CR)'); C3FR3 means compression after third round impact and third round 2-D confined recovery; C3CR3 means compression after third round impact and third round 3-D confined recovery; etc.

5.3 Thermomechanical Programming

In order to make the sandwich smart, they were subjected to a thermomechanical programming cycle. A compression molding fixture with a top platen and a bottom platen was employed for the programming process. The top platen is fixed and the bottom platen was moved with the help of a lever. The top and bottom platens were heated separately with different control knobs. The specimen was first inserted between the two platens. Then the platens were heated until the temperature reached 79.4^{o}C (above the T_g of the SMP-62^{o}C). Once the temperature in the specimen became uniform; it was compressed to the designed displacement (depending on the prestrain levels) by moving the bottom platen up. The displacement was measured with the help of an LVDT (Cooper Instruments LDT 200 series) system, which has a stroke length of about 3 inches attached to the top platen and measured the movement of the bottom platen. The displacement was recorded on a Data Chart 2000 series data acquisition system. The recorded data was post-processed to an ASCI file for analyzing the data. Once the specimen was compressed at 79.4^{o}C to the designed prestrain level, the heating was stopped and the platens were allowed to cool down to room temperature while maintaining the prestrain constant (strain controlled programming). Once room temperature was reached, the platens were released and the

strain-controlled programming was completed. In this study, two prestrain levels, 3% and 20%, were used to program the specimens, respectively. The purpose was to investigate how the prestrain levels affect the healing efficiency. Also, these two strain levels resided on the linear elastic region and plateau region of the foam, respectively. The programming setup is shown in Figure 33.

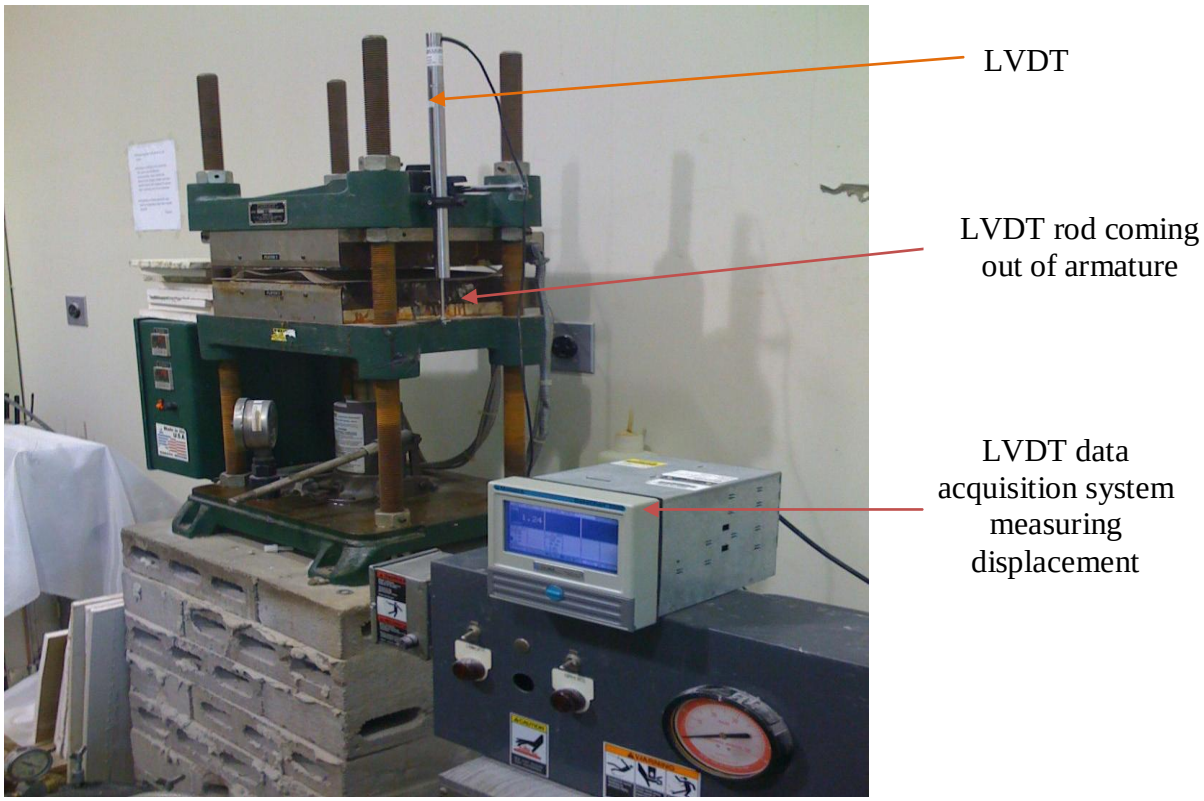

Figure 33. LVDT setup for Thermomechanical Programming

5.4 Low Velocity Impact (LVI) Tests and Self-Healing

Except for control specimens, low velocity impact tests were performed on each programmed specimen at the same impact location (center of the specimen) repeatedly using an Instron Dynatup 8250 HV drop tower machine. The tup nose is semi-spherical with a radius of 12.5mm. The impact velocity was respectively 3 m/s and 4m/s with a hammer weight of 6.64 kg, leading

to impact energy of 30J and 53J. The test was conducted per ASTM D 2444 at room temperature. For each impact at least five effective specimens were tested and the load and energy traces were obtained. The maximum impact force, maximum deflection, and impact duration were directly obtained from the load and energy traces. The initiation energy and propagation energy were calculated based on the traces.

The recovery/healing for the grid stiffened sandwich structures were done following 2 routes. After each impact, one set of the specimens was brought to an oven for shape recovery (2-D confined recovery/healing) at a temperature of 121.1°C for 3 hours. Another set was healed in a 3-D constrained way. This was performed in the same compression molding equipment with both the top and bottom platens heated to the required temperature and both of them were in contact with the specimen thereby preventing free recovery. This setup will make the specimen recover in a 3-D confined way. The same process of impact and healing was continued until 7 rounds.

Impact energy is dissipated in terms of energy transfer (elastic strain energy and kinetic energy), energy absorption (through damage and plastic deformation), temperature rising, and sound. Usually, energy transfer and energy absorption constitutes a major part of energy dissipation. In some cases with perforation, energy absorption through temperature rising is considerable. As for the energy dissipation through sound, the amount of energy consumed is minimal. It is noticed that the energy transfer and energy absorption can be obtained through the energy traces in terms of initiation energy and propagation energy.

5.4.1 Low Energy Impact (30 J)

The temperature profile immediately before and after impact of the smart sandwich specimen is shown in Figure 34 (a) and (b), respectively. It can be noticed that, with an incident energy of 30J, the maximum temperature rising is only 2.5^{o}C. This temperature is not sufficient to trigger

the phase change in the smart polymer because the temperature immediately after impact (24.8^{o}C) is still much lower than the glass transition temperature of the SMP (62^{o}C), suggesting that the orthogrid stiffened smart foam under impact is still in its glassy state.

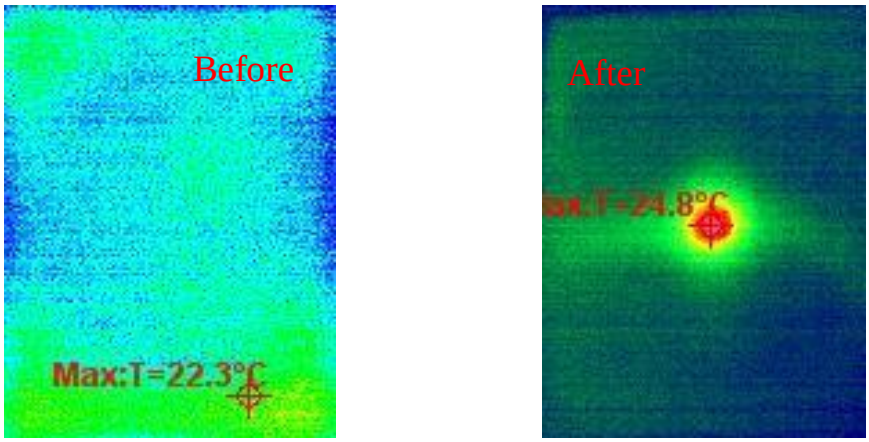

(a) (b)

Figure 34. Infrared image showing temperature profile of smart sandwich specimen (a) immediately before impact and (b) immediately after impact

Figure 35 (a) and (b) shows the effect of 7 rounds of impact and healing on the maximum load, initiation energy and propagation energy obtained from the LVI tests for 3% and 20% programmed specimens, respectively. The error bar represents standard deviation. The effect of different levels of prestrain programming can be visualized. From Figure 35(a), the maximum impact load for the 3% programmed specimen is constant within the experimental errors after 7 rounds of impact and healing. This suggests that the recovery process (both 2-D and 3-D) employed was able to effectively heal the damage induced due to each cycle of impact. On the other hand, the initiation energy keeps increasing until the 4th round of impact and then is a constant until the 7th round. The propagation energy follows exactly the opposite trend when compared with the initiation energy. These LVI results strongly support the claim that the load carrying capacity is effectively recovered and better healing efficiency has been achieved. The impact behavior for the 20% prestrained specimen also follows a similar trend. However, it is

found that the maximum impact load for the 20% prestrained specimen (7.27 kN) is about 17% higher than its 3% counterpart (6.22 kN). This suggests that the increase in the prestrain level enabled an increase in the load carrying capacity of the sandwich structure.

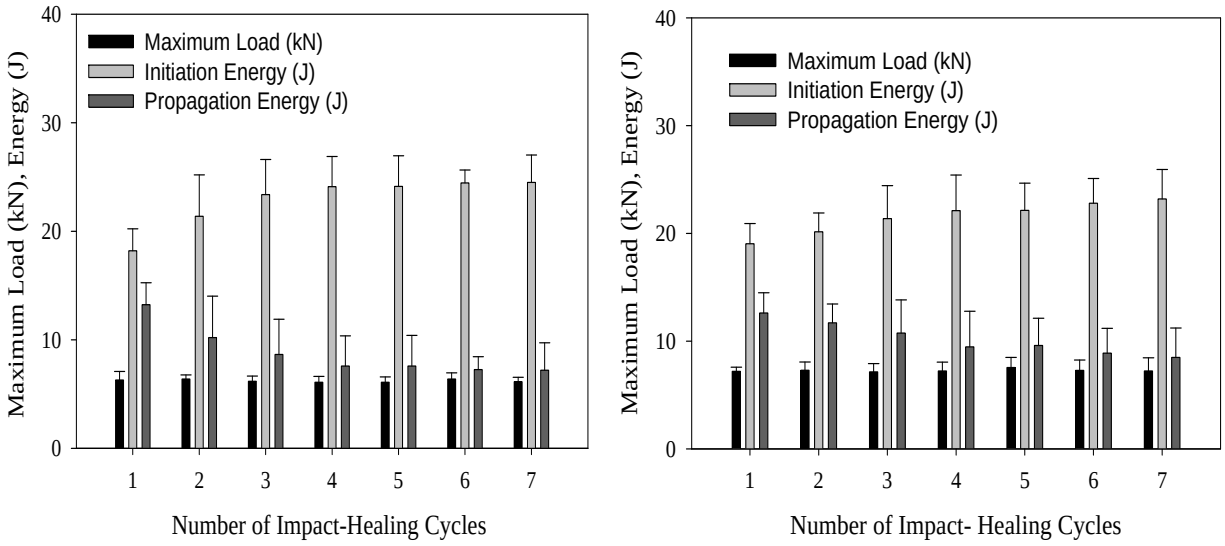

(a) Programmed 3% prestrain (b) Programmed 20% prestrain

Figure 35. Effect of programming strain levels on the impact responses

Table 3 summarizes the deflection at peak load, initiation energy, propagation energy, total energy and total time for the 3% prestrained, 30 Joules impacted grid stiffened sandwich structure for seven cycles of impact and healing. From Table 3, it can be seen that the deflection at peak load increases from the first impact until the third impact-healing cycle and then remains more or less a constant till the end of the seventh round of impact. Table 4 summarizes the deflection at peak load, initiation energy, propagation energy, total energy and total time for the 20% prestrained sandwich specimen impacted at 30 Joules of energy for seven impact healing cycles. From both tables it can be seen that the deflection at peak load increases as the impact cycles increases, showing the specimen is undergoing more damage.

Table 3. Low Velocity Impact Results of 3% prestrained sandwich impacted at 30 Joules

Number of Impact Cycles	Deflection at Peak Load (mm)	Maximum Load (kN)	Initiation Energy (J)	Total energy (J)	Propagation Energy (J)	Total Time (ms)
1	4.13	6.29	18.20	31.42	13.22	4.87
2	5.61	6.38	21.38	31.58	10.20	5.19
3	6.20	6.17	23.38	32.02	8.65	5.26
4	6.19	6.08	24.11	31.70	7.59	5.27
5	6.27	6.09	24.13	31.71	7.58	5.13
6	6.15	6.39	24.45	31.70	7.26	4.93
7	6.21	6.13	23.96	31.56	7.60	5.04

Table 4. Low Velocity Impact Results of 20% prestrained sandwich impacted at 30 Joules

Number of Impact Cycles	Deflection at Peak Load (mm)	Maximum Load (kN)	Initiation Energy (J)	Total energy (J)	Propagation Energy (J)	Total Time (ms)
1	4.26	7.20	19.04	31.64	12.61	4.44
2	4.75	7.29	20.14	31.84	11.70	4.70
3	5.11	7.15	21.36	32.11	10.75	4.77
4	5.22	7.22	22.79	31.67	8.89	4.83
5	5.10	7.54	22.11	31.71	9.60	4.49
6	5.19	7.29	23.20	31.68	8.48	4.57
7	5.27	7.23	22.13	31.61	9.47	4.66

On the other hand, the consistency in the peak load shows that most of the damage has been recovered effectively by the healing process employed. The deflection at peak load from Table 4 indicates an increment from impact cycle 1 until impact cycle 3. This follows a similar trend as for the 3% prestrained specimen. After the 3rd cycle, the deflection is more or less a constant. Also the deflection values of the 20% prestrained specimen are less than that of the corresponding 3% prestrained ones. This shows that the 20% prestrained specimen were capable of taking equivalent loads to the 3% prestrained specimen with less deflection.

A better visualization of the aforementioned results can be seen in Figure 36. Figure 36 shows a typical load and energy versus time plot for the 3% and 20% prestrained specimen after the first round of impact. It can be seen that the 20% prestrained specimen shows a higher load when compared with its 3% counterpart.

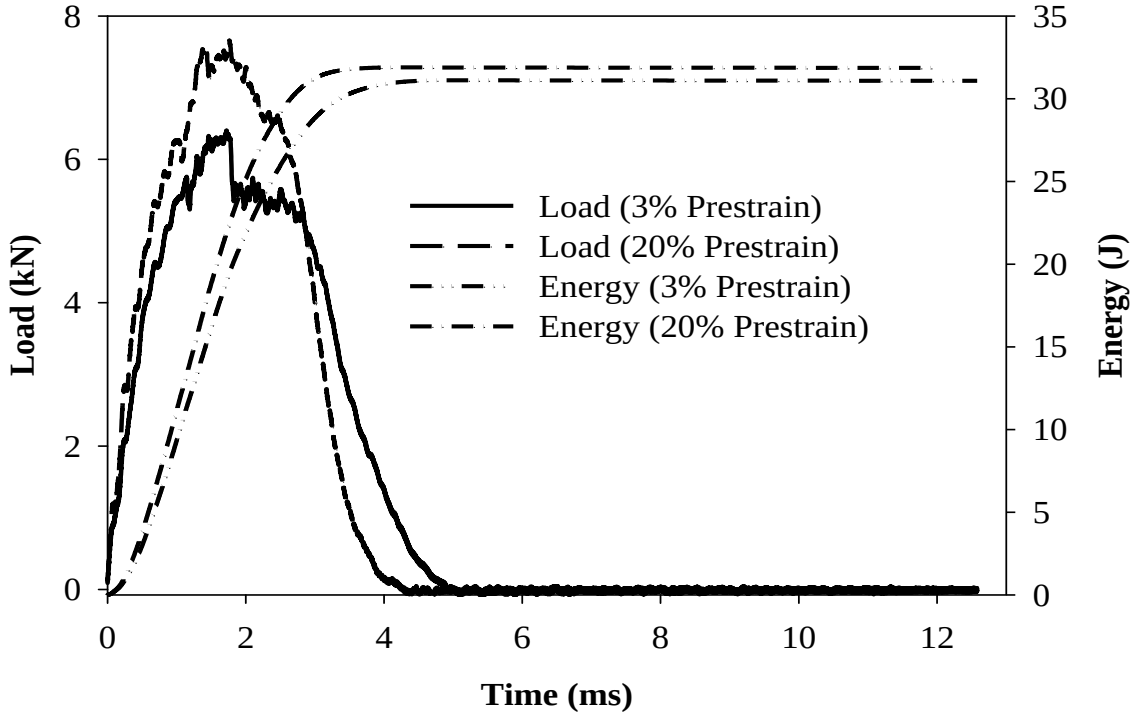

Figure 36. Load and Energy versus time plots for 3% and 20% prestrained sandwich

This fact was emphasized in Figure 35 and is more clearly evident from the typical load and energy versus time plots in Figure 36.

5.4.2 High Energy Impact (53 J)

In order to evaluate the effect of impact energy or the degree of damage on the self-healing efficiency, a higher impact energy (53J) impact test was also conducted. Because it was found that specimens programmed by 20% prestrain and recovered under 3-D confinement had better healing efficiency than specimens programmed by 3% prestrain and recovered under 2-D confinement as discussed in 5.4.1, only specimens programmed by 20% prestrain and recovered under 3-D confinement was tested by the higher energy impact.

Figure 37 shows the effect of higher energy impact on the maximum impact load, initiation energy and propagation energy of 20% programmed and 3-D confined specimens. The error bars represent the standard deviation. It can be noted that the maximum impact force reduced from 8.11 kN for the first impact cycle to 6.71 kN for the 7^{th} impact cycle. This reflects a decrease in the load bearing capacity by about 17%. Also, the initiation energy was almost constant and the propagation energy decreased slightly as the impact/healing cycle increased. This is again an indication of the reduction in the load bearing capacity due to impact by a higher energy. The slight reduction in propagation energy suggests that the healing efficiency was decreasing as the impact cycle increased, because the foam that was not fully healed could not further absorb impact energy through damage. These findings will be further validated in section 5.6.

Table 5 summarizes the deflection at peak load, maximum load, initiation energy, propagation energy, total energy and total time from the low velocity impact tests until seven rounds at 20% prestrain and 53 Joules of energy.

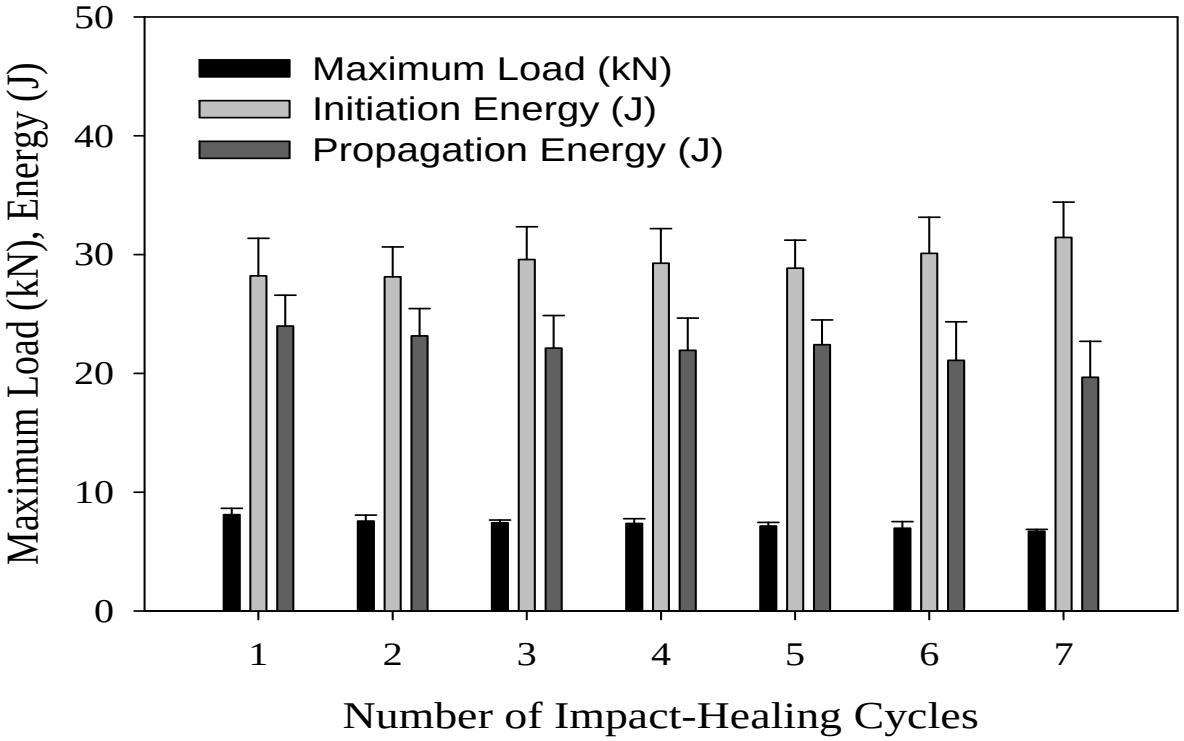

Figure 37. Effect of 7 rounds of impact-healing cycles on the maximum impact load (kN), initiation energy (J), and propagation energy (J)

From Table 5 it can be seen that the deflection at peak load increases with the number of impact cycles. It can be noticed that the 20% prestrained specimen impacted at a lower energy (30J) had less deflection when compared with the 20% prestrained specimen impacted at higher energy (53J). Thus the sandwich panels impacted at the higher energy (53J) resulted in more damaged regions when compared with the ones impacted at a lower energy (30J).

The corresponding load and energy versus time plots for the first and seventh rounds of impact are depicted in Figure 38 to show the reduction in peak load after the seventh round of high energy impact. There is a considerable reduction in the peak load for the 7^{th} impacted specimen when compared with the 1^{st} one. This could be due to partial healing resulting in absorption of less impact energy.

Table 5. Low Velocity Impact Results of 20% prestrained sandwich impacted at 53 Joules

Number of Impact Cycles	Deflection at Peak Load (mm)	Maximum Load (kN)	Initiation Energy (J)	Total energy (J)	Propagation Energy (J)	Total Time (ms)
1	5.49	8.11	28.21	52.19	23.98	4.65
2	5.68	7.56	28.12	51.28	23.15	4.71
3	6.03	7.42	29.58	51.70	22.12	4.85
4	6.12	7.15	29.26	51.19	21.93	4.91
5	6.62	7.37	28.86	51.26	22.41	4.75
6	6.96	6.97	30.09	51.17	21.09	5.11
7	7.01	6.71	31.44	51.10	19.66	4.95

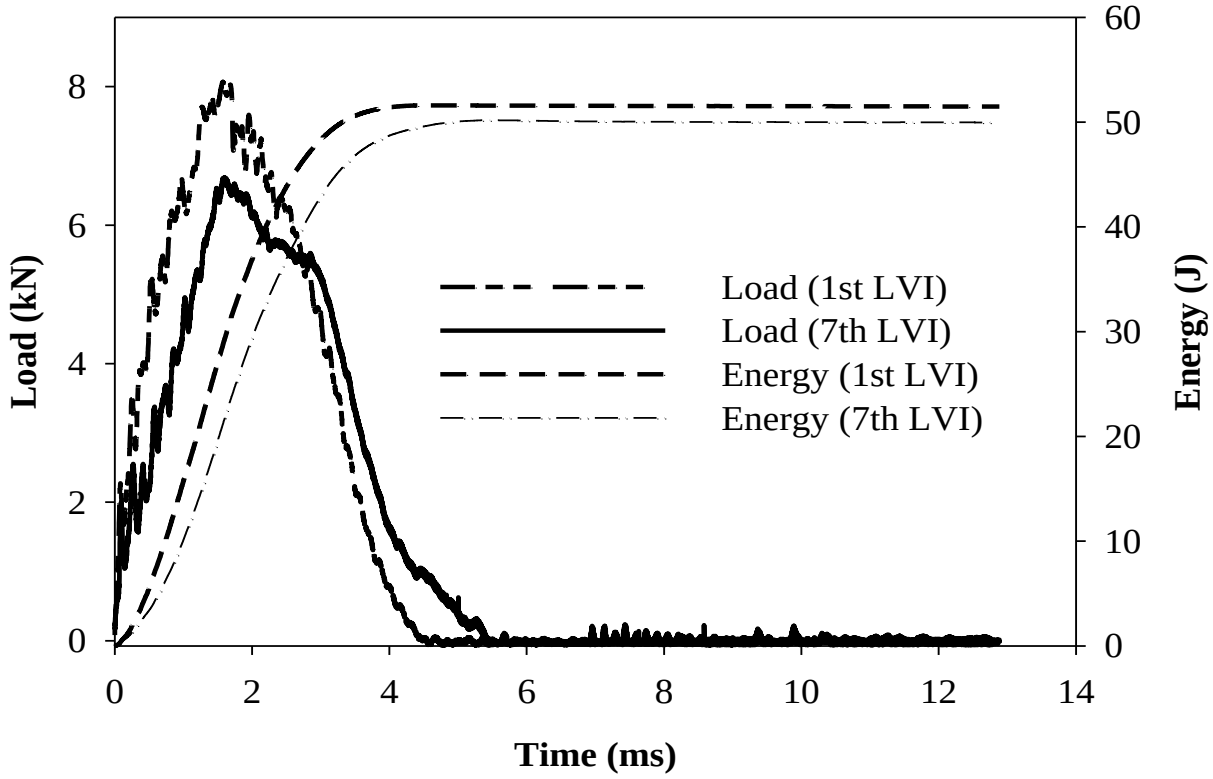

Figure 38. Load and Energy versus Time plots for 53 Joule impacted sandwich

5.5 Wave Propagation during Impact in Grid Stiffened Sandwich

In this study, the claim from the previous work [54] that the orthogrid stiffened foam cored sandwich responds to impact quasi-statically was validated by analyzing the wave propagation within the bay directly under impact during the impact event. One strain gage was attached along one of the boundary ribs of the bay directly under impact and the other diagonally on one of the nodes of the selected bay; see Figure 39 (a). The strain gages were in turn connected to a strain gage conditioner (Vishay Micro-measurements). The strain gage conditioner was programmed such that 1 mV of voltage was equivalent to 1με. The signal from the strain gage conditioner was amplified with the help of an oscilloscope and the oscilloscope was in turn connected to a laptop which monitored both the strain gage channels using a Wavestar software package. The data were saved and analyzed as an ASCI file. Figure 39 (b) shows the sandwich specimen attached with the gages and the data acquisition system.

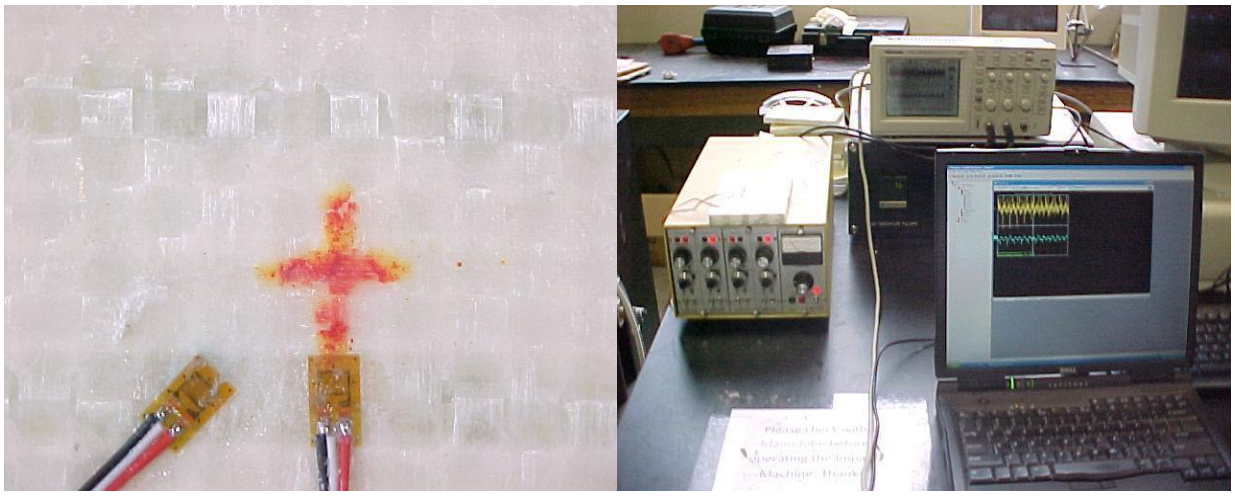

(a) Strain Gages attached (b) Waveform measurement setup

Figure 39. Strain gages attached to the sandwich with strain gage conditioner and oscilloscope

Figure 40 shows the wave propagation along the boundary rib of the bay. The waveform from the strain gage attached diagonally on the node did not show any change during the impact event,

possibly due to the debonding of the strain gage from the sandwich under impact. Therefore, the data from the second strain channel is not shown here. From the impact data, the impact duration was about 4.7 milliseconds for this gauged specimen. The wave propagation during the impact can be easily identified by the voltage/strain peaks for the first 4.7 milliseconds. It is found that there are two crests and two troughs during this time period, which suggests that the impact wave reached and was reflected by the boundary of the bay directly under impact twice. Therefore, it is concluded that the impact response of the bay directly under impact is boundary controlled and it is quasi-static. This validates the previous claim in [54]. The change in voltage of the wave form due to impact is zoomed in and shown in the inset picture for better visualization.

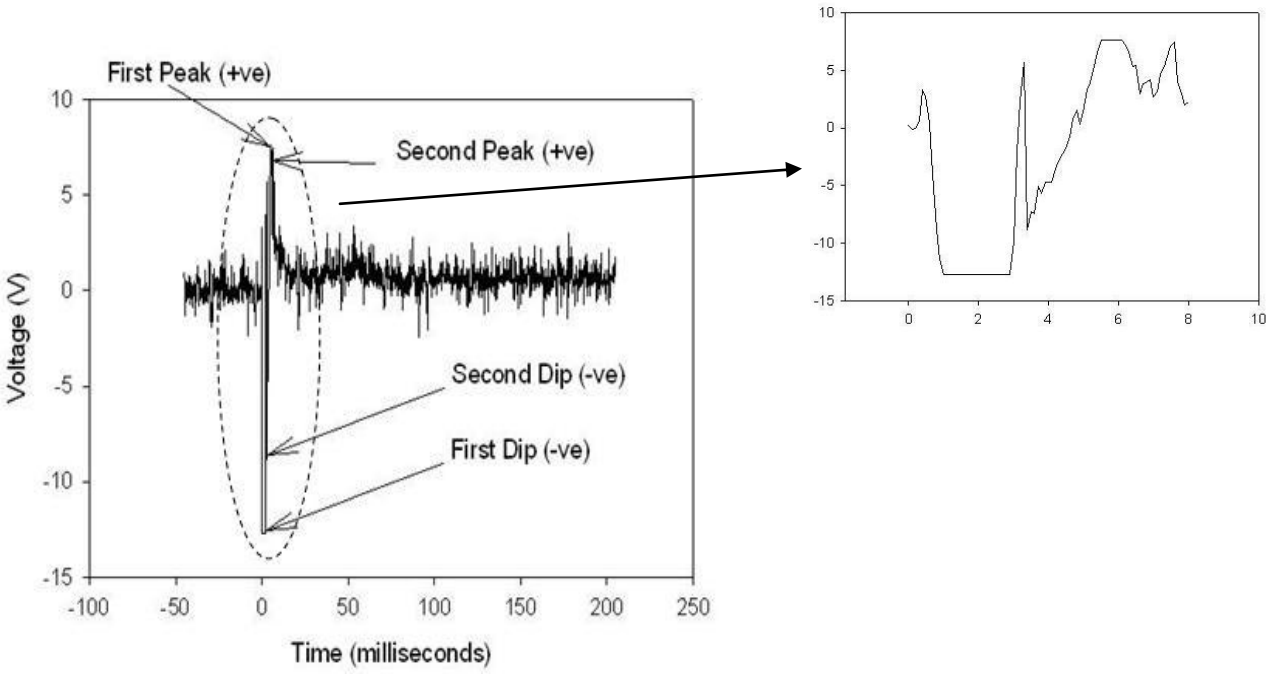

Figure 40. Wave propagation within the bay area of the sandwich specimen

5.6 Compression After Impact (CAI)

Compression after impact (CAI) test was conducted to evaluate the residual strength after impact and the healing efficiency after confined shape recovery. Specimens without

programming and programmed specimens without impact were also tested as control. The testing was conducted using an MTS Q TEST 150 machine and the fixture used was a "Boeing Compression after Impact Compression Test Fixture" per BSS7260 standard. A strain controlled testing mode experiment was conducted at room temperature and the loading rate was 1.3 mm/min.

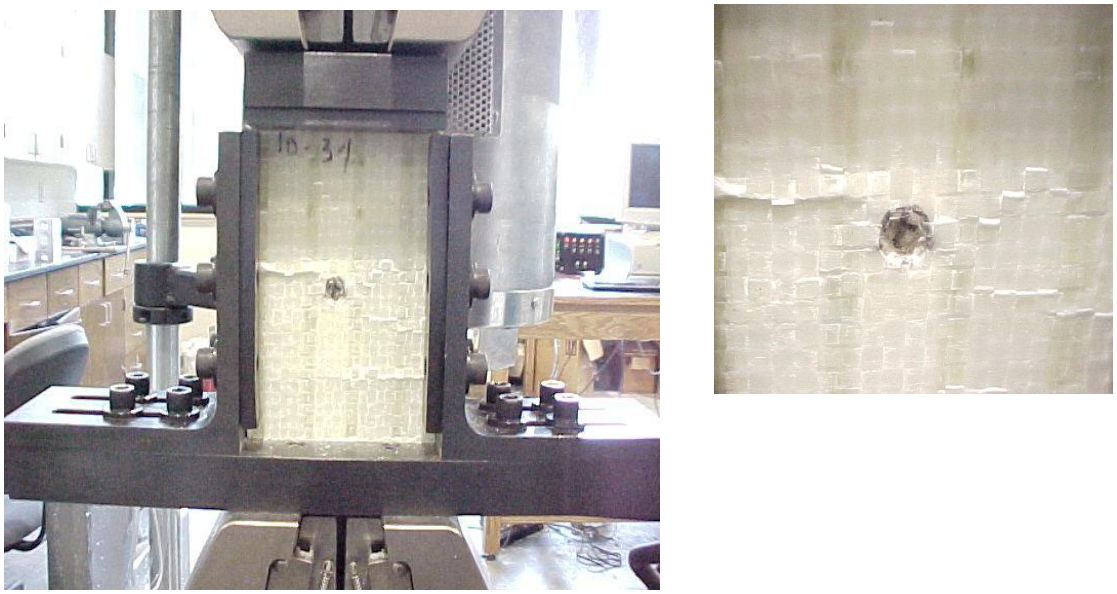

Figure 41. Compression After Impact setup for 3% prestrained sandwich specimen

5.6.1 Low Energy Impact (30 J)

The compression after impact test setup for the grid stiffened smart foam sandwich structure is depicted in Figure 41. The inset shows a clearer picture of the damage at the impact location.

The different modes of failure of the impacted and healed sandwich structures during compression tests were visually identified by capturing digital images. Figure 42 shows a series of pictures captured at different intervals during the compression tests of the programmed sandwich structure subjected to impact and Figure 43 depicts the corresponding compression test images of the programmed sandwich structure that was impacted and healed in a 3-D constrained

manner. From Figure 42, it can be seen that for the impacted sandwich specimen, damage starts to propagate from the impact location and the damage gets more severe with progress of time. The direction of the arrows depicts the sequence of the damage in the specimen during the compression tests.

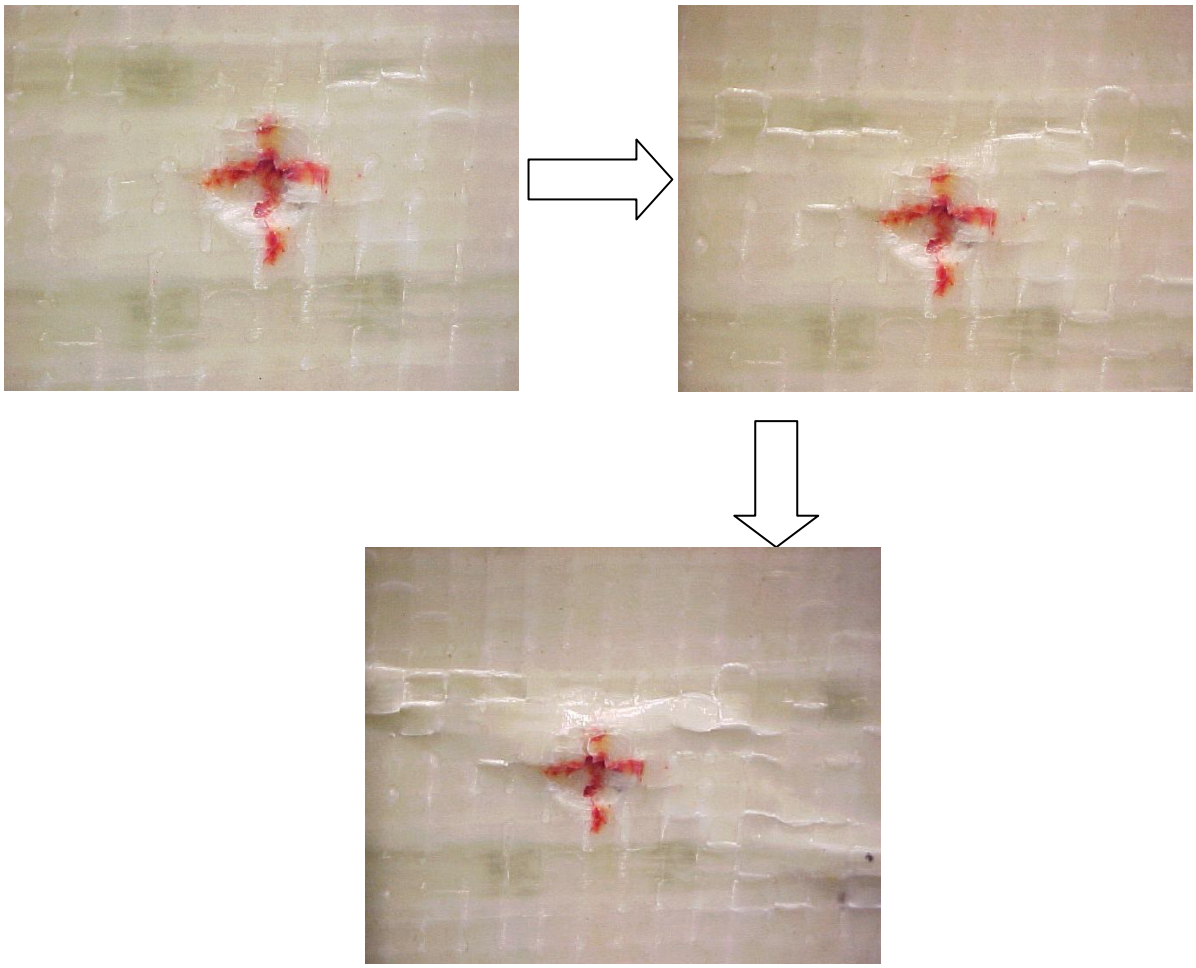

Figure 42. Failure modes of sandwich specimen subjected to compression after impact

On the other hand, from Figure 43, it can be noticed that even though the damage is initiated somewhat close to the impact location for the impacted and healed specimen, it doesn't grow drastically when compared with the impacted specimen that was not healed. This fact is further substantiated with compressive strength values in the upcoming sections. Hence it can be

concluded from these images that the 3-D constrained recovery process helped in healing the damage due to impact and also regaining the strength of the structure.

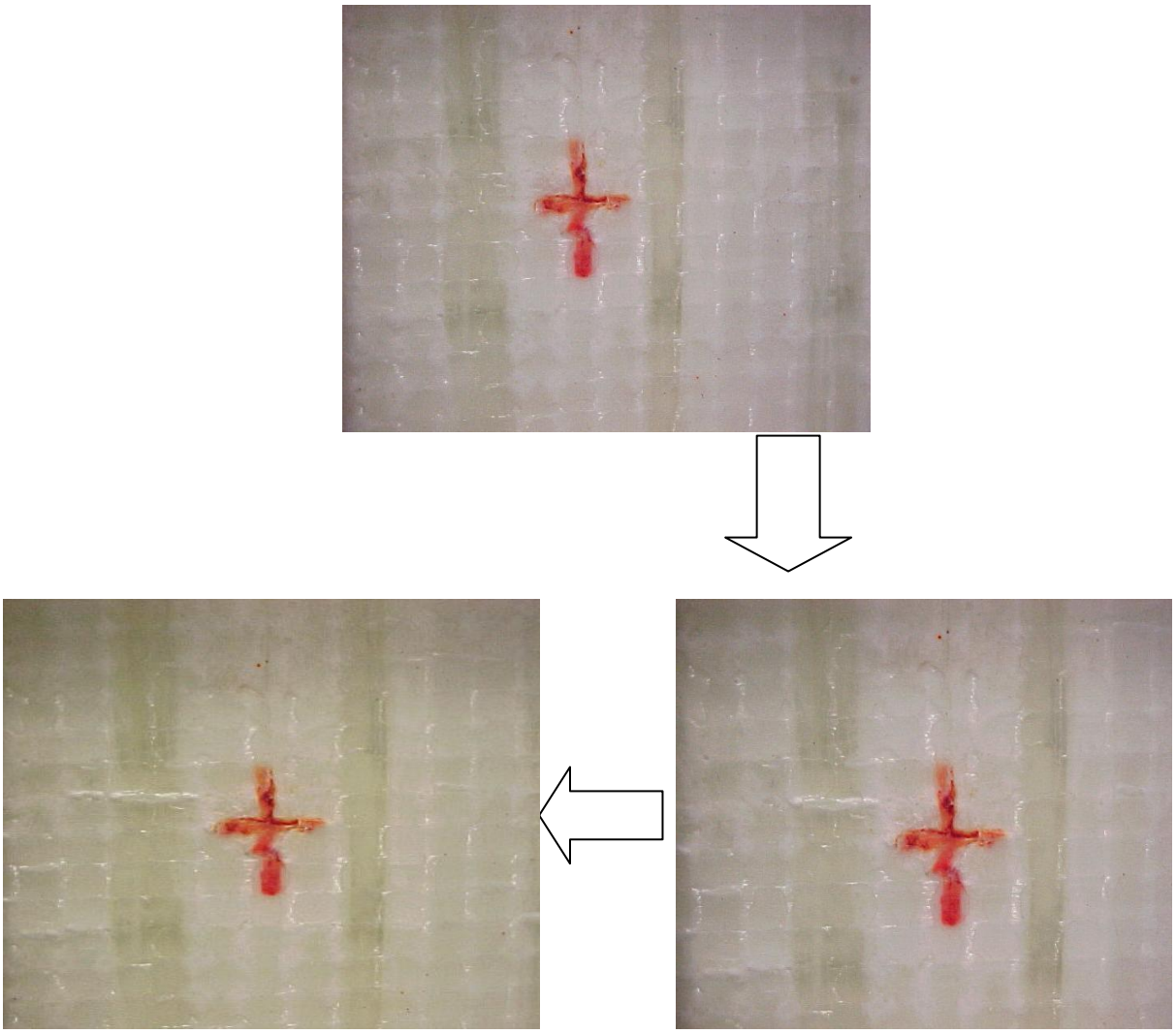

Figure 43. Failure modes of sandwich specimen impacted and healed subjected to compression

Figure 44 shows the effect of one round of impact on the programmed sandwich, and the healing efficiency of the 2-D (free) recovery and 3-D (constrained) recovery process on the compressive strength of the sandwich. Figure 44 (a) depicts the case for the 3% prestrained specimen. It can be noticed that after the first impact, the compressive strength of the sandwich

(20.12 MPa) reduces by about 15% when compared with the programmed unimpacted specimen (23.21 MPa). On the other hand, after both 2-D and 3-D recovery the sandwich regains 100% of its compressive strength. Also, there is a slight increase in the strength regained for the 3-D recovered sandwich. A similar trend can be noticed for the 20% prestrained specimen in Figure 44 (b). However, the reduction in compressive strength for the 20% prestrained sandwich (22.72 MPa) was only 4% of the programmed unimpacted specimen (23.63 MPa). This shows that the 20% prestrained specimen was capable of containing the damage and thereby improving the residual strength after recovery. Also, the programming made the foam denser, resulting in a more stiff structure.

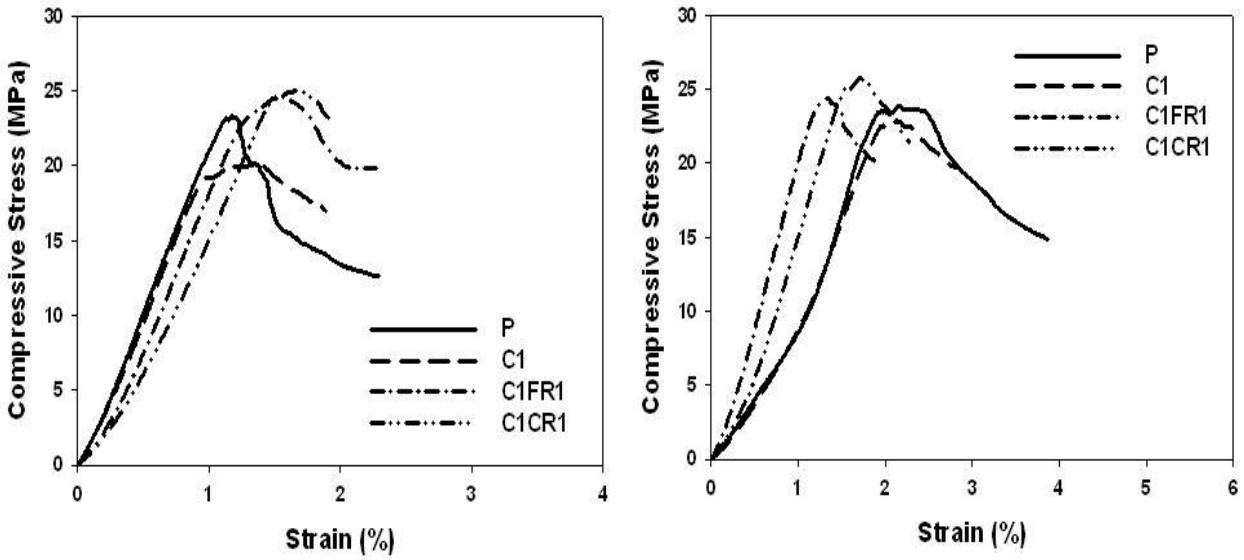

(a) 3% prestrained (b) 20% prestrained

Figure 44. Compressive Stress-Strain Plots for different prestrains

Figure 45 (a) and (b) shows the effect of the prestrain levels during programming and the confinement levels during shape recovery on the CAI strength. From Figure 45, the following observations can be made: (1) programming itself increased the compressive strength of the

sandwich when comparing specimens NP with specimens P. This is due to the densification of the specimens by the strain-controlled programming. (2) As expected, impact reduced the CAI strength of all the specimens due to the creation of impact damage. (3) Specimens programmed by 20% prestrain consistently shows a higher CAI strength than those programmed by 3% prestrain, regardless of the impact/healing cycles. Again, this is because 20% prestrain made the specimen denser and thus stiffer and stronger. (4) Specimens healed under 3-D confinement consistently shows a higher CAI strength than those healed under 2-D confinement, again regardless of the impact/healing cycles.

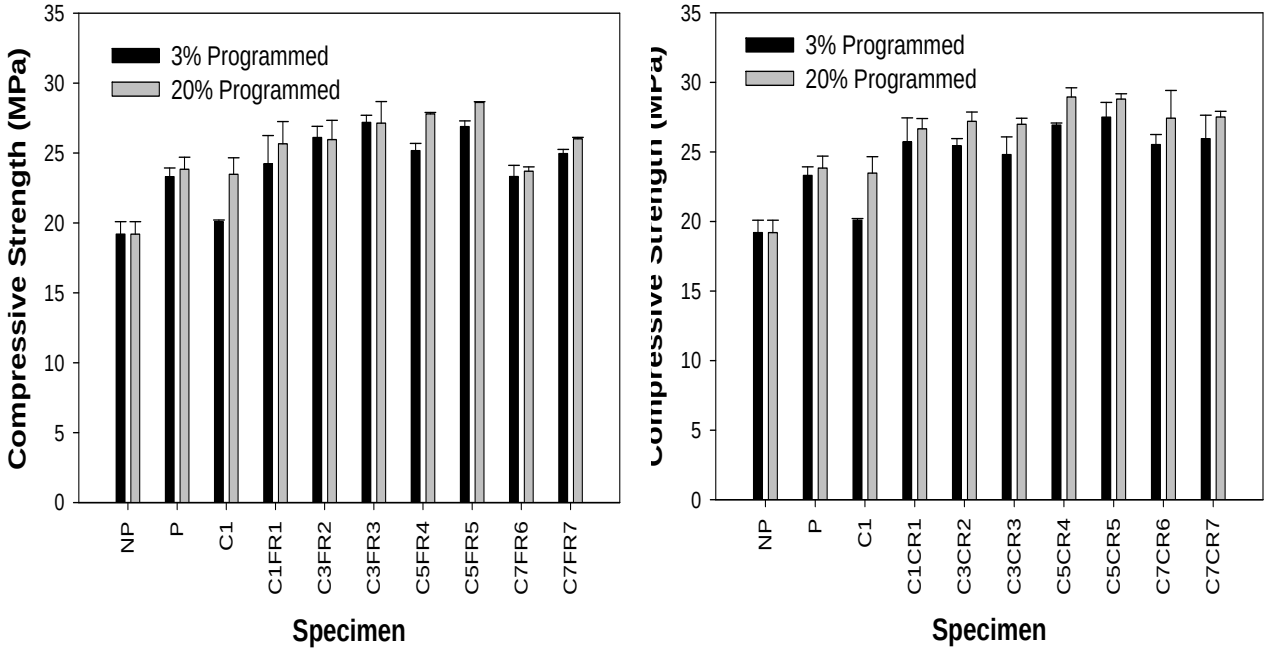

(a) 2-D confined (b) 3-D confined

Figure 45. Effect of Programming and Recovery methods on the Compressive Strength of the Sandwich Structure

This is because 3-D confinement resisted the growth in the specimen volume more effectively during the shape recovery process; consequently, the crack within the specimen was narrowed or closed more effectively. (5) For each impact/healing cycle, the CAI strength shows some

increases as compared to the control specimens without impact and without programming (P and NP). This fact is desired as it makes the sandwich stronger after healing. This may be due to the adjustment of the microstructure during the impact/healing cycles, which can be validated by the C-scan results later.

5.6.2 High Energy Impact (53 J)

Figure 46 shows the compressive stress versus strain plots for the 20% prestrained specimen subjected to 53J of impact. As expected, high impact energy resulted in more damage in the sandwich specimens.

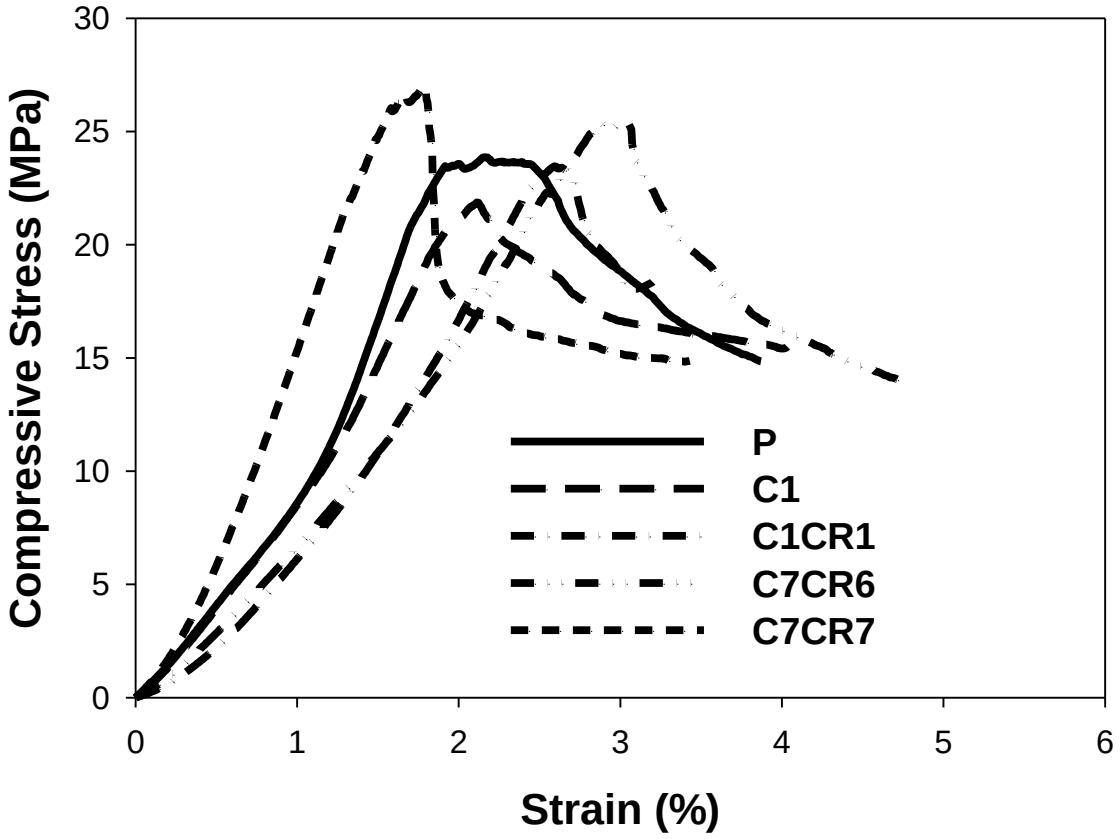

Figure 46. Compressive Stress versus Strain Plots for 20% prestrained and 53 J Impacted specimens

After the first impact, the residual strength of the sandwich is about 21.87 MPa as compared to 23.84 MPa for the programmed unimpacted specimen. This is a reduction of about 8.3%. After the first 3-D confined recovery, the specimen regains 100% of the compressive strength. In fact, after the 7th impact and healing, the residual strength (26.88 MPa) has increased. This can be attributed to the change in microstructure as seen from the C-scan images in section 5.7. A more detailed study on the effect of post curing on the healing characteristics will be discussed towards the end of this section.

From Figure 47, the CAI strength of the specimens impacted by 53J of energy is consistently lower than that impacted by 30J of energy.

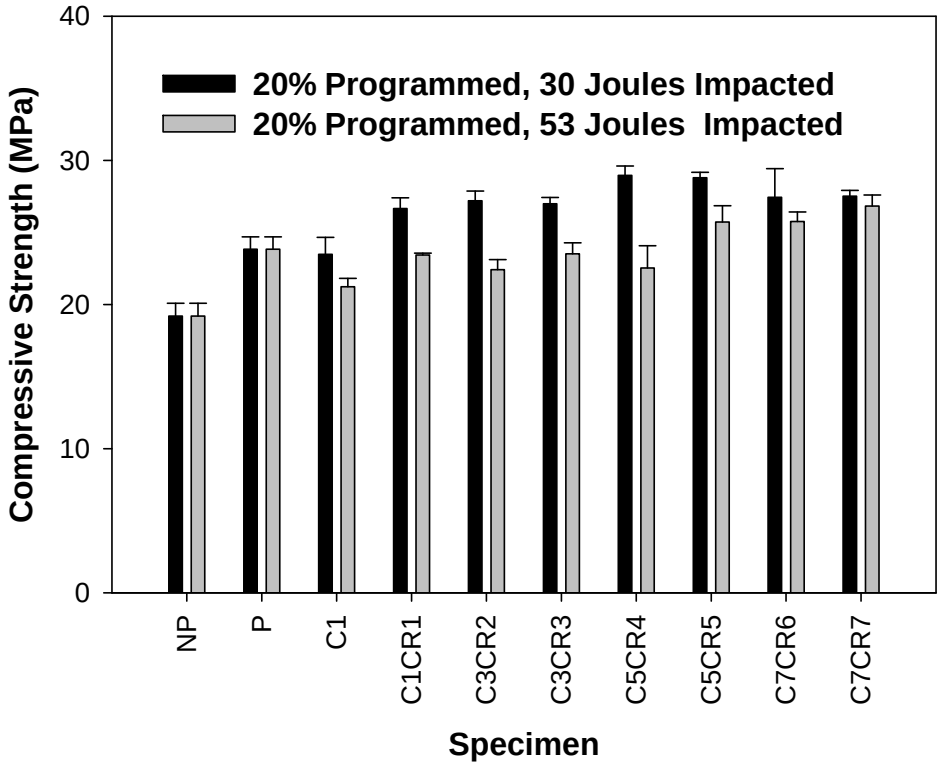

Figure 47. Effect of impact energy on the CAI strength of the sandwich structure

However, it is interesting to note that as the impact/healing cycle increases, the difference between the two types of specimens becomes smaller. Actually, at the 7th round of

impact/healing cycle, the CAI strength of the two types of specimens is very close. While the strength of the specimens after healing is slightly lower than that of the programmed control specimens (P) without impact and without healing for the first four impact/healing cycles, the strength of the healed specimens becomes slightly higher than that of the control specimens during the 5^{th}, 6^{th}, and 7^{th} impact/healing cycle, which is in agreement with the healed strength of specimens impacted by the lower energy (30J).

Thus it can be concluded that even though the higher energy impact resulted in more damage, the confined recovery was able to recover and enhance the strength of the sandwich. This claim of better healing efficiency for the 3-D constrained recovery specimen will be further validated by the Ultrasonic C-scan images and visual inspection of these sandwich specimens.

Before reporting the C-scan results, there is one question that needs to be clarified. As discussed in Chapter 4, the healing efficiency greater than 100% is due to the post-curing effect during the shape recovery process for each healing cycle. Therefore, it is quite obvious to ask the same question: is the healing efficiency greater than 100% due to the post-curing effect? To answer this question, uniaxial compression tests were also conducted to evaluate the variation of the compressive strength of the foam with the time period of the shape recovery. First, foam specimens cured following the normal curing cycle as mentioned in section 2.7 was fabricated. Compression specimens were then cut out of the big foam panel and transferred into an oven. The oven was maintained at a temperature of 121.1^{o}C. After every 3 hours a set of 4 specimens were taken out of the oven to simulate the 3 hours of shape recovery used for each healing cycle. This was continued until 21 hours corresponding to the 7^{th} healing cycle. The results of the post-cured foams are summarized in Table 6.

Table 6. Uniaxial compressive yield strength of the foam after post-curing up to 21 hours

Post curing time (Hours)	Compressive Strength (MPa)	Standard Deviation
0(regularly cured as shown in section 2.7)	20.22	0.49
3	19.50	0.53
6	19.67	0.50
9	19.79	0.24
12	19.36	0.39
15	19.45	0.30
18	19.52	0.56
21	19.41	0.15

It can be noticed that post-curing had negligible effect on the compressive yield strength of the foam specimen. Thus the effect of post-curing on the compressive strength enhancements for the healed specimens can be ruled out. In another word, the healing efficiency greater than 100% as reported in the CAI test is a fact.

5.7 Non-Destructive Ultrasonic C-scan Inspection

Ultrasonic inspection was performed on all specimens both after impact and after healing for each impact-healing cycle using a 2.5 MHz transducer for the grid stiffened sandwich respectively. An UltraPac inspection machine from Physical Acoustics Laboratory was used in conjunction with UltraWin software to acquire the C-scan images and identify damages. A typical C-scan image on the software that acquires the image is shown in Figure 48.

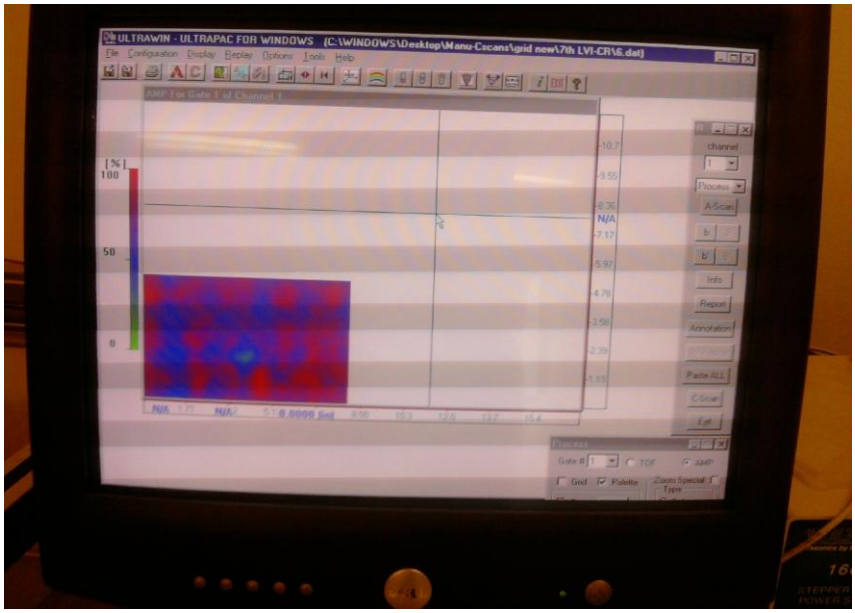

Figure 48. Ultrapac ultrasonic C-scan Image

Ultrasonic C-scan images of the sandwich structure impacted at 53 Joules were captured in order to investigate the impact damage and also to analyze the healing efficiency achieved. C-scanning was conducted on 2 different specimens: one was a 2-D confined specimen and the other was a 3-D confined specimen. This was to compare the healing efficiency achieved by employing 2 different routes of recovery. Figure 49 shows the C-scan images of the 2-D confined specimen before impact, after 1st impact, after 1st healing, until after 7th impact and 7th healing; and Figure 50 shows the corresponding C-scan images for the 3-D confined specimen. In these pulse-echo C-scan images, red color represents an excess of 80% of the signal returning to the receiver, whereas blue color indicates that 50–80% of the signal is being received. The green color indicates that less than 50% signal has been received by the transducer due to attenuation of the ultrasonic signal by damage. From Figure 49 it is seen that the damage area increases as impact cycle increases. Also, after the 2-D confined recovery, the damage is not fully healed as the green color region is reduced but did not fully disappear. From Figure 50, the

impact damage after each impact has been effectively healed by the 3-D confined shape recovery, as evidenced by the disappearance of the green color after each healing cycle.

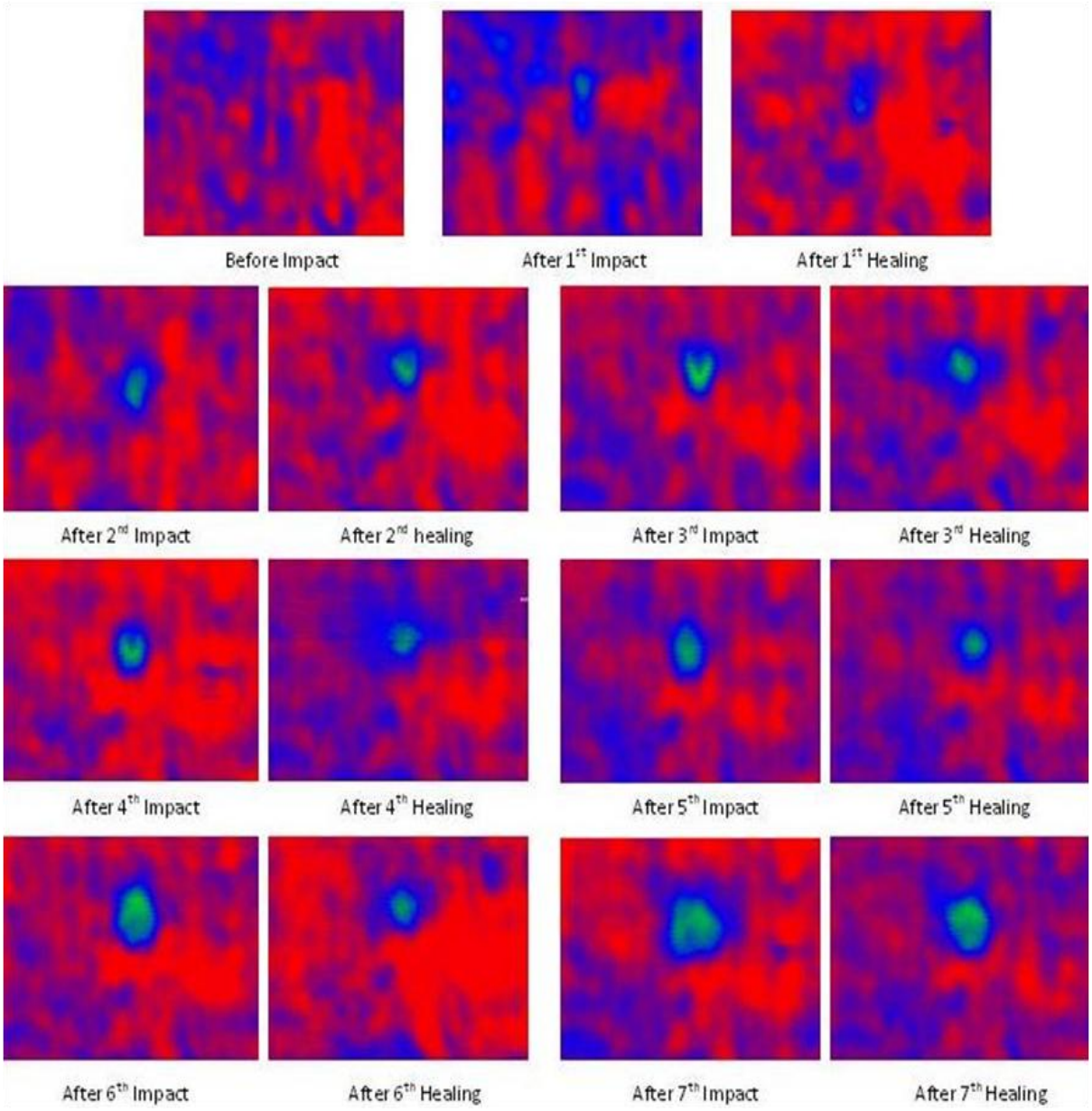

Figure 49. C-scan Images of the sandwich specimen after each impact and 2-D confined recovery

Also, it seems that the red color region becomes brighter or the reflected signal becomes stronger after each healing cycle, suggesting that the sandwich is actually becomes stronger. This is in agreement with the impact response and the CAI strength test results.

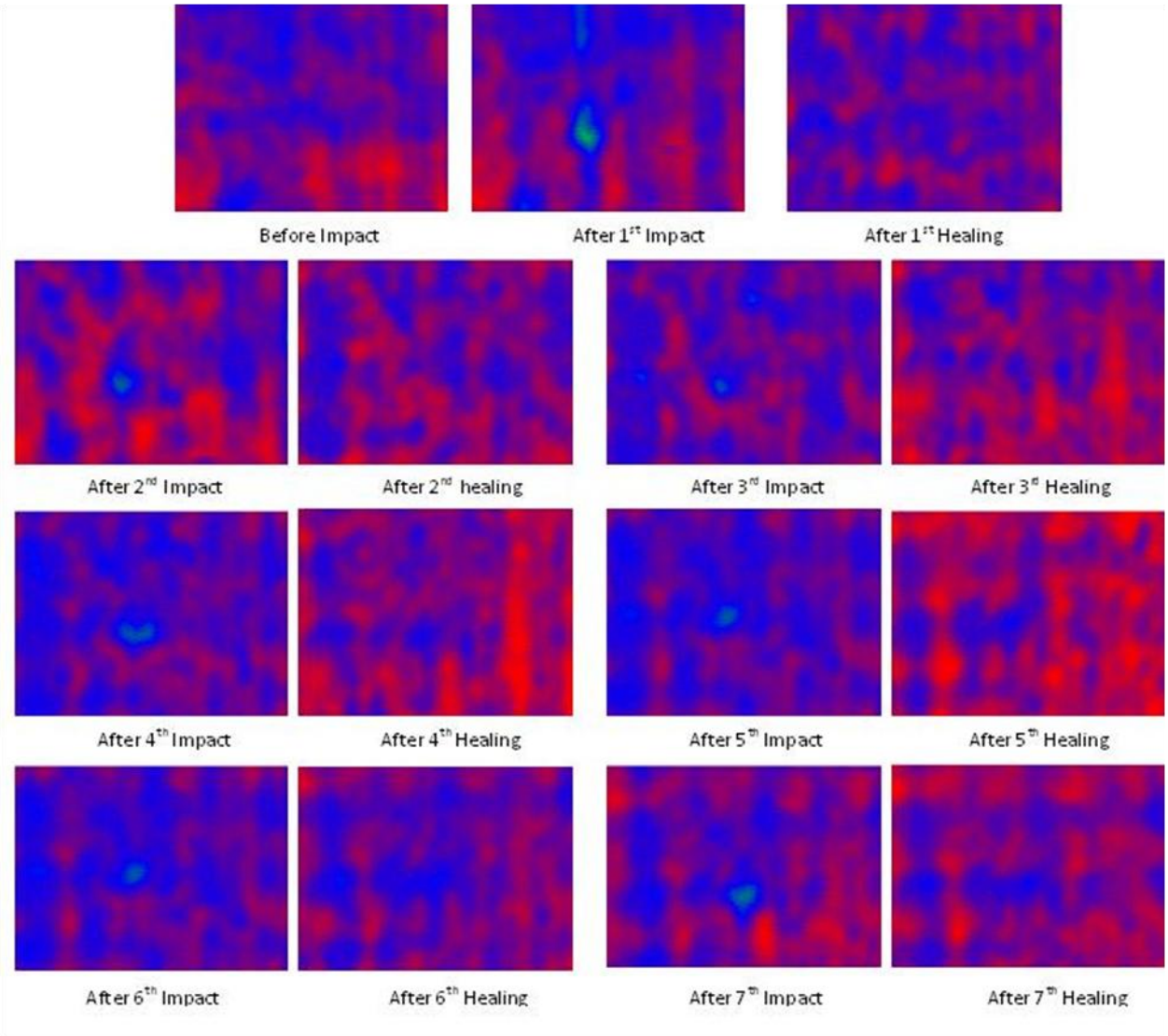

Figure 50. C-scan images of the sandwich specimen after each impact and 3-D confined recovery

This also is an indication of the change in microstructure of the foam during each healing cycle employed. Since there was lot of attenuation of the ultrasonic signals from the foam sandwich a clear distinct boundary of the ribs in the grid structure could not be visualized.

5.8 Visual Inspection

The above observations can also be echoed by visual inspection. After the 7th round of impact and healing cycle, optical microscopic images of the impacted/healed areas were captured. Figure 51 (a) and (b) shows the optical pictures for the 3% prestrained specimen and Figure 52

(a) and (b) shows the corresponding pictures for the 20% prestrained specimen. It can be clearly visualized that the healing efficiency of the 3-D constrained recovery specimen is almost 100%, while the 2-D confined specimen did not fully recover the impact damage on the surface of the sandwich.

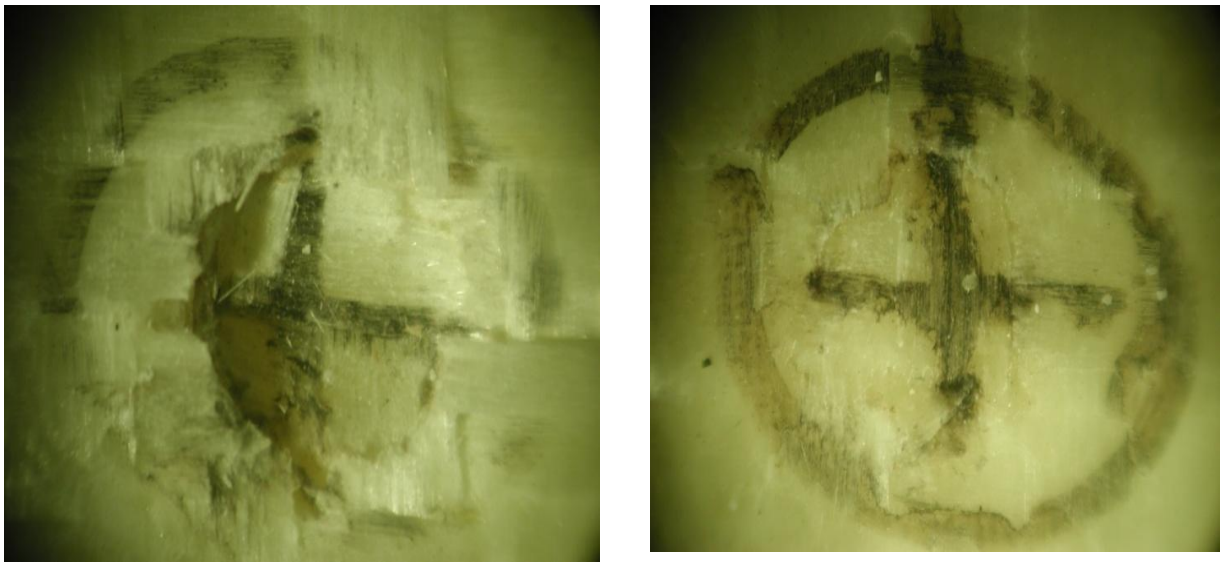

(a) After 7th LVI and 2-D recovery (b) After 7th LVI and 3-D recovery

Figure 51. Optical Microscopic images after 7th impact and healing of 3% prestrained sandwich

This is evidenced from the uniformity and continuity of the 3-D constrained recovery specimen (Figure 51 (b)) when compared with the 2-D confined specimen in Figure 51 (a). A similar trend in the recovery process can be visualized for the 20% prestrained sandwich specimen in Figure 52. From Figure 52 it can be seen that after the 3-D confined recovery process, the 20% prestrained specimen was able to recover more efficiently than the corresponding 2-D recovered sandwich specimen. These visual inspection pictures strongly support the efficient healing achieved for the 3-D confined sandwich specimen in the LVI and CAI tests, and C-scans.

(a) After 7th LVI and 2-D recovery (b) After 7th LVI and 3-D recovery

Figure 52. Optical Microscopic images after 7th impact and healing of 20% prestrained sandwich

CHAPTER 6. CONCLUSIONS AND FUTURE WORK

6.1 Conclusions

In this dissertation, an extensive literature review of the current syntactic foams and the foam cored sandwiches were first conducted in detail. It was concluded from this survey that the damage induced in these load-carrying structural components was on a macro-length scale and these type of damages inflicted in the structure was beyond repair or in some cases might result in large amounts of financial burdens associated with the repair work. It was also concluded that there is an urgent need to design systems that can account for this type of damages. Detailed review on the current healing schemes used in thermoset polymers which are used as a matrix in sandwich structures were also discussed in the introduction part. It was inferred that no existing self-healing scheme can satisfy all the requirements for self-healing structural length-scale damage, i.e., autonomously, repeatedly, efficiently and on a molecular length scale. Shape memory polymer based syntactic foam cored sandwich systems were suggested as a viable alternative to contain the drawbacks in the present self healing systems. It is envisioned that the development of SMP based syntactic foam cored and grid stiffened foam cored sandwiches will account for the drawbacks in the existing healing methods.

This research work was further subdivided into four subsections as detailed in chapters 2, 3, 4 and 5. Chapters 2 and 3 primarily detailed the fabrication, characterization and modeling of a smart shape memory polymer based syntactic foam core to be used in sandwich constructions. Chapter 4 gave the details of the fabrication, thermomechanical programming, impact and recovery, compression after impact testing, non-destructive testing and morphological analysis of the smart foam cored sandwich. Chapter 5 enumerates the fabrication, programming to two prestrain levels, impact and recovery under two confinement levels, compression after impact

testing, quasi-static response evaluation, non-destructive testing and visual inspection of the healing of a grid stiffened smart foam cored sandwich structure. The conclusions from each chapter are listed separately in the upcoming sections.

6.1.1 SMP Based Smart Syntactic Foam Core

The following conclusions are obtained from the detailed characterization and modeling of the smart syntactic foam core:

(1) The combination of ultrasonic and three-roll mill mixing was found to be effective in dispersing the carbon nanotubes in the foam as evidenced from the TEM images.

(2) From the DSC results it can be inferred that the glass transition temperature of the foam with carbon nanotubes is similar to its polymer matrix with a much flattened peak.

(3) From the thermal conductivity studies conducted on the smart foam, it was concluded that the specific heat of the smart foam was reduced by about 2.2% when compared with the neat SMP and this could probably be due to the presence of voids in the hollow glass microballoons. Also this reduction in specific heat of the smart foam is an indication that the amount of heat energy required to increase the heat of a unit quantity of the foam is less than that of the neat SMP.

(4) Uniaxial compression tests were conducted on the foam with nanotubes and without nanotubes. The yield strength of the foam without nanotubes was higher than that of the one with nanotubes. This could be attributed to the presence of more voids and less curing in the foam with carbon nanotubes.

(5) A four-phase microstructure consisting of a solid glass shell, a void within the glass shell, an Interfacial Transition Zone (ITZ) and a layer of SMP was identified within the smart foam. A clear picture of the microstructure of the smart foam was developed by employing a

micromechanics based four-phase sphere model to estimate the effective modulus of the equivalent SMP layer in the smart foam. The equivalent smart foam was quantified as well.

6.1.2 Smart Foam Cored Sandwich

The following can be concluded based on the systematic testing of the smart foam cored sandwich:

(1) The shape memory functionality of the shape memory polymer based syntactic foam can be utilized for the purpose of self-sealing impact damage repeatedly, efficiently, and almost autonomously.

(2) For the foam cored sandwich, programming itself can increase the in-plane compressive strength of the sandwich. The shape fixity and shape recovery values for the smart foam cored sandwich was close to 100%, suggesting good shape memory functionality of the smart foam.

(3) From the LVI tests and partially confined healing process employed, it can be concluded that the damage induced by each impact was effectively sealed by the shape recovery process. In other words, the impact tolerance and the load carrying capacity has been effectively recovered.

(4) The compression after impact studies also strongly supports the LVI test results. It was found that each impact cycle reduced the CAI strength and each healing cycle helped in recovering the compressive strength lost due to impact. There is also a need to study the yield strength reduction with 3 hours of additional post-curing time.

(5) From the ultrasonic C-scan images it can be concluded that the damage due to each impact cycle has been effectively healed and also the microstructure has changed after each impact-healing cycle employed.

(6) The SEM images also show evidence of crack sealing in the smart foam due to the partial confinement by the top and bottom skins and the surrounding materials. Thus depending on the degree of the confinement used, the healing achieved in the smart foam could be improved. The

visual inspection images also depict the healing efficiency achieved due to the unconstrained healing process used.

6.1.3 Grid Stiffened Smart Syntactic Foam Cored Sandwich

Based on the extensive testing procedure followed on the grid stiffened smart sandwich structures the following conclusions can be obtained:

(1) The orthogrid stiffened SMP based syntactic foam cored sandwich responds to impact quasi-statically. The low velocity impact leads to a slight temperature rising, which is not sufficient to trigger the shape recovery process.

(2) The developed sandwich can heal structural-length scale damage such as impact damage repeatedly, efficiently, and almost autonomously.

(3) As impact energy increases, the healing efficiency decreases for the first four rounds of impact/healing cycles. For impact/healing up to seven cycles, the healing efficiency is almost the same, regardless of the impact energy (30J and 53J).

(4) The prestrain level during programming has a significant effect on the impact response and healing efficiency of the smart sandwich. Programming by 20% prestrain consistently shows a higher impact tolerance and higher CAI strength than that by 3% prestrain.

(5) The healing efficiency depends on the external confinement provided to the damaged specimen during the shape recovery process. The stronger the external confinement, the higher the healing efficiency.

(6) The fact that the healed sandwich has a higher compressive strength than the control sandwich suggests that the developed material and structure is ideal for impact mitigations. The increase in strength can be explained by the favorable change in microstructure, as evidenced by the C-scan images. The damage propagation in the impacted and healed specimen indicates how

efficiently the healing process has helped in improving the load bearing capacity of the grid stiffened smart syntactic foam cored sandwich structures.

(7) For the case of the smart foam cored sandwich (smart foam core with carbon nanotubes), the post-curing effect due to three additional hours of healing after each impact-healing cycle, contributed to a healing efficiency of more than 100%. However, post-curing had no effect on the higher healing efficiency of the grid stiffened smart foam cored sandwich (smart foam core without nanotubes).

6.2 Future Work

The research done in this work can be further substantiated by conducting the following experimental and fabrication methodologies:

(1) In the current study, it was shown that the SMP based foam cored sandwich and the grid stiffened sandwich was able to repair impact damage repeatedly, efficiently, and almost autonomously. But the SEM images do not show molecular-level healing, which is one of the essential requirements in developing self healing smart polymer systems. In order to achieve healing at molecular level, it is essential to reestablish chemical bonds between the broken polymer chains. Thus, the incorporation of thermoplastic materials into the thermoset SMP polymer system could be a novel option to achieve molecular level healing. It is envisioned that the thermoplastics at the time of recovery, will melt and flow into the damaged area, thereby closing the crack and also reestablishing links with the broken chains. It is very crucial that the SMP and the thermoplastic have good compatibility and also the melting temperature of the thermoplastic should be a few degrees above the T_g of the SMP. Care should also be taken to select the thermoplastic such that the melting temperature is not above or even close to the

permissible/degradation temperature of the SMP. This study will be conducted with the support by an NSF grant NSF/CMMI 0900064.

(2) Based on the intensive set of tests and micromechanics based modeling of the effective modulus, it can be realized that the key for the sandwich structure to self-heal damage is to program the sandwich autonomously and at the same time provide transverse confinement during the shape recovery process of the SMP based syntactic foam core. Transverse confinement can be provided in the form of a shape memory alloy (SMA) z-pinned sandwich structure with a hybrid core – a continuous fiber reinforced polymer grid skeleton that is filled in with a light weight shape memory polymer (SMP) based self-healing smart syntactic foam. This study will be conducted with the support by an NSF grant with contract number NSF/CMMI 0946740.

REFERENCES

[1] K.K. Chawla and G. M. Gladysz, "Syntactic and composite foams", 2006, Journal of Materials Science, volume 4, pp: 3959–3960.

[2] M. Puterman, M. Narkis and S. Kenig, "Syntactic foam Part I: Preparation, structure and properties", 1980, Journal of Cellular Plastics, volume 16, pp: 223-229.

[3] L. Hollaway, "Polymer, fiber and composite material properties and manufacturing techniques", 1990, In: Hollaway, L. (Ed.), Polymers and Polymers Composites in Construction. Thomas/Telford, London, pp: 5-31.

[4] D. Hull and T.W Clyne, "An Introduction to Composite Materials", 1996, Cambridge University Press, Cambridge.

[5] E. Rizzi, E. Papa and A. Corigliano, "Mechanical behavior of a syntactic foam: experiments and Modeling", 2000, International Journal of Solids and Structures, volume 37, pp: 5773-5794.

[6] F.A. Shutov, "Syntactic polymer foams", 1986, Advances in Polymer Science, volume 73/74, pp: 63-123.

[7] A.R. Luxmoore and D.R.J. Owen, "Syntactic foams", 1982, In: Hilyard, N.C. (Ed.), Mechanics of Cellular Plastics. Applied Science Publishers, London, pp: 359-391.

[8] N. Gupta and R. Nagorny, "Tensile Properties of Glass Microballoon-Epoxy Resin Syntactic Foams", 2006, Journal of Applied Polymer Science, volume 102, pp: 1254–1261.

[9] Kishore, R. Shankar and S. Sankaran, "Gradient syntactic foams: Tensile strength, modulus and fractographic features", 2005, Materials Science and Engineering A, volume 412, pp: 153–158.

[10] C.S. Karthikeyan, S. Sankaran and Kishore, "Flexural Behavior of Fibre-Reinforced Syntactic Foams", 2005, Macromolecular. Materials and. Engineering, volume 290, pp: 60–65.

[11] M.V Alonso, M.L. Auad and S. Nutt, "Short-fiber-reinforced epoxy foams", 2006, Composites: Part A, volume 37, pp: 1952–1960.

[12] C.S. Karthikeyan, S. Sankaran and Kishore, "Elastic behavior of plain and fiber-reinforced syntactic foams under compression", 2004, Materials Letters, volume 58, pp: 995– 999.

[13] N Gupta, S. Priya, R. Islam and W. Ricci, "Characterization of Mechanical and Electrical Properties of Epoxy-Glass Microballoon Syntactic Composites", 2006, Ferroelectrics, volume 345, pp: 1–12.

[14] H.S. Kim and P. Plubrai, "Manufacturing and failure mechanisms of syntactic foam under compression", 2004, Composites: Part A, volume 35, pp: 1009–1015.

[15] M. Koopman, K. K. Chawla, K. K. Carlisle and G. M. Gladysz, "Microstructural failure modes in three-phase glass syntactic foams", 2006, Journal of Materials Science, volume 41, pp: 4009–4014.

[16] G. Li and J. Nji, "Development of rubberized syntactic foam", 2007, Composites: Part A, volume 38, pp: 1483–1492.

[17] J .Nji and G. Li, "A CaO enhanced rubberized syntactic foam", 2008, Composites: Part A, volume 39, pp: 1404–1411.

[18] G. Li and M. John, "A crumb rubber modified syntactic foam", 2008, Materials Science and Engineering: A, volume 474, Issues 1-2, pp: 390-399.

[19] H. R. Azimi, R. A. Pearson, and R. W. Hertzberg "Fatigue of Hybrid Epoxy Composites: Epoxies Containing Rubber and Hollow Glass Spheres", 1996, Polymer Engineering and Science, volume 36, number 18, pp: 2352-2365.

[20] B. Song, W. Chen and D.J. Frew, "Dynamic compressive response and failure behavior of an epoxy syntactic foam", 2004, Journal of Composite Materials, volume 38, pp: 915-936.

[21] L. Bardella and F. Genna, "On the elastic behavior of syntactic foams", 2001, International Journal of Solids and Structures, volume 38, pp: 7235-7260.

[22] P.R. Marur, "Effective elastic moduli of syntactic foams", 2005, Materials Letters, volume 59, pp: 1954-1957.

[23] G. Subhash and Q. Liu, "Quasistatic and dynamic crushability of polymeric foams in rigid confinement", 2009, International Journal of Impact Engineering, volume 36, pp: 1303–1311.

[24] S. Sankaran, K. Ravi Shekhar, G. Raju and M. N. Jagdish Kumar, "Characterization of epoxy syntactic foams by dynamic mechanical analysis", 2006, Journal of Materials Science, volume 41, pp: 4041–4046.

[25] M.A. El-Hadek and H.V.Tippur, "Dynamic fracture parameters and constraint effects in functionally graded syntactic epoxy foams", 2003, International Journal of Solids and Structures, volume 40, pp: 1885-1906.

[26] N. Gupta, "A functionally graded syntactic foam material for high energy absorption under compression", 2007, Materials Letters, volume 61, pp: 979-982.

[27] D. Jegley, "Impact-damaged graphite-thermoplastic trapezoidal-corrugation sandwich and semi-sandwich panels", 1993, Journal of Composite Materials, volume 27, pp: 526-538.

[28] E.S.C. Chin, "Army focused research team on functionally graded armor composites", 1999, Materials Science and Engineering A-Structural Materials Properties, Microstructure and Processing, volume 259, pp: 155-161.

[29] B.A. Gama, T.A. Bogetti, B.K. Fink, C.J. Yu, T.D. Claar, H.H. Eifert and J.W. Gillespie Jr, "Aluminum foam integral armor: a new dimension in armor design", 2001, Composite structures, volume 52, pp: 381-395.

[30] B.A. Cheeseman and T.A. Bogetti" "Ballistic impact into fabric and compliant composite laminates", 2003, Composite Structures, volume 61, pp: 161-173.

[31] Columbia Accident Investigation Board, 2003, volume 1, Printing and Distributed by the National Aeronautics and Space Administration and the Government Printing Office, Washington, D.C.

[32] G.S. Langdon, W.J. Cantwell and G.N. Nurick, "The blast response of novel thermoplastic-based fiber-metal laminates-some preliminary results and observations", 2003, Composites Science and Technology, volume 65, pp: 861-872.

[33] G.J. Dvorak and A.P. Suvorov, "Protection of sandwich plates from low-velocity impact", 2006, Journal of Composite Materials, volume 40, pp: 1317-1331.

[34] C. Berggreen, B.C. Simonsen and K.K. Borum, "Experimental and numerical study of interface crack propagation in foam-cored sandwich beams", 2007, Journal of Composite Materials, volume 41, pp: 493-519.

[35] R. Ferri and B.V. Sankar, "A Comparative Study on the Impact Resistance of Composite Laminates and Sandwich Panels", Journal of Thermoplastic Composite Materials, 1997, volume 10, pp: 304-315.

[36] U. K. Vaidya, C. Ulven, S. Pillay and H. Ricks, "Impact Damage of Partially Foam-filled Co-injected Honeycomb Core Sandwich Composites", 2003, Journal of Composite Materials, volume 37, number 7, pp: 611-626.

[37] M.A. Hazizan and W.J. Cantwell, "Low Velocity Impact Response of Foam Core Sandwich Structure", 2004, Advances in Technology of Materials and Materials Processing Journal, volume 6, number 2, pp: 276-285.

[38] T.S. Lim, C.S. Lee and D.G. Lee, "Failure Modes of Foam Core Sandwich Beams under Static and Impact Loads", 2004, Journal of Composite Materials, volume 38, number 18, pp: 1639-1662.

[39] N. Gupta and E. Woldsenbet, "Characterization of Flexural Properties of Syntactic Foam Core Sandwich Composites and Effect of Density Variation", 2005, Journal of Composite Materials, volume 39, number. 24, pp: 2197-2212.

[40] A. Corigliano, E. Rizzi and E. Papa, "Experimental characterization and numerical simulations of a syntactic-foam/glass-fiber composite sandwich", 2000, Composites Science and Technology, volume 60, pp: 2169-2180.

[41] S.V. Rocca and A. Nanni, "Mechanical Characterization Of Sandwich Structure Comprised of Glass Fiber Reinforced Core: Part 1", 2005, Composites in Construction – Third International Conference Lyon, France, July 11 – 13.

[42] G. Griffith, "Carbon foam: a next-generation structural material", 2002, Industrial Heating, volume 69, pp: 47-52.

[43] M.F. Ashby, A.G. Evans, N.A. Fleck, L.J. Gibson, J.W. Hutchinson and H.N.G Wadley, "Metal Foams: A Design Guide", 2000, Butterworth Heinemann, Oxford.

[44] V.S. Deshpande, M.F. Ashby and N.A. Fleck, "Foam topology bending versus stretching dominated architectures" 2001, Acta Materialia, volume 49, pp: 1035-1040.

[45] V.S. Deshpande and N.A. Fleck, "Collapse of truss core sandwich beams in 3-point bending" 2001, International Journal of Solids and Structures, volume 38, pp: 6275-6305.

[46] A. Valdevit, J.W. Hutchinson and A.G. Evans, "Structurally optimized sandwich panels with prismatic cores", 2004, International Journal of Solids and Structures, volume 41, pp: 5105-5124.

[47] L.J. Gibson and M.F. Ashby, "Cellular Solids: Structure and Properties", 1997, 2nd ed., Cambridge University Press, Cambridge.

[48] A.G. Evans, J.W. Hutchinso, and M.F. Ashby, "Multifunctionality of cellular metal systems", 1998, Progress in Materials Science, volume 43, pp: 171-221.

[49] A.W. Van Vuure, "Composite panels based on woven sandwich-fabric performs", 1997, Ph.D. Thesis, Katholieke Universiteit Leuven, Belgium.

[50] M.V. Hosur, M. Abdullah, S. Jeelani, "Manufacturing and low-velocity impact characterization of foam filled 3-D integrated core sandwich composites with hybrid face sheets", 2005, Composite Structures, volume 69, pp: 167-181.

[51] H.L.Fan, W. Yang and Z.M. Chao, "Microwave absorbing composite lattice grids", 2007, Composites Science and Technology, volume 67, pp: 3472-3479.

[52] R.S. Hasebe and C.T. Sun, "Performance of sandwich structures with composite reinforced core", 2000, Journal of Sandwich Structures and Materials, volume 2, pp: 75-100.

[53] F. Laurin and A.J. Vizzini, "Energy absorption of sandwich panels with composite-reinforced foam core", 2005, Journal of Sandwich Structures and Materials, volume 7, pp: 113-132.

[54] G. Li and V.D. Muthyala, "Impact Characterization of Sandwich Structures with an Integrated Orthogrid Stiffened Syntactic Foam Core," 2008, Composites Science and Technology, volume 68, number. 9, pp: 2078-2084.

[55] G. Li and V.S. Chakka, "Isogrid Stiffened Syntactic Foam Cored Sandwich Structure under Low Velocity Impact," Composites Part A: Applied Science and Manufacturing, (Accepted October 12, 2009) doi: 10.1016/j.compositesa.2009.10.007.

[56] G.Li, N. Pourmohamadian, A. Cygan, J. Peck, J.E. Helms, and S.S. Pang, "Fast repair of laminated beams using UV curing composites", 2003, Composite Structures, volume 60, pp: 73-81.

[57] A.C. Balazs, "Modeling self-healing materials", 2007, Materials Today, volume 10, pp: 18–23.

[58] C.M. Dry and N.R. Sottos, "Passive smart self-repair in polymer matrix composite materials", 1992, In: Conference on recent advances in adaptive and sensory materials and their applications. Virginia, USA: Technomic, pp: 438–444.

[59] C.M. Dry, "Alteration of matrix permeability and associated pore and crack structure by timed release of internal chemicals", 1991, Ceramic Transactions, volume 16, pp: 729–768.

[60] C.M. Dry, "Smart materials for sensing and/or remedial action to reduce damage to materials", 1991, In: ADPA/AIAA/ ASME/SPIE conference on active materials and adaptive structures, Virginia, USA, pp: 191–193.

[61] M. Motuku, U.K. Vaidya and G.M. Janowski, "Parametric studies on self-repairing approaches for resin infused composites subjected to low velocity impact", 1999, Smart Materials and Structures, volume 8, pp: 623–638.

[62] S.M. Bleay, C.B. Loader, V.J. Hawyes, L. Humberstone and P.T. Curtis, "A smart repair system for polymer matrix composites", 2001, Composites Part A—Applied Science and Manufacturing, volume 32, pp: 1767–1776.

[63] J.W.C. Pang and I.P. Bond, "A hollow fiber reinforced polymer composite encompassing self-healing and enhanced damage visibility", 2005, Composites Science and Technology; volume 65, pp: 1791–1799.

[64] R.S Trask, G.J Williams and I.P Bond, "Bioinspired self-healing of advanced composite structures using hollow glass fibers", 2007, Journal of Royal Society of Interface, volume 4, pp: 363-371.

[65] C.R. Hickenboth, J.S. Moore, S.R. White, N.R. Sottos, J. Baudry and S.R. Wilson, " Biasing reaction pathways with mechanical force", 2007, Nature, volume 446, pp: 423–427.

[66] A. Hegeman, "Self repairing polymers: repair mechanisms and micromechanical modeling", 1997, Master thesis, University of Illinois at Urbana-Champaign, Urbana, USA.

[67] Jung D, “Performance and properties of embedded microspheres for self-repairing applications”, 1997, Master thesis, University of Illinois at Urbana-Champaign, Urbana, USA.

[68] M.R. Kessler, “Characterization and performance of a self healing composite material”, 2002, Doctor of Philosophy thesis, University of Illinois at Urbana-Champaign, Urbana, USA.

[69] A. Skipor, S. Scheifer and B. Olson, “Self healing polymer compositions”, 2004, (Motorola Inc. U) US: 2004007784-A1.

[70] M. Zako and N. Takano, “Intelligent material systems using epoxy particles to repair microcracks and delamination damage in GFRP”, 1999, Journal of Intelligent Material Systems and Structures, volume 10, pp: 836–841.

[71] S.A. Hayes, F.R. Jones, K. Marshiya and W. Zhan, “A self-healing thermosetting composite material”, 2007, Composites Part A - Applied Science and Manufacturing, volume 38, pp: 1116-1120.

[72] X. Chen, F. Wudl F, A.K. Mal, H. Shen and S.R. Nutt, “New thermally remendable highly cross-linked polymeric materials”, 2003, Macromolecules, volume 36, pp: 1802–1807.

[73] B. Rickborn, “The retro-Diels–Alder reaction- Part I. C–C dienophiles”, 1998, In: Org Reactions, pp: 1–394.

[74] Y.L. Liu and Y.W. Chen, “Thermally reversible cross-linked polyamides with high toughness and self-repairing ability from maleimide- and furan-functionalized aromatic polyamides”, 2007, Macromolecular Chemistry and Physics, volume 208, pp: 224–232.

[75] Y.L. Liu and C.Y. Hsieh, “Crosslinked epoxy materials exhibiting thermal remendabilility and removability from multifunctional maleimide and furan compounds”, 2006, Journal of Polymer Science Part A—Polymer Chemistry, volume 44, pp: 905–913.

[76] D. Ratna and J. Karger-Kocsis J, “Recent advances in shape memory polymers and composites: a review”, 2008, Journal of Materials Science, volume 43, pp: 254–269.

[77] C. Liang, C. A. Rogers and E. Malafeew, “Investigation of Shape Memory Polymers and Their Hybrid Composites”, Journal of Intelligent Material Systems and Structures, 1997, volume 8, pp: 380-386.

[78] V. Brent, “Characterization of Shape Memory Polymers”, Research and Technology Directorate Mechanics of Structures and Materials Branch, Texas A & M University.

[79] C.S. Zhang and Q. Q. Ni, “Bending behavior of shape memory polymer based laminates”, 2007, Composite Structures, volume 78, pp: 153-161.

[80] S.C. Arzberger, M.L. Tupper, M.S. Lake, R. Barrett, K. Mallick, C. Hazelton, W. Francis, P.N. Keller, D. Campbell, S. Feucht, D. Codell, J. Wintergerst, L. Adams, J. Mallioux, R. Denis, K. White, M. Long, and N.A. Munshi, "Elastic Memory Composites (EMC) for deployable industrial and commercial applications", 2005, Proceedings of SPIE -Smart Structures and Materials: Industrial and Commercial Applications of Smart Structures Technologies, volume 5762, pp: 35-47.

[81] L. Yiping, K. Gall, M.L. Dunn and P. McCluskey, "Thermomechanical recovery couplings of shape memory polymers in flexure", 2003, Smart Materials Structures, volume 12, pp: 947–954.

[82] W. Francis, M.S. Lake, K. Mallick, G.E. Freebury, and A. Maji, Presented at the 44th AIAA/ASME/ ASCE/AHS/ASC SDM Conference, 2003, AIAA Paper No. 2003-1496, Norfolk, VA.

[83] A. Lendlein and S. Kelch, "Shape Memory Polymers", 2002, Angewandte Chemie International Edition, volume 41, issue 12, pp: 2034-2057.

[84] P. Miaudet, A. Derré, M. Maugey, C. Zakri, P.M. Piccione, R. Inoubli, and P.Poulin, "Shape and temperature memory of nanocomposites with broadened glass transition, 2007, Science, volume 318, pp: 1294-1296.

[85] J. Diani and K. Gall, "Molecular dynamics simulations of the shape-memory behavior of polyisoprene", 2007, Smart Materials and Structures, volume 16, pp: 1575-1583.

[86] I.S. Gunes and S.C. Jana, "Shape Memory Polymer and Their Nanocomposites: A Review of Science and Technology of New Functional Materials", 2008, Journal of Nanoscience and Nanotechnology, volume 8, pp: 1616-1637.

[87] H. Tobushi, R. Matsui, S. Hayashi and D. Shimada, "The influence of shape-holding conditions on shape recovery of polyurethane-shape memory polymer foams", 2004, Smart Materials and Structures, volume 13, pp: 881–887.

[88] H. Tobushi, K. Okumura, M. Endo and S. Hayashi, "Thermomechanical Properties of Polyurethane-Shape Memory Polymer Foam", 2001, Journal of Intelligent Material Systems and Structures, volume 12, pp: 283-287.

[89] W.M. Huang, C.W. Lee and H.P. Teo, "Thermomechanical Behavior of a Polyurethane Shape Memory Polymer Foam", 2006, Journal of Intelligent Material Systems and Structures, volume 17, pp: 753-760.

[90] S.J. Tey, W.M. Huang and W.M. Sokolowski, "Influence of long-term storage in cold hibernation on strain recovery and recovery stress of polyurethane shape memory polymer foam", 2001, Smart Materials and Structures, volume 10, pp: 321–325.

[91] H. Koerner, G. Price, N.A. Pearce, M. Alexander and R.A. Vaia, "Remotely actuated polymer nanocomposites stress recovery of carbon-nanotube-filled thermoplastic elastomers, 2004, Nature Materials, volume 3, pp: 115-120.

[92] A. Lendlein, H. Jiang, O. Jünger, and R. Langer, "Light-induced shape-memory polymers", 2005, Nature, volume 434, pp: 879-882.

[93] R. Mohr, K. Kratz, T. Weigel, M. Lucka-Gabor, M. Moneke and A. Lendlein, "Initiation of shape-memory effect by inductive heating of magnetic nanoparticles in thermoplastic polymers", 2006, Proceedings of the National Academy of Sciences of the United States of America, volume 103, pp: 3540-3545.

[94] H. Tobushi, H. Hara, E. Yamada, and S. Hayashi, "Thermomechanical properties in a thin film of shape memory polymer of polyurethane series", 1996, Smart Materials and Structures, volume 5, pp: 483-49.

[95] M. Irie, "Shape memory polymers", 1998, Cambridge University Press, Cambridge, UK.

[96] G.J. Monkman, "Advances in shape memory polymer actuation", 2000, Mechatronics, volume 10, pp: 489-498.

[97] F. Li, L. Qi, J. Yang, M. Xu, X. Luo, and D. Ma, "Polyurethane/conducting carbon black composites: structure, electrical conductivity, strain recovery behavior and their relationships", 2000, Journal of Applied Polymer Science, volume75, pp: 68-77.

[98] H.M. Jeong, B.K. Ahn, and B.K. Kim, "Miscibility and shape memory effect of thermoplastic polyurethane blends with phenoxy resin", 2001, European Polymer Journal, volume 37, pp: 2245-2252.

[99] A. Lendlein and R. Langer, "Biodegradable, elastic shape-memory polymers for potential biomedical applications", 2002, Science, volume 296, pp: 1673-1676.

[100] T.H. Tong, "Shape Memory Styrene Copolymer", 2004, United States Patent US 6,759,481 B2.

[101] J.N. Coleman, U. Khan, and Y.K. Gun'ko, "Mechanical Reinforcement of Polymers Using Carbon Nanotubes", 2006, Advanced Materials, volume 18, pp: 689–706.

[102] G. Ji and G. Li, "Effects of nanoclay morphology on the mechanical, thermal, and fire-retardant properties of vinyl ester based nanocomposite", 2008, Materials Science and Engineering A, volume 498, pp: 327-334.

[103] J. Berriot, H. Montes, F. Lequeux, D. Long and P. Sotta, "Gradient of glass transition temperature in filled elastomers", 2003, Europhysics Letters, volume 64, pp: 50-56.

[104] W. Xu and G. Li, "Constitutive Modeling of Shape Memory Polymer Based Self-healing Syntactic Foam", International Journal of Solids and Structures, (Submitted October 21, 2009).

[105] G. Li and D. Nettles, "Thermomechanical Characterization of a Shape Memory Polymer Based Self-Sealing Syntactic Foam", Polymer, (Submitted September 24, 2009).

[106] J. Berriot, F. Lequeux, L. Monnerie, H. Montes, D. Long and P. Sotta, "Filler–elastomer interaction in model filled rubbers, a 1H NMR study", 2002, Journal of Non-Crystalline Solids, volume 307–310, pp: 719–724.

[107] S. Kaufman, W.P. Slichter and D.D. Davis, "Nuclear Magnetic Resonance Study of Rubber-Carbon Black Interactions", 1971, Journal of Polymer Science: Part A, volume 9, pp: 829-839.

[108] G. Li, Y. Zhao Y and S.S. Pang, "Four-phase sphere modeling of effective bulk modulus of concrete", 1999, Cement and Concrete Research, volume 29, pp: 839-845.

[109] P.S. Timoshenko and J.N. Goodier, "Theory of Elasticity", 1970, 3rd ed., McGraw- Hill, New York.

[110] J.D. Eshelby, "The determination of the elastic field of an ellipsoidal inclusion, and related problems", 1957, Proceedings of the Royal Society of London, volume A241, pp: 376–392.

[111] R.M. Christensen, "Mechanics of Composite Materials", 1979, John Wiley & Sons, Inc., New York.

APPENDIX: PERMISSION

ELSEVIER LICENSE
TERMS AND CONDITIONS

Oct 26, 2009

This is a License Agreement between Manu John ("You") and Elsevier ("Elsevier") provided by Copyright Clearance Center ("CCC"). The license consists of your order details, the terms and conditions provided by Elsevier, and the payment terms and conditions.

All payments must be made in full to CCC. For payment instructions, please see information listed at the bottom of this form.

Supplier	Elsevier Limited The Boulevard,Langford Lane Kidlington,Oxford,OX5 1GB,UK
Registered Company Number	1982084
Customer name	Manu John
Customer address	3550 Nicholson Dr, Apt#2080 Baton Rouge, LA 70802
License Number	2293950063406
License date	Oct 21, 2009
Licensed content publisher	Elsevier
Licensed content publication	Composites Science and Technology
Licensed content title	A self-healing smart syntactic foam under multiple impacts
Licensed content author	Guoqiang Li and Manu John
Licensed content date	December 2008
Volume number	
Issue number	
Pages	0
Type of Use	Thesis / Dissertation
Portion	Full article
Format	Both print and electronic
You are an author of the Elsevier article	Yes
Are you translating?	No
Order Reference Number	
Expected publication date	Dec 2009
Elsevier VAT number	GB 494 6272 12

Permissions price	0.00 USD
Value added tax 0.0%	0.00 USD
Total	0.00 USD

Terms and Conditions

INTRODUCTION

1. The publisher for this copyrighted material is Elsevier. By clicking "accept" in connection with completing this licensing transaction, you agree that the following terms and conditions apply to this transaction (along with the Billing and Payment terms and conditions established by Copyright Clearance Center, Inc. ("CCC"), at the time that you opened your Rightslink account and that are available at any time at http://myaccount.copyright.com).

GENERAL TERMS

2. Elsevier hereby grants you permission to reproduce the aforementioned material subject to the terms and conditions indicated.

3. Acknowledgement: If any part of the material to be used (for example, figures) has appeared in our publication with credit or acknowledgement to another source, permission must also be sought from that source. If such permission is not obtained then that material may not be included in your publication/copies. Suitable acknowledgement to the source must be made, either as a footnote or in a reference list at the end of your publication, as follows:

"Reprinted from Publication title, Vol /edition number, Author(s), Title of article / title of chapter, Pages No., Copyright (Year), with permission from Elsevier [OR APPLICABLE SOCIETY COPYRIGHT OWNER]." Also Lancet special credit - "Reprinted from The Lancet, Vol. number, Author(s), Title of article, Pages No., Copyright (Year), with permission from Elsevier."

4. Reproduction of this material is confined to the purpose and/or media for which permission is hereby given.

5. Altering/Modifying Material: Not Permitted. However figures and illustrations may be altered/adapted minimally to serve your work. Any other abbreviations, additions, deletions and/or any other alterations shall be made only with prior written authorization of Elsevier Ltd. (Please contact Elsevier at permissions@elsevier.com)

6. If the permission fee for the requested use of our material is waived in this instance, please be advised that your future requests for Elsevier materials may attract a fee.

7. Reservation of Rights: Publisher reserves all rights not specifically granted in the combination of (i) the license details provided by you and accepted in the course of this licensing transaction, (ii) these terms and conditions and (iii) CCC's Billing and Payment terms and conditions.

8. License Contingent Upon Payment: While you may exercise the rights licensed immediately upon issuance of the license at the end of the licensing process for the transaction, provided that you have disclosed complete and accurate details of your proposed use, no license is finally effective unless and until full payment is received from you (either by publisher or by CCC) as provided in CCC's Billing and Payment terms and conditions. If full payment is not received on a timely basis, then any license preliminarily granted shall be deemed automatically revoked and shall be void as if never granted. Further, in the event that you breach any of these terms and conditions or any of CCC's Billing and Payment terms and conditions, the license is automatically revoked and shall be void as if never granted. Use of materials as described in a revoked license, as well as any use of the materials beyond the scope of an unrevoked license, may constitute copyright infringement and publisher reserves the right to take any and all action to protect its copyright in the materials.

9. Warranties: Publisher makes no representations or warranties with respect to the licensed material.

10. Indemnity: You hereby indemnify and agree to hold harmless publisher and CCC, and their respective officers, directors, employees and agents, from and against any and all claims arising out of your use of the licensed material other than as specifically authorized pursuant to this license.

11. No Transfer of License: This license is personal to you and may not be sublicensed, assigned, or transferred by you to any other person without publisher's written permission.

12. No Amendment Except in Writing: This license may not be amended except in a writing signed by both parties (or, in the case of publisher, by CCC on publisher's behalf).

13. Objection to Contrary Terms: Publisher hereby objects to any terms contained in any purchase order, acknowledgment, check endorsement or other writing prepared by you, which terms are inconsistent with these terms and conditions or CCC's Billing and Payment terms and conditions. These terms and conditions, together with CCC's Billing and Payment terms and conditions (which are incorporated herein), comprise the entire agreement between you and publisher (and CCC) concerning this licensing transaction. In the event of any conflict between your obligations established by these terms and conditions and those established by CCC's Billing and Payment terms and conditions, these terms and conditions shall control.

14. Revocation: Elsevier or Copyright Clearance Center may deny the permissions described in this License at their sole discretion, for any reason or no reason, with a full refund payable to you. Notice of such denial will be made using the contact information provided by you. Failure to receive such notice will not alter or invalidate the denial. In no event will Elsevier or Copyright Clearance Center be responsible or liable for any costs, expenses or damage incurred by you as a result of a denial of your permission request, other than a refund of the amount(s) paid by you to Elsevier and/or Copyright Clearance Center for denied permissions.

LIMITED LICENSE

The following terms and conditions apply only to specific license types:

15. **Translation**: This permission is granted for non-exclusive world **English** rights only unless your license was granted for translation rights. If you licensed translation rights you may only translate this content into the languages you requested. A professional translator must perform all translations and reproduce the content word for word preserving the integrity of the article. If this license is to re-use 1 or 2 figures then permission is granted for non-exclusive world rights in all languages.

16. **Website**: The following terms and conditions apply to electronic reserve and author websites:
Electronic reserve: If licensed material is to be posted to website, the web site is to be password-protected and made available only to bona fide students registered on a relevant course if:
This license was made in connection with a course,
This permission is granted for 1 year only. You may obtain a license for future website posting,
All content posted to the web site must maintain the copyright information line on the bottom of each image,
A hyper-text must be included to the Homepage of the journal from which you are licensing at http://www.sciencedirect.com/science/journal/xxxxx or the Elsevier homepage for books at http://www.elsevier.com , and
Central Storage: This license does not include permission for a scanned version of the material to be stored in a central repository such as that provided by Heron/XanEdu.

17. **Author website** for journals with the following additional clauses:

All content posted to the web site must maintain the copyright information line on the bottom of each image, and
he permission granted is limited to the personal version of your paper. You are not allowed to download and post the published electronic version of your article (whether PDF or HTML, proof or final version), nor may you scan the printed edition to create an electronic version,
A hyper-text must be included to the Homepage of the journal from which you are licensing at http://www.sciencedirect.com/science/journal/xxxxx , As part of our normal production process, you will receive an e-mail notice when your article appears on Elsevier's online service ScienceDirect (www.sciencedirect.com). That e-mail will include the article's Digital Object Identifier (DOI). This number provides the electronic link to the published article and should be included in the posting of your personal version. We ask that you wait until you receive this e-mail and have the DOI to do any posting.
Central Storage: This license does not include permission for a scanned version of the material to be stored in a central repository such as that provided by Heron/XanEdu.

18. **Author website** for books with the following additional clauses:
Authors are permitted to place a brief summary of their work online only.
A hyper-text must be included to the Elsevier homepage at http://www.elsevier.com

All content posted to the web site must maintain the copyright information line on the bottom of each image
You are not allowed to download and post the published electronic version of your chapter, nor may you scan the printed edition to create an electronic version.
Central Storage: This license does not include permission for a scanned version of the

material to be stored in a central repository such as that provided by Heron/XanEdu.

19. **Website** (regular and for author): A hyper-text must be included to the Homepage of the journal from which you are licensing at http://www.sciencedirect.com/science/journal/xxxxx. or for books to the Elsevier homepage at http://www.elsevier.com

20. **Thesis/Dissertation**: If your license is for use in a thesis/dissertation your thesis may be submitted to your institution in either print or electronic form. Should your thesis be published commercially, please reapply for permission. These requirements include permission for the Library and Archives of Canada to supply single copies, on demand, of the complete thesis and include permission for UMI to supply single copies, on demand, of the complete thesis. Should your thesis be published commercially, please reapply for permission.

21. **Other Conditions**None

v1.6

Gratis licenses (referencing $0 in the Total field) are free. Please retain this printable license for your reference. No payment is required.

If you would like to pay for this license now, please remit this license along with your payment made payable to "COPYRIGHT CLEARANCE CENTER" otherwise you will be invoiced within 30 days of the license date. Payment should be in the form of a check or money order referencing your account number and this license number 2293950063406.
If you would prefer to pay for this license by credit card, please go to http://www.copyright.com/creditcard to download our credit card payment authorization form.

Make Payment To:
Copyright Clearance Center
Dept 001
P.O. Box 843006
Boston, MA 02284-3006

If you find copyrighted material related to this license will not be used and wish to cancel, please contact us referencing this license number 2293950063406 and noting the reason for cancellation.

Questions? customercare@copyright.com or +1-877-622-5543 (toll free in the US) or +1-978-646-2777.

VITA

Mr. Manu Kuruvila John was born in November, in Ibadan, Nigeria. He completed his schooling from St. Thomas Central School, India, in 1997. He received his bachelor's degree in mechanical engineering (B.Tech) from Mar Athanasius College of Engineering, India, in May 2001 and his master's degree in mechanical engineering (MS) from Tuskegee University, Alabama, in Summer 2004. He joined Louisiana State University in Fall 2004 and will graduate with the degree of Doctor of Philosophy in mechanical engineering in Fall 2009.